

EFFECTIVE NUCLEAR OPERATORS WITH THE
COUPLED-CLUSTER METHOD

By

Samuel John Novario

A DISSERTATION

Submitted to
Michigan State University
in partial fulfillment of the requirements
for the degree of

Physics—Doctor of Philosophy

2017

PUBLIC ABSTRACT

EFFECTIVE NUCLEAR OPERATORS WITH THE COUPLED-CLUSTER METHOD

By

Samuel John Novario

Your public abstract goes here. This is a preview of the dissertation/thesis template. General instructions for the template can be found in Chapter 7.

—

Lorem ipsum dolor sit amet, consectetur adipiscing elit. Vivamus tristique pretium ipsum nec bibendum. Vestibulum eleifend viverra dui, non molestie libero tincidunt a. Duis commodo odio eget rhoncus cursus. Quisque mattis scelerisque purus in facilisis. Ut consectetur luctus venenatis. Phasellus pulvinar congue tellus, eu tempor augue congue at. In hac habitasse platea dictumst. In accumsan tristique neque quis convallis. Duis quis portitor orci. Vestibulum ante ipsum primis in faucibus orci luctus et ultrices posuere cubilia Curae; Sed sit amet elit sit amet elit scelerisque mattis. Nam a cursus sapien.

ABSTRACT

EFFECTIVE NUCLEAR OPERATORS WITH THE COUPLED-CLUSTER METHOD

By

Samuel John Novario

Your abstract goes here. This is a preview of the dissertation/thesis template. General instructions for the template can be found in Chapter 7.

—

Lorem ipsum dolor sit amet, consectetur adipiscing elit. Vivamus tristique pretium ipsum nec bibendum. Vestibulum eleifend viverra dui, non molestie libero tincidunt a. Duis commodo odio eget rhoncus cursus. Quisque mattis scelerisque purus in facilisis. Ut consectetur luctus venenatis. Phasellus pulvinar congue tellus, eu tempor augue congue at. In hac habitasse platea dictumst. In accumsan tristique neque quis convallis. Duis quis portitor orci. Vestibulum ante ipsum primis in faucibus orci luctus et ultrices posuere cubilia Curae; Sed sit amet elit sit amet elit scelerisque mattis. Nam a cursus sapien.

(Only needed if you intend
to register for a copyright.)

Copyright by
SAMUEL JOHN NOVARIO
2017

Your dedication goes here. It is optional.

Lorem ipsum dolor sit amet, consectetur adipiscing elit. Donec mollis mauris vitae massa
aliquet, at accumsan lorem lobortis.

ACKNOWLEDGMENTS

Your acknowledgments goes here. It is optional. You can also use the variant spelling “Acknowledgements” (note the extra “e”).

—

Lorem ipsum dolor sit amet, consectetur adipiscing elit. Donec vel nisl aliquam, tincidunt lacus et, sollicitudin lectus. Mauris quis sagittis risus. Lorem ipsum dolor sit amet, consectetur adipiscing elit. Vestibulum aliquet odio leo, eget laoreet leo dictum luctus. Aliquam at nisi eu turpis posuere rhoncus id ac neque. Nunc iaculis turpis id rhoncus rutrum.

In pharetra neque luctus, vestibulum diam quis, vehicula turpis. Proin magna magna, feugiat sed luctus consectetur, vehicula id erat. Phasellus non nisi ac ipsum vehicula aliquet. Proin pulvinar sit amet metus id finibus. Mauris et justo et mi sollicitudin commodo. Cras tempus interdum lectus ac iaculis. Proin purus purus, euismod non magna aliquet, gravida volutpat velit. Praesent eu erat purus. Cras tempus eu dolor vitae malesuada.

PREFACE

Your preface goes here. It is optional. This is a preview of the dissertation/thesis template. General instructions for the template can be found in Chapter 7.

Lorem ipsum dolor sit amet, consectetur adipiscing elit. In id pellentesque lacus. Praesent scelerisque eros sit amet felis faucibus pretium. Pellentesque cursus maximus consectetur. Suspendisse at congue eros. Cras tincidunt tellus lorem, ut viverra ligula sagittis eget. Praesent egestas viverra leo a rutrum. Vivamus finibus magna eu sapien tristique, eget congue mi facilisis. Integer porttitor dignissim dolor ut porta. Nulla congue hendrerit nulla, et volutpat elit scelerisque vitae.

Donec convallis, nunc eget efficitur lacinia, magna ipsum dignissim dolor, vitae mollis neque sem in ipsum. In quam mi, laoreet ac nibh sed, imperdiet tincidunt tellus. Sed dictum ante ac facilisis ornare. Curabitur sit amet purus quis nulla dictum blandit in ut purus. Praesent eget ligula in nisl interdum facilisis vitae vitae magna. Ut quis ornare augue. Cras aliquet ac ex iaculis rutrum. Vestibulum volutpat fermentum orci, sed laoreet neque auctor eu. Fusce ac lorem congue, blandit eros a, tincidunt leo. Cras luctus ultricies mollis. Phasellus laoreet nulla sit amet ipsum sollicitudin facilisis. Donec sit amet est volutpat, accumsan nisi sed, fringilla mi.

TABLE OF CONTENTS

LIST OF TABLES	ix
LIST OF FIGURES	x
KEY TO SYMBOLS AND ABBREVIATIONS	xii
Chapter 1 Introduction	1
1.1 A Brief History of Nuclear Structure Theory	2
1.2 Electroweak Theory and Nuclear Structure	4
1.3 Ab-Initio Descriptions of Beta Decay	6
1.4 Thesis Structure	7
Chapter 2 Many-Body Quantum Mechanics	8
2.1 Independent-Particle Model	8
2.2 Second Quantization	11
2.3 Normal Ordering	13
2.4 Wick's Theorem	15
2.5 Hartree-Fock Method	19
2.6 Configuration-Interaction	23
2.7 Many-Body Perturbation Theory	26
Chapter 3 Coupled-Cluster Theory	32
3.1 Connection to MBPT	45
3.2 Solving the Coupled Cluster Equations	46
3.3 Example: Pairing Model	46
3.4 Example: Infinite Matter	49
3.4.1 Two-body interaction	54
Chapter 4 Equation-of-Motion Method	63
Chapter 5 Effective Operators	71
5.1 Beta Decay	73
5.2 Sum Rules	74
5.3 Calculating Beta-Decay Matrix Elements	75
Chapter 6 Conclusions and Perspectives	77
Chapter 7 Instructions	78
7.1 Preamble	78
7.2 Front matter	79
7.3 Main matter	79
Chapter 8 Appendix	80

Chapter 9 Lorem ipsum	81
9.1 Pellentesque Scelerisque	81
9.1.1 Fusce Convallis	82
9.2 Curabitur	83
APPENDICES	85
Appendix A Etiam a Convallis	86
Appendix B Nulla Feugiat	88
Appendix C Diagrammatic Rules	89
Appendix D Angular Momentum Coupling	90
Appendix E Coupled Two-Body State	91
Appendix F Convergence Acceleration: Direct-Inversion of the Iterative Subspace	92
Appendix G CCSD Diagrams	93
Appendix H Computational Implementation	100
Appendix I Angular Momentum Coupling	111
REFERENCES	114

LIST OF TABLES

Table 3.1:	Single-particle states and their quantum numbers and their energies from Eq. (3.40). The degeneracy for every quantum number p is equal to 2 due to the two possible spin values.	47
Table 3.2:	Total number of particle filling $N_{\uparrow\downarrow}$ for various $n_x^2 + n_y^2 + n_z^2$ values for one spin-1/2 fermion species. Borrowing from nuclear shell-model terminology, filled shells corresponds to all single-particle states for one $n_x^2 + n_y^2 + n_z^2$ value being occupied. For matter with both protons and neutrons, the filling degree increased with a factor of 2.	52
Table 3.3:	Parameters used to define the Minnesota interaction model [?].	58
Table 3.4:	CCD and MBPT2 results for infinite neutron matter with $N = 66$ neutrons and a maximum number of single-particle states constrained by $N_{max} = 36$	61
Table 5.1:	Single-particle states and their quantum numbers and their energies from Eq. (3.40). The degeneracy for every quantum number p is equal to 2 due to the two possible spin values.	73
Table 9.1:	Nulla suscipit ultricies massa at sagittis.	84
Table B.1:	Lorem ipsum dolor sit amet, consectetur adipiscing elit. Nulla feugiat ante quis consectetur pellentesque. In tincidunt orci in justo tempor, non tempor metus congue.[30]	88

LIST OF FIGURES

Figure 1.1:	Nuclear chart of nuclei with ground-state energies which have been calculated with ab-initio methods and NN+3N interactions. Figure taken from [51].	3
Figure 1.2:	Progress of ab-initio nuclear structure from calculations of ground-state energies with NN+3N interactions. Early progress was approximately linear as the problem size scaled with Moore’s law while more recent progress has taken advantage of new algorithms which have outpaced Moore’s law. Data taken from [51].	5
Figure 2.1:	A depiction of the closed-shell reference state in the independent particle model. Each horizontal line represents a shell of single-particle orbits, and the dotted line represents the Fermi level which separates <i>particle</i> states from <i>hole</i> states.	13
Figure 2.2:	A depiction of $1p\text{-}1h$, $2p\text{-}2h$, $1p\text{-}0h$, and $0p\text{-}1h$ Slater determinants defined relative to the reference state in the independent particle model. .	14
Figure 2.3:	Scaling of the matrix size and number of non-zero matrix elements for nuclear CI calculations of light nuclei. Even for modest N_{max} , the memory requirements approach the limit of petascale supercomputers (10^{10}). Figure taken from [81].	25
Figure 3.1:	(Color online) Diagrammatic representation of \bar{H} of Eq. (3.6), excluding terms involving the one-body interaction \hat{H}_1 and first-order terms involving only the bare Hamiltonian. Open circles represent the excitation cluster operators \hat{T}_1 and \hat{T}_2 , and filled circles represent the two-body interaction \hat{H}_2 . As before, the diagrams are implicitly antisymmetrized (Hugenholtz diagrams). Lines connected to \hat{T} are always directed upward because they represent an excitation operator while the directions of external lines connected to \hat{H}_2 are unconstrained.	35
Figure 3.2:	Correlation energy for the pairing model with exact diagonalization, MBPT2 and perturbation theory to third order MBPT3 for a range of interaction values. A canonical Hartree-Fock basis has been employed in all MBPT calculations.	46
Figure 3.3:	ab-initio progress blah blah blah	49
Figure 3.4:	Correlation energy for the pairing model with exact diagonalization, MBPT2 and perturbation theory to third order MBPT3 for a range of interaction values. A canonical Hartree-Fock basis has been employed in all MBPT calculations.	50

Figure 3.5:	Energy per particle for pure neutron matter as function of density from coupled cluster calculations with doubles correlations only. The reference energy is included for comparison. The results have been obtained with Minnesota interaction model using periodic boundary conditions and $N = 66$ neutrons and single-particle states up to $N_{max} = 36$, resulting in a total of 2377 single-particle states.	60
Figure 3.6:	Energy per particle for pure neutron matter as function of density from coupled cluster calculations with doubles correlations only. The reference energy is included for comparison. The results have been obtained with Minnesota interaction model using periodic boundary conditions and $N = 66$ neutrons and single-particle states up to $N_{max} = 36$, resulting in a total of 2377 single-particle states.	62
Figure 4.1:	Progress of ab-initio nuclear structure from calculations of ground-state energies with NN+3N interactions. Early progress was approximately linear as the problem size scaled with Moore’s law while more recent progress has taken advantage of new algorithms which have outpaced Moore’s law. Data taken from [51].	69
Figure 4.2:	Progress of ab-initio nuclear structure from calculations of ground-state energies with NN+3N interactions. Early progress was approximately linear as the problem size scaled with Moore’s law while more recent progress has taken advantage of new algorithms which have outpaced Moore’s law. Data taken from [51].	70
Figure 9.1:	Lorem ipsum dolor sit amet, consectetur adipiscing elit. Ut et leo non tortor viverra sodales.	82
Figure 9.2:	Ut condimentum odio orci, a varius sapien vehicula quis.	82

KEY TO SYMBOLS AND ABBREVIATIONS

$Ap-Bh$ A -particle, B -hole excitation or de-excitation from the reference state

$|0\rangle$ vacuum state

$|\Phi_0\rangle$ reference state

$|\Psi\rangle$ correlated ground state

$|\Phi_{i_1 \dots i_B}^{a_1 \dots a_A}\rangle$ specific $Ap-Bh$ state

$\{\dots\}$ normal-ordered with respect to the reference state

$\hbar\omega$ harmonic oscillator energy scale

\hat{H} Hamiltonian

\bar{H} similarity-transformed Hamiltonian

\hat{H}_N normal-ordered Hamiltonian

\bar{H}_N normal-ordered similarity-transformed Hamiltonian

\hat{T} cluster operator

$\varepsilon_{i_1 \dots i_B}^{a_1 \dots a_A}$ energy denominator, $f_{i_1}^{i_1} + \dots + f_{i_B}^{i_B} - f_{a_1}^{a_1} - \dots - f_{a_A}^{a_A}$

CC coupled cluster

CCD coupled cluster with doubles

CCSD coupled cluster with singles and doubles

CCSDT coupled cluster with singles, doubles, and triples

CCSD(T) coupled cluster with singles, doubles, and triples approximation

Λ -CCSD(T) coupled cluster with singles, doubles, and Λ -triples approximation

CI configuration interaction

FCI full configuration interaction

COM center of mass

EOM equations-of-motion

PA particle-attached

PR particle-removed

EOM equations-of-motion

EOM-CC equations-of-motion coupled cluster

EOM-CCSD equations-of-motion coupled cluster with singles and doubles

HF Hartree-Fock

IM-SRG in-medium similarity renormalization group

HO harmonic oscillator

LECs low-energy constants

MBPT many-body perturbation theory

WS Woods-Saxon

DIIS direct-inversion of the iterative subspace

QCD quantum chromodynamics

EFT effective field theory

NN nucleon-nucleon

3N three-nucleon

NLO next-to leading order

N²LO next-to-next-to leading order

N³LO next-to-next-to-next-to leading order

Chapter 1

Introduction

Steady progress in any modern scientific endeavor requires a strong, dynamic relationship between experimental data to paint an accurate picture of some natural phenomena and theoretical models to interpret those phenomena with respect to the growing network of other scientific models. Conversely, the predictive capability of theoretical models can highlight blurry or unfinished areas of that picture which can be clarified or completed by new or improved experimental techniques. In the pursuit to understand and describe the atomic nucleus and the corresponding implications from quarks to neutron stars, this push-and-pull coordination between theory and experiment makes progress in modern nuclear physics robust and persistent.

An integral component of modern nuclear physics is describing the structure and emergent properties of self-bound systems of protons and neutrons. The systems in questions can be stable nuclei, rare isotopes far from stability, and even infinite nuclear matter which can be used to model neutron stars. Relevant properties to nuclear structure include ground-state energies—for determining nuclear masses, excited-state energies—for identification in gamma or neutron spectroscopy, and transition or decay amplitudes—for calculating the respective rates for those processes. This wide array of emergent properties inserts both nuclear structure theory and experiment into a prominent role within every other subfield of modern nuclear physics, from lattice quantum chromodynamics (QCD) to nuclear astrophysics, and beyond, to questions about fundamental symmetries and dark matter. However, two inextricable characteristics of a comprehensive model of nuclear structure—the increasingly large

size of many-body nuclear systems and the complexity and strength of the nucleon-nucleon interactions—have been imposing hurdles for theorists to overcome.

1.1 A Brief History of Nuclear Structure Theory

The project to solve the correlation problem in many-fermion systems began with the work of Brueckner, Bethe, and Goldstone [18, 8, 1] with the reformulation of the nuclear interaction by accounting for two-body correlations from the nuclear medium. This work continued with the work of Coester and Kummel [26, 27, 62] with a further resummation of nuclear correlations in the form of an exponential ansatz into what would become coupled-cluster (CC) theory. However, there were two major obstacles that hindered the progress in this area for decades. First, while these methods were systematically improvable by including progressively higher-level correlations, the highly-nonperturbative nature of the nuclear force required computationally infeasible summations. Second, there wasn't a reliable and consistent theory to model nucleon-nucleon interactions.

However, the well-known and highly-perturbative Coulomb force, which underlies the many-electron systems in atoms and molecules, made consistent advances in ab-initio quantum chemistry possible since the 1950s. Along with the quasi-exact method of configuration interaction (CI) [84, 28, 3, 102] which physicists have utilized since the formulation of quantum mechanics, chemists successfully employed approximate methods like many-body perturbation theory (MBPT) [53, 54, 80, 82] and coupled-cluster theory [24, 22, 23, 73, 82].

Fortunately, within the past decade, two breakthroughs have allowed ab-initio nuclear structure to resurface and thrive the way that quantum chemistry had done in the previous decades. First was the invention of chiral effective field theory (EFT) [34, 65] which gave theorists the ability to construct nucleon-nucleon interactions consistent with the underlying

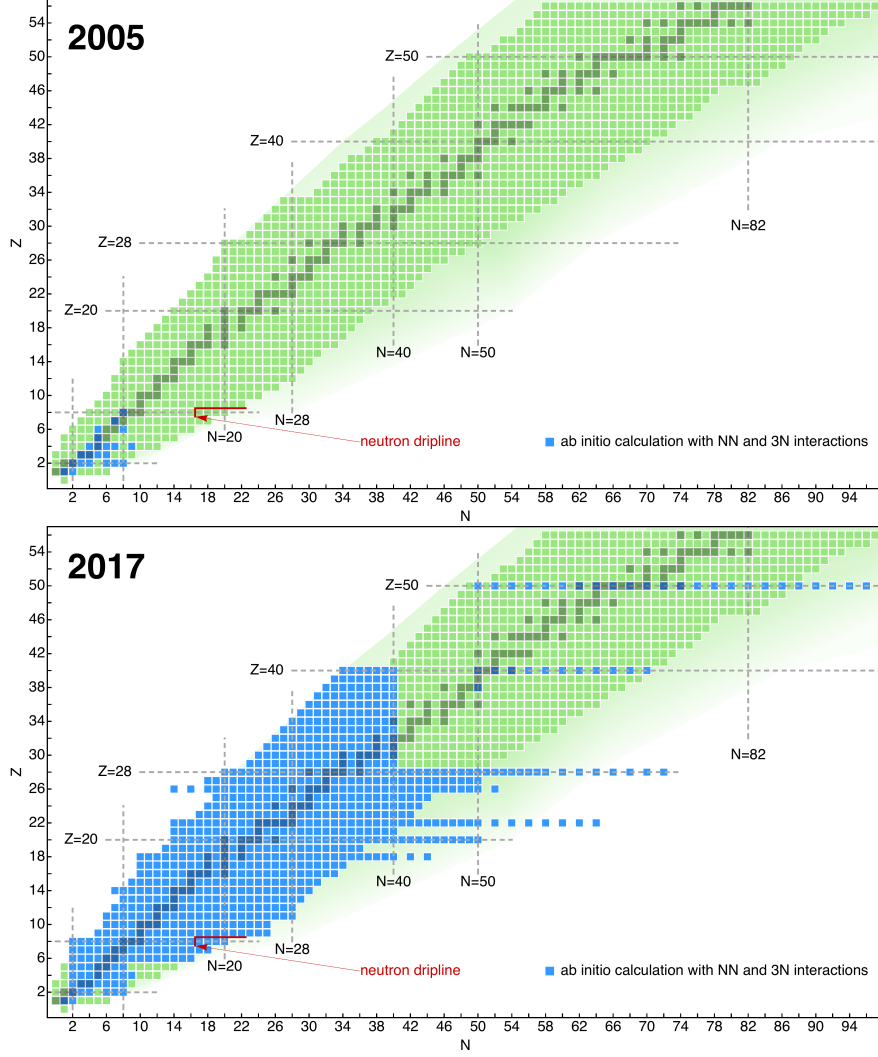


Figure 1.1: Nuclear chart of nuclei with ground-state energies which have been calculated with ab-initio methods and NN+3N interactions. Figure taken from [51].

QCD of the strong nuclear force. Second was the application of renormalization group (RG) methods to the nuclear force [13, 79]. This procedure can “soften” the NN interaction, to decouple the high- and low-momentum components of the nuclear force and generate less-correlated systems that can be calculated at a reasonable computational cost. These major changes to nuclear structure theory made it possible to merge the field with the progress of quantum chemistry and open a new area for additional developments in ab-initio descriptions of many-fermion systems, see Fig. 1.1.

Along with exponential improvements to high-performance computing, these novel techniques have allowed modern many-body methods to extend their reach and deepen their applicability across the nuclear chart, see Fig. 1.2. The no-core shell model (NCSM), a quasi-exact method, has been able to reach the sd shell and useful in calculating the radii, transition strengths, and effective interactions of light nuclei [68, 69, 5]. Another quasi-exact technique which follows a completely different methodology than NCSM, quantum Monte Carlo (QMC), has also progressed and is now capable of calculating properties of light nuclei with modern chiral forces [75, 74, 21]. In addition to these exponentially scaling techniques' successes with lighter nuclei, polynomially scalling techniques—such as the in-medium similarity renormalization group (IMSRG) [100, 101, 49, 11, 50, 48, 90, 89], self-consistent Green's functions (SCGF) [86, 87, 88], and coupled cluster theory [107, 108, 55, 56, 42, 60, 40, 9]—have been able to reach open-shell nuclei through the pf shell and even up to the chain of even tin isotopes with equations-of-motion and multi-reference techniques.

1.2 Electroweak Theory and Nuclear Structure

Nuclear structure is implicated in performing and analyzing experiments to probe fundamental symmetries and physics beyond the Standard Model. One example is determining the V_{ud} component of the Cabbibo-Kobayashi-Maskawa (CKM) matrix, which relates quark eigenstates of the weak interaction to their mass eigenstates [20, 58]. This matrix element can be determined from by measuring the half-lives of superallowed Fermi beta decays [94] and applying a nucleus-dependent structure correction [95, 99, 98, 4, 57]. The value of $|V_{ud}|$ is used to test the unitarity of the CKM matrix and the conserved-vector current hypothesis, which relates the ft -values of superallowed Fermi beta decays of different nuclei, both predicted by the standard model [44].

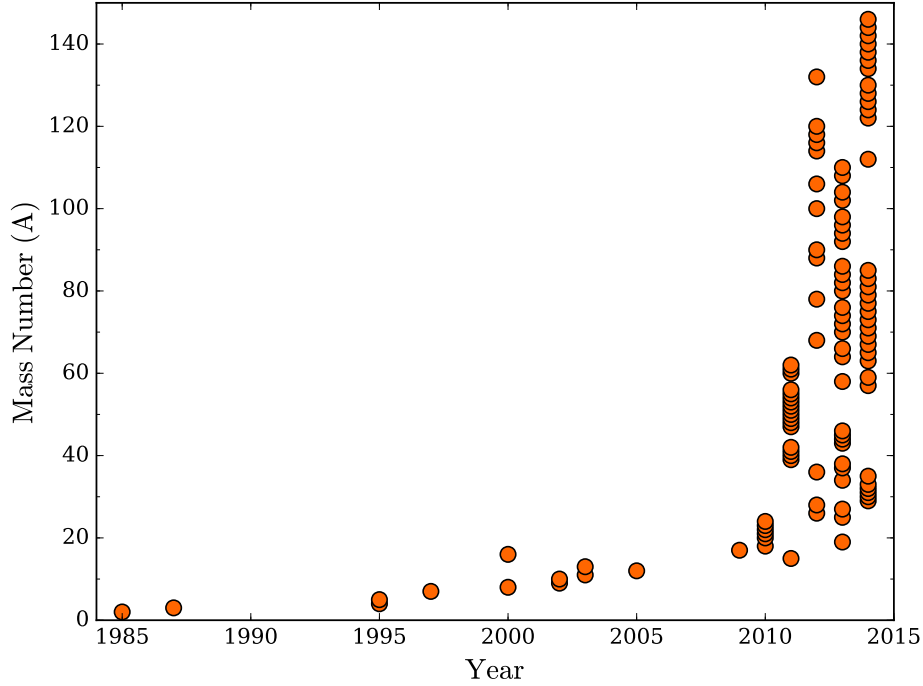


Figure 1.2: Progress of ab-initio nuclear structure from calculations of ground-state energies with NN+3N interactions. Early progress was approximately linear as the problem size scaled with Moore’s law while more recent progress has taken advantage of new algorithms which have outpaced Moore’s law. Data taken from [51].

Another example of physics beyond the standard model is the neutrinoless double-beta decay ($0\nu\beta\beta$) [91, 2]. The extremely-rare, two-neutrino double-beta decay ($2\nu\beta\beta$) has been observed in many experiments [32, 66], which has motivated the search for its neutrinoless counterpart, in which two Majorana neutrinos—being their own antiparticles—annihilate one another, which is not possible in the standard electro-weak theory. The long half-lives of these theoretical decays depend on a phase-space factor, which is highly dependent on the decay Q -value, and a nuclear matrix element. The Q -value can be determined from high-precision mass measurements of the relevant nuclei [64, 41, 78, 19], while the nuclear matrix element, which contributes the largest source of uncertainty, must be calculated with a sufficient many-body theory.

The weak interaction and nuclear structure can also be exploited for supernova neutrino

detection and spectroscopy. While these original detectors were based on electron-neutrino scattering [52, 10], more recent experiments utilize correlated nucleon effects of large nuclei to enhance the scattering cross section and therefore the ability to resolve energies and distinguish neutrino flavors [46, 25, 35, 63]. Supernova models predict distinct distributions for different neutrino flavors based on the temperatures at which they are emitted [59, 7]. With nuclear structure calculations that include sufficient nuclear correlations, these high-resolution detectors can be used to verify specific models.

1.3 Ab-Initio Descriptions of Beta Decay

Since Enrico Fermi’s originally rejected paper describing β decay in 1934 [36, 106], theorists have worked to refine this description within the ever-growing library of knowledge concerning the nature of the weak force, the characteristics of the neutrino, and the structure of nuclei. With the success of ab-initio calculations for nuclear properties such as masses, radii, and electromagnetic phenomena, these techniques also seem promising ways to calculate relevant quantities involved in nuclear β decay. Because the kinematics of the decay and the underlying weak process are well understood, the remaining task for nuclear theory to tackle is calculating the transition amplitudes between the initial and final nuclei.

Modern calculations of these β -decay matrix elements were originally performed using phenomenological interactions in the shell model framework [105, 16, 103, 70]. Also, predecessors to current ab-initio techniques like the random-phase approximation (RPA) [97] included core-correlation effects in these early descriptions. These methods were able to successfully reproduce experimental lifetime data and address technical issues such as the quenching of the axial-vector coupling constant. More recently, the success of the shell model has inspired an extension to the new method, known as the ab-initio shell model, where an

effective interaction is constructed within a certain valence space using a many-body method such as CC [31] or IMSRG [12]. However, these techniques are computationally expensive and cannot currently reach heavy nuclei of interest. The most common method used in their place is known as the quasiparticle random-phase approximation (QRPA) [92, 33]. While these calculations can be performed for heavy nuclei in large spaces, they also rely on phenomenological effective interactions. Therefore, there is a demand for computationally-economical, ab-initio techniques that can capture the relevant many-body correlations needed to accurately describe the nuclear structure aspects of electro-weak processes.

1.4 Thesis Structure

The main goal of this work is to explore the ab-initio description of nuclear beta decay within the coupled-cluster theory framework of EOM-CCSD using renormalized chiral NN and 3N interactions. The organization of the thesis builds from a general description of the many-body problem of quantum mechanics in chapter 2. Then, in chapter 3, this many-body framework is applied within the coupled-cluster theory and applied to various systems including atomic nuclei. In chapter 4, coupled-cluster theory is extended to the equations-of-motion method to describe open-shell systems. Chapter 5 outlines the procedure to express observables as effective coupled-cluster operators and how to calculate those observables in the equations-of-motion framework. Then, in chapter 5.1, the ability to calculate effective operators is applied to Fermi- and Gamow-Teller- beta-decay operators and relevant quantities are determined for various nuclei. Lastly, conclusions and future perspectives are given in chapter 6 while technical details concerning the formalism and implementation are given in the appendix 8.

Chapter 2

Many-Body Quantum Mechanics

Ab-initio structure calculations of many-fermion systems such as those in nuclear and electronic structure aim to describe emergent phenomena from the constituent particles subject to the underlying microscopic Hamiltonian. This amounts to finding the solution to the many-body Schrödinger equation. However, a calculation of the exact solution needs to account for all possible correlations among the particles and thus scales factorially. This motivates the need for approximations to the exact solution that account for the most important correlations. This chapter first establishes the formalism necessary to define the many-body problem then illustrates several successive approximations to its solution. Because the type of fermions and the underlying Hamiltonian can be kept generic until specific systems are considered, the formalism and many-body methods can be kept generic as well.

2.1 Independent-Particle Model

The nonrelativistic A-body quantum problem begins with the Schrödinger equation,

$$\hat{H}\Psi_{\nu}(\mathbf{r}_1, \dots, \mathbf{r}_A) = E_{\nu}\Psi_{\nu}(\mathbf{r}_1, \dots, \mathbf{r}_A), \quad (2.1)$$

for the correlated wave function $\Psi_{\nu}(\mathbf{r}_1, \dots, \mathbf{r}_A)$ and the corresponding energy E_{ν} . The Hamiltonian can be written generically as a sum of k -body pieces which, in principle, can

contain up to A -body interactions,

$$\begin{aligned}\hat{H} &= {}^{(1)}\hat{H} + {}^{(2)}\hat{H} + {}^{(3)}\hat{H} + \dots \\ &= \sum_i^A {}^{(1)}\hat{H}(\mathbf{r}_i) + \sum_{i<j}^A {}^{(2)}\hat{H}(\mathbf{r}_i, \mathbf{r}_j) + \sum_{i<j<k}^A {}^{(3)}\hat{H}(\mathbf{r}_i, \mathbf{r}_j, \mathbf{r}_k) + \dots\end{aligned}\quad (2.2)$$

Regardless of the system, the one-body term contains the kinetic energy operator $\frac{\hbar^2}{2m}\nabla_i^2$, while the higher-order terms result from inter-particle interactions.

An intuitive way to formulate the solution to the many-body Schrödinger equation is to express the collective wave function in terms of independent single-particle wave functions, or orbitals $\phi(\mathbf{r})$. In this independent-particle model, a selection of single-particle wave functions, known as the single-particle basis, are constructed by solving the Schrödinger equation for a single particle in some mean-field potential, for bound systems, or in free space, for infinite systems. Then a many-body wave function is constructed as a product of these single-particle orbits. This simple model is justified because it becomes exact when inter-particle interactions are completely suppressed and is useful because it provides an intuitive way to interpret complicated many-body dynamics as processes involving few single-particle wave functions.

A many-body wave function of fermions must be anti-symmetric with respect to particle exchange so that the Pauli exclusion principle is followed, such that no single-particle wave function is occupied by more than one fermion. This condition is satisfied by a wave function

in the form of a *Slater determinant* [85],

$$\Phi(\mathbf{r}_1, \dots, \mathbf{r}_A) = \frac{1}{\sqrt{A!}} \begin{vmatrix} \phi_1(\mathbf{r}_1) & \phi_1(\mathbf{r}_2) & \cdots & \phi_1(\mathbf{r}_A) \\ \phi_2(\mathbf{r}_1) & \phi_2(\mathbf{r}_2) & \cdots & \phi_2(\mathbf{r}_A) \\ \vdots & \vdots & \ddots & \vdots \\ \phi_A(\mathbf{r}_1) & \phi_A(\mathbf{r}_2) & \cdots & \phi_A(\mathbf{r}_A) \end{vmatrix}, \quad (2.3)$$

where A is the number of particles in the system and $\phi_p(\mathbf{r}_\mu)$ is the p -th orbital filled with the μ -th particle.

If the orbitals are constructed from an appropriate phenomenological potential, a Slater determinant composed of the A lowest orbitals can represent a fairly good approximations to the ground state for a closed-shell system, where the lowest-energy Slater determinant can be uniquely determined. The set of all Slater determinants in a certain model space of single-particle wave functions defines a complete A -body Hilbert space such that a generic wave function can be written as a linear combination of Slater determinants,

$$\Psi_\nu(\mathbf{r}_1, \dots, \mathbf{r}_A) = \sum_{\mu=1}^{\mathcal{N}} C_\nu^\mu \Phi_\mu(\mathbf{r}_1, \dots, \mathbf{r}_A), \quad (2.4)$$

where $C_\nu^\mu = \langle \Psi(\mathbf{r}_1, \dots, \mathbf{r}_A) | \Phi_\nu^\mu(\mathbf{r}_1, \dots, \mathbf{r}_A) \rangle$. The number of Slater determinants \mathcal{N} in an A -body Hilbert space with N orbits is given by,

$$\mathcal{N} = \binom{N}{A} = \frac{N!}{A!(N-A)!}, \quad (2.5)$$

which shows the factorial scaling of the exact problem. However, to reduce the size of the problem, progressively more significant Slater determinants can be chosen to systematically

refine approximations to the full solution.

2.2 Second Quantization

Even with the simplification of the independent-particle model, the many-body Schrödinger equation is an unwieldy and complex system of coupled differential equations. A useful reformulation of this equation is to promote the single-particle orbits to operators in a step known as *second quantization* (see e.g., [82, 37]). In this framework, a Slater determinant is represented by a string of occupied orbitals,

$$\Phi(\mathbf{r}_1, \dots, \mathbf{r}_A) \equiv \mathcal{A}(\phi_{p_1} \phi_{p_2} \phi_{p_3} \cdots \phi_{p_N}) \equiv |p_1 p_2 p_3 \cdots p_N\rangle, \quad (2.6)$$

where \mathcal{A} represents a permutation and normalization operator to correspond with Eq. (2.3). These second-quantized Slater determinants can be constructed with the use of operators that correspond to specific orbitals. A *creation* operator, \hat{a}_p^\dagger , places a particle in the p orbital, and an *annihilation* operator, \hat{a}_p , removes a particle from the p orbital,

$$\hat{a}_p^\dagger |0\rangle = |p\rangle \quad \hat{a}_p |p\rangle = |0\rangle, \quad (2.7)$$

where $|0\rangle$ represents the true vacuum, a state void of any particles. Because there must be a correspondence between the original first quantization and second quantization, these creation and annihilation operators obey the following anticommutation relations ($[\hat{A}, \hat{B}]_+ = \hat{A}\hat{B} + \hat{B}\hat{A}$),

$$[\hat{a}_p^\dagger, \hat{a}_q]_+ = \delta_{pq} \quad [\hat{a}_p^\dagger, \hat{a}_q^\dagger]_+ = [\hat{a}_p, \hat{a}_q]_+ = 0, \quad (2.8)$$

which guarantee that wave functions comprised of these operators obey antisymmetry and the Pauli exclusion principle required of fermionic systems.

The Hamiltonian in the form of Eq. (2.2) can be written with second-quantized operators as,

$$\hat{H} = \sum_{pq} {}^{(1)}H_q^p \hat{a}_p^\dagger \hat{a}_q + \frac{1}{4} \sum_{pqrs} {}^{(2)}H_{rs}^{pq} \hat{a}_p^\dagger \hat{a}_q^\dagger \hat{a}_s \hat{a}_r + \frac{1}{36} \sum_{pqrstu} {}^{(3)}H_{stu}^{pqr} \hat{a}_p^\dagger \hat{a}_q^\dagger \hat{a}_r^\dagger \hat{a}_u \hat{a}_t \hat{a}_s + \dots, \quad (2.9)$$

where the prefactors account for the double counting of particle-particle interactions, and the matrix elements represent integrals over the relevant single-particle wave functions,

$$\begin{aligned} {}^{(1)}H_q^p &\equiv \int d\mathbf{r}_1 \phi_p^*(\mathbf{r}_1) {}^{(1)}\hat{H}(\mathbf{r}_1) \phi_q(\mathbf{r}_1) \\ {}^{(2)}H_{rs}^{pq} &\equiv \int d\mathbf{r}_1 d\mathbf{r}_2 \phi_p^*(\mathbf{r}_1) \phi_q^*(\mathbf{r}_2) {}^{(2)}\hat{H}(\mathbf{r}_1, \mathbf{r}_2) [\phi_r(\mathbf{r}_1) \phi_s(\mathbf{r}_2) - \phi_s(\mathbf{r}_1) \phi_r(\mathbf{r}_2)] \\ &\vdots \end{aligned} \quad (2.10)$$

Matrix elements involving two or more particles include exchange terms which guarantee that they are also antisymmetric,

$$\begin{aligned} {}^{(2)}H_{rs}^{pq} &= -{}^{(2)}H_{rs}^{qp} = -{}^{(2)}H_{sr}^{pq} = {}^{(2)}H_{sr}^{qp} \\ {}^{(3)}H_{stu}^{pqr} &= -{}^{(3)}H_{stu}^{qpr} = -{}^{(3)}H_{tsu}^{pqr} = {}^{(3)}H_{tsu}^{qpr} = \dots \end{aligned} \quad (2.11)$$

These definitions apply regardless of the form of the Hamiltonian, and thus this formalism remains generic to the particular system. Second quantization is a crucial step in simplifying the many-body Schrödinger equation because it reduces the complexity of the spatial and spin degrees of freedom within the single-particle wave functions and interactions into precomputed matrix elements. The remaining effort is reduced to algebraic expressions in-

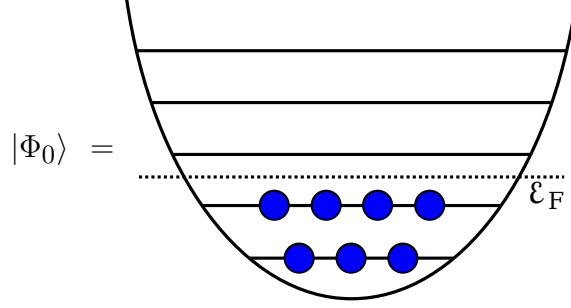


Figure 2.1: A depiction of the closed-shell reference state in the independent particle model. Each horizontal line represents a shell of single-particle orbits, and the dotted line represents the Fermi level which separates *particle* states from *hole* states.

volving creation and annihilation operators.

2.3 Normal Ordering

It's convenient to define an A-particle reference state, where states are filled from the true vacuum up to a closed shell, known as the Fermi level. This reference state must be uniquely determined from the number of particles in the system and therefore nondegenerate with other Slater determinants,

$$|\Phi_0\rangle = \left\{ \prod_i^A \hat{a}_i^\dagger \right\} |0\rangle. \quad (2.12)$$

This reference determinant defines a new *Fermi vacuum*. States above the Fermi vacuum are called *particle* states and will be denoted with the indices a, b, c, d, \dots while states below the Fermi vacuum are called *hole* states and will be denoted with the indices i, j, k, l, \dots . Generic states above or below the Fermi vacuum will be denoted with the indices p, q, r, s, \dots .

Any other Slater determinant can be constructed relative to this reference state by adding particles and/or removing holes. A Slater determinant with A particles added and B holes

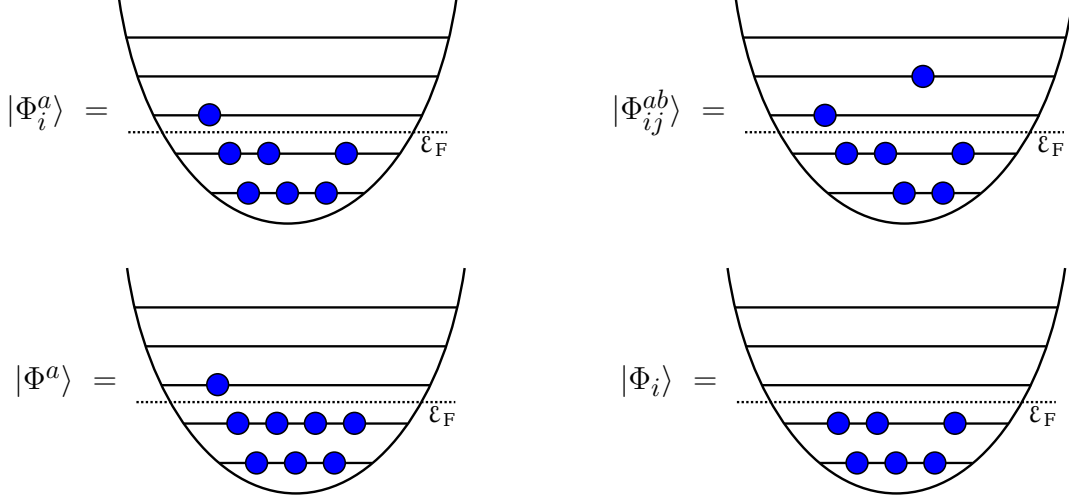


Figure 2.2: A depiction of $1p-1h$, $2p-2h$, $1p-0h$, and $0p-1h$ Slater determinants defined relative to the reference state in the independent particle model.

removed from reference state is known as a $Ap-Bh$ excitation.

$$\begin{aligned}
 |\Phi_i^a\rangle &\equiv \hat{a}_a^\dagger \hat{a}_i |\Phi\rangle \\
 |\Phi_{ij}^{ab}\rangle &\equiv \hat{a}_a^\dagger \hat{a}_b^\dagger \hat{a}_j \hat{a}_i |\Phi\rangle \\
 |\Phi^a\rangle &\equiv \hat{a}_a^\dagger |\Phi\rangle \\
 |\Phi_i\rangle &\equiv \hat{a}_i |\Phi\rangle
 \end{aligned} \tag{2.13}$$

Using these definitions, hole-creation and particle-annihilation operators vanish when acting on the Fermi vacuum from the left, $\hat{a}_i^\dagger |\Phi_0\rangle = \hat{a}_a |\Phi_0\rangle = 0$. Conversely, hole-annihilation and particle-creation operators vanish when acting on the Fermi vacuum from the right, $\langle \Phi_0 | \hat{a}_i = \langle \Phi_0 | \hat{a}_a^\dagger = 0$.

These results can be exploited to simplify expressions involving strings of creation and annihilation operators by a procedure called *normal ordering* with respect to the Fermi vacuum. Denoted by $\{\cdots\}$, normal ordering permutes a string of creation and annihilation operators so that hole-annihilation and particle-creation operators are to the left of hole-

creation and particle-annihilation operators, which guarantees that normal ordered operators vanish on the Fermi vacuum, $\langle \Phi_0 | \{ \dots \} = 0$ and $\{ \dots \} | \Phi_0 \rangle = 0$.

$$\left\{ \hat{a}_j^\dagger \cdots \hat{a}_i \cdots \hat{a}_b \cdots \hat{a}_a^\dagger \right\} = (-1)^\sigma \hat{a}_i \cdots \hat{a}_a^\dagger \cdots \hat{a}_j^\dagger \cdots \hat{a}_b, \quad (2.14)$$

where σ is the number of two-state permutations required to do the normal ordering.

2.4 Wick's Theorem

At this point, the many-body problem has been reduced to computing long strings of creation and annihilation operators between the normal-ordered Hamiltonian and the correlated wave function using Eq. (2.8). Instead of using a brute-force approach by permuting over and over, a further simplification known as *Wick's theorem* [104] can be introduced. A Wick contraction of two operators with respect to the reference state is defined as

$$\overline{\hat{A}\hat{B}} = \hat{A}\hat{B} - \left\{ \hat{A}\hat{B} \right\}. \quad (2.15)$$

Which, given the definition in Eq. (2.14) and the anticommutation relations in Eq. (2.8), means that the only nonzero contractions are of the form,

$$\overline{\hat{a}_i^\dagger \hat{a}_j} = \delta_{ij} \quad \text{and} \quad \overline{\hat{a}_a \hat{a}_b^\dagger} = \delta_{ab}. \quad (2.16)$$

Because contracted operators simply represent a Kronecker delta, they can be removed from a normal ordered product by permuting the product σ times so that the contracted operators

are next to each other,

$$\{\hat{A} \cdots \overbrace{\hat{B} \cdots \hat{C}} \cdots \hat{D}\} = (-1)^\sigma \{\hat{A} \cdots \overbrace{\hat{B} \hat{C}} \cdots \hat{D}\} = (-1)^\sigma \overbrace{\hat{B} \hat{C}} \{\hat{A} \cdots \hat{D}\}. \quad (2.17)$$

These different definitions for operator manipulation come together to define the time-independent Wick's theorem, which reformulates a product of operators as the sum of its normal-ordered form and all possible contractions of its normal-ordered form.

$$\hat{A} \hat{B} \hat{C} \cdots = \left\{ \hat{A} \hat{B} \hat{C} \cdots \right\} + \sum_{\substack{\text{one-} \\ \text{contractions}}} \left\{ \overbrace{\hat{A} \hat{B} \hat{C} \cdots} \right\} + \sum_{\substack{\text{two-} \\ \text{contractions}}} \left\{ \overbrace{\overbrace{\hat{A} \hat{B} \hat{C} \cdots}} \right\} + \cdots + \sum_{\substack{\text{all-} \\ \text{contractions}}} \left\{ \overbrace{\overbrace{\overbrace{\hat{A} \hat{B} \hat{C} \cdots}}} \right\} \quad (2.18)$$

Wick's theorem is incredibly useful in many-body techniques because complicated expressions of operators can be expressed as diagrams that are easy to compute with simple diagrammatic rules which correspond to Eqs. (2.8), (2.16), and (2.17). These diagrammatic techniques are an integral component to deriving expressions used in this work, and their underlying rules are summarized in C and are extensively discussed in [82].

A powerful application of Wick's theorem is to rewrite the Hamiltonian in normal-ordered form.

$$\hat{H} = E_0 + \sum_{pq} f_q^p \left\{ \hat{a}_p^\dagger \hat{a}_q \right\} + \frac{1}{4} \sum_{pqrs} V_{rs}^{pq} \left\{ \hat{a}_p^\dagger \hat{a}_q^\dagger \hat{a}_s \hat{a}_r \right\} + \frac{1}{36} \sum_{pqrstu} W_{stu}^{pqr} \left\{ \hat{a}_p^\dagger \hat{a}_q^\dagger \hat{a}_r^\dagger \hat{a}_u \hat{a}_t \hat{a}_s \right\} + \cdots, \quad (2.19)$$

where the newly defined normal-ordered Hamiltonian terms are defined as,

$$\begin{aligned}
E_0 &= \text{diagram with a circle and an incoming line labeled } i \text{ meeting a dashed line with a cross} + \text{diagram with two circles and incoming lines } i, j \text{ meeting a dashed line} + \text{diagram with three circles and incoming lines } i, j, k \text{ meeting a dashed line} + \dots \\
&= \sum_i {}^{(1)}H_i^i + \frac{1}{2} \sum_{ij} {}^{(2)}H_{ij}^{ij} + \frac{1}{6} \sum_{ijk} {}^{(3)}H_{ijk}^{ijk} \dots
\end{aligned} \tag{2.20}$$

$$\begin{aligned}
\text{diagram with two vertices connected by a dashed line, each vertex having two incoming lines (p, q)} &= \text{diagram with two vertices connected by a dotted line, each vertex having two incoming lines (p, q)} + \text{diagram with two vertices connected by a dotted line, the right vertex having a self-loop labeled } i \text{ and two incoming lines (p, q)} + \text{diagram with two vertices connected by a dotted line, the right vertex having two self-loops labeled } i, j \text{ and two incoming lines (p, q)} + \dots \\
f_q^p &= {}^{(1)}H_q^p + \sum_i {}^{(2)}H_{qi}^{pi} + \frac{1}{2} \sum_{ij} {}^{(3)}H_{qij}^{pij} + \dots
\end{aligned} \tag{2.21}$$

$$\begin{aligned}
\text{diagram with two vertices connected by a dashed line, each vertex having two incoming lines (p, r) and (q, s)} &= \text{diagram with two vertices connected by a dotted line, each vertex having two incoming lines (p, r) and (q, s)} + \text{diagram with two vertices connected by a dotted line, the right vertex having a self-loop labeled } i \text{ and two incoming lines (p, r) and (q, s)} + \dots \\
V_{rs}^{pq} &= {}^{(2)}H_{rs}^{pq} + \sum_i {}^{(3)}H_{rsi}^{pqi} + \dots
\end{aligned} \tag{2.22}$$

$$\begin{aligned}
\text{diagram with two vertices connected by a dashed line, each vertex having two incoming lines (p, s) and (q, t) and (r, u)} &= \text{diagram with two vertices connected by a dotted line, each vertex having two incoming lines (p, s) and (q, t) and (r, u)} + \dots \\
W_{stu}^{pqr} &= {}^{(3)}H_{stu}^{pqr} + \dots
\end{aligned} \tag{2.23}$$

This has the effect of shuffling higher-order interactions into lower-order terms, and makes it feasible to include computationally expensive many-body interactions as normal-ordered few-body interactions. Also, it reorganizes many-body correlations into the reference state so that additional correlations around the Fermi surface can be treated as a perturbation. Therefore, from this point forward, the many-body problem will be formulated in terms of the normal-ordered Hamiltonian, and the bare interactions will be truncated beyond the three-body level for computational feasibility. Electronic systems are naturally truncated at the two-body Coulomb force, while nuclear systems can be successfully described with the two-body normal-ordered piece of the three-body force.

In this form, the Hamiltonian is written as a sum of the *reference energy*, E_0 , which is the fully-contracted expectation value of the Hamiltonian with respect to the reference state,

$$E_0 = \langle \Phi | \hat{H} | \Phi \rangle, \quad (2.24)$$

and the remaining normal-ordered pieces of the Hamiltonian, \hat{H}_N . Rewriting the many-body Schrödinger equation for the ground state, $|\Psi\rangle$, and using this partition gives,

$$\begin{aligned} \hat{H}|\Psi\rangle &= (E_0 + \hat{H}_N)|\Psi\rangle = E|\Psi\rangle \\ \longrightarrow \hat{H}_N|\Psi\rangle &= (E - E_0)|\Psi\rangle = \Delta E|\Psi\rangle, \end{aligned} \quad (2.25)$$

where ΔE is known as the *correlation energy*.

Now that the many-body quantum problem has been formulated, different approaches to solving that problem can be proposed and analyzed. Because taking account of correlations from all particles simultaneously is a demanding—and for some systems, computationally impossible—endeavor, methods for solving the many-body Schrödinger equation should be

systematically improvable. Successful methods with this quality incorporate the most dominant correlations in lower-order solutions and approach the exact solution when more and more orders are included.

2.5 Hartree–Fock Method

A successful, first-order approximation to any many-body method comes from noticing that each individual particle feels a mean-field potential from the cumulative interactions with all the other particles. The *Hartree-Fock* (HF) method [47, 38] aims to transform the original single-particle basis to a Hartree-Fock basis where each orbital is the eigenfunction of its corresponding mean-field. Because the transformation of a single orbital changes its effect on every other particle, this process must be performed iteratively until self-consistency between all the orbitals is reached, which is why this method is also known as the *Self-Consistent Field* (SCF) method.

This mean-field picture results from the following procedure. It begins by minimizing the reference energy with respect to the reference state. This functional is just the zero-body piece of the normal-ordered Hamiltonian,

$$E_{\text{HF}}[\Phi_0] = \langle \Phi_0 | \hat{H} | \Phi_0 \rangle = \sum_i {}^{(1)}H_i^i + \frac{1}{2} \sum_{ij} {}^{(2)}H_{ij}^{ij} + \frac{1}{6} \sum_{ijk} {}^{(3)}H_{ijk}^{ijk}. \quad (2.26)$$

Transforming the reference determinant can be accomplished by rotating the state within the single-particle basis by use of the *Thouless theorem* [93], which states that any Slater determinant can be written as the product of any other Slater determinant and an exponentiated

single-excitation operator,

$$|\Phi'\rangle = e^{\hat{C}_1} |\Phi_0\rangle, \quad \text{where } \hat{C}_1 = \sum_{ai} C_i^a \{ \hat{a}_a^\dagger \hat{a}_i \}. \quad (2.27)$$

If the difference between the two Slater determinants is dominated by single excitations, this transformation can be approximated by expanding the exponential and ignoring higher-order terms,

$$|\Phi'\rangle \simeq \left(1 + \sum_{ai} C_i^a \{ \hat{a}_a^\dagger \hat{a}_i \} \right) |\Phi_0\rangle. \quad (2.28)$$

The reference energy functional can now be written as a sum of the original reference state and new terms that incorporate the single-excitation variation,

$$E_{\text{HF}} [\Phi'] = \langle \Phi' | \hat{H} | \Phi' \rangle \simeq E_{\text{HF}} [\Phi_0] + \sum_{ai} C_i^a \langle \Phi_0 | \hat{H} | \Phi_i^a \rangle + \sum_{ai} C_i^{a*} \langle \Phi_i^a | \hat{H} | \Phi_0 \rangle. \quad (2.29)$$

The minimum of this functional is found by differentiating the expression with respect to the coefficients C_i^a and setting the result to zero,

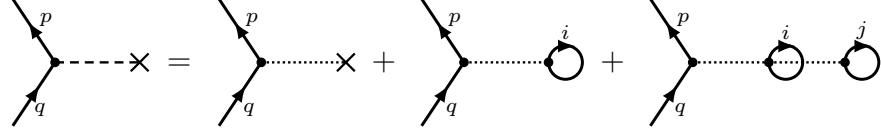
$$\delta E_{\text{HF}} [\Phi'] \simeq \sum_{ai} \delta C_i^a \langle \Phi_0 | \hat{H} | \Phi_i^a \rangle + \sum_{ai} \delta C_i^{a*} \langle \Phi_i^a | \hat{H} | \Phi_0 \rangle = 0 \quad (2.30)$$

Because this expression is Hermitian, both terms must vanish independently so that,

$$\langle \Phi_0 | \hat{H} | \Phi_i^a \rangle = \langle \Phi_i^a | \hat{H} | \Phi_0 \rangle = 0. \quad (2.31)$$

This condition is the result of the *Brillouin theorem* [15], which states that the Hamiltonian matrix element must vanish between an optimized Hartree-Fock ground state and any single excitation from it. The Brillouin condition is satisfied by diagonalizing the one-body piece

of the normal-ordered Hamiltonian f_q^p , known as the *Fock* operator, such that off-diagonal pieces like $\langle \Phi_0 | \hat{H} | \Phi_i^a \rangle = f_a^i$ and $\langle \Phi_i^a | \hat{H} | \Phi_0 \rangle = f_i^a$ vanish.



$$f_q^p = {}^{(1)}H_q^p + \sum_i {}^{(2)}H_{qi}^{pi} + \frac{1}{2} \sum_{ij} {}^{(3)}H_{qij}^{pij} \longrightarrow \varepsilon_q^p \delta_{pq}, \quad (2.32)$$

where ε_q^p is the eigenvalue of the Fock operator.

A practical way of solving this system of equations is to express each new orbital in the unknown Hatree-Fock basis, $|p'\rangle \equiv \phi_{p'}(\mathbf{r})$, denoted with primed labels, as a linear combination of the known single-particle basis states, $|p\rangle \equiv \phi_p(\mathbf{r})$, denoted without primed labels.

$$|p'\rangle = \sum_p \langle p | p' \rangle |p\rangle = \sum_p C_{p'}^p |p\rangle \quad (2.33)$$

Then the Fock matrix can be written in terms of the Hartree-Fock basis,

$$\begin{aligned} f_{q'}^{p'} &= {}^{(1)}H_{q'}^{p'} + \sum_{i'} {}^{(2)}H_{q'i'}^{p'i'} + \frac{1}{2} \sum_{i'j'} {}^{(3)}H_{q'i'j'}^{p'i'j'} \\ &= \sum_{pq} C_p^{p'*} {}^{(1)}H_q^p C_{q'}^q + \sum_{\substack{i' \\ prqs}} C_p^{p'*} C_r^{i'*} {}^{(2)}H_{qs}^{pr} C_{q'}^q C_{i'}^s + \frac{1}{2} \sum_{\substack{i'j' \\ prsqtu}} C_p^{p'*} C_r^{i'*} C_s^{j'*} {}^{(3)}H_{qtu}^{prs} C_{q'}^q C_{i'}^t C_{j'}^u. \end{aligned} \quad (2.34)$$

Defining the first-order density matrix γ_q^p as the product of expansion coefficients, summed over all shared hole states,

$$\gamma_q^p = \sum_{i'} C_{i'}^p C_q^{i'*}, \quad (2.35)$$

Eq. (2.5) is simplified to,

$$f_{q'}^{p'} = \sum_{pq} C_p^{p'*} \left[{}^{(1)}H_q^p + \sum_{rs} \gamma_s^r {}^{(2)}H_{qs}^{pr} + \frac{1}{2} \sum_{rstu} \gamma_t^r \gamma_u^s {}^{(3)}H_{qtu}^{prs} \right] C_{q'}^q \longrightarrow \varepsilon_{q'}^{p'} \delta_{p'q'}. \quad (2.36)$$

Therefore, the Hartree-Fock equations are ultimately expressed as an eigenvalue problem where the matrix to diagonalize is the Fock matrix in the form,

$$\hat{F}_q^p(\hat{C}) = {}^{(1)}H_q^p + \sum_{rs} \gamma_r^s {}^{(2)}H_{qs}^{pr} + \frac{1}{2} \sum_{rstu} \gamma_r^t \gamma_s^u {}^{(3)}H_{qtu}^{prs}, \quad (2.37)$$

and the matrix of coefficients, $\hat{C} = C_{p'}^p$, is the unitary operator that transforms the matrix to a diagonal form,

$$\sum_{pq} C_p^{p'*} \hat{F}_q^p(\hat{C}) C_{q'}^q = \varepsilon_{q'}^{p'} \delta_{p'q'} \quad (2.38)$$

The iterative nature of the solution comes from the dependence of the Fock matrix on the transformation coefficients. These Hartree-Fock equations are solved numerically by using an iterative algorithm where the Fock matrix is built using a known set of coefficients and diagonalized to obtain an updated set of coefficients. This process is repeated until the unitary set of coefficients is unchanged within a certain tolerance. For most calculations, using the identity matrix as an initial guess for the coefficients is sufficient. To improve the rate of convergence, techniques such as the direct inversion of the iterative subspace (DIIS) [77, 76] or Broyden's method [17] can be implemented. And, to avoid any oscillatory behavior around the solution, techniques such as the level-shifting method or *ad hoc* linear mixing can be implemented to dampen the large changes between iterations.

To make use of the HF solution as the reference state for post-HF calculations, the Hamiltonian matrix elements must be transformed to the new basis and the normal-ordered

version redefined to account for the additional reordering of one-particle correlations into the HF energy.

$$f_{q'}^{p'} = \varepsilon_{q'}^{p'} \delta_{p'q'} \quad (2.39)$$

$$V_{r's'}^{p'q'} = \sum_{pqrs} C_p^{p'*} C_q^{q'*} \left({}^{(2)}H_{rs}^{pq} + {}^{(3)}H_{rsu}^{pqt} \gamma_t^u \right) C_{r'}^r C_{s'}^s \quad (2.40)$$

$$\begin{aligned} E_0 &= \sum_{i'} {}^{(1)}H_{i'}^{i'} + \frac{1}{2} \sum_{i'j'} {}^{(2)}H_{i'j'}^{i'j'} + \frac{1}{6} \sum_{i'j'k'} {}^{(3)}H_{i'j'k'}^{i'j'k'} \\ &= \sum_{i'} \varepsilon_{i'}^{i'} - \frac{1}{2} \sum_{i'j'} V_{i'j'}^{i'j'} + \frac{1}{6} \sum_{i'j'k'} {}^{(3)}H_{i'j'k'}^{i'j'k'} \end{aligned} \quad (2.41)$$

Additionally, any operators that are constructed in the original basis must be transformed in a similar manner. For example, a one-body operator \hat{O} in the Hartree-Fock basis is,

$$\begin{aligned} \hat{O} &= \sum_{p'q'} O_{q'}^{p'} \left\{ \hat{a}_{p'}^\dagger \hat{a}_{q'} \right\} = \sum_{p'q'pq} C_p^{p'*} O_q^p C_{q'}^q \left\{ \hat{a}_{p'}^\dagger \hat{a}_{q'} \right\} \\ &\longrightarrow O_{q'}^{p'} = \sum_{pq} C_p^{p'*} O_q^p C_{q'}^q. \end{aligned} \quad (2.42)$$

Because the Hartree-Fock basis is diagonal in the one-body piece of the Hamiltonian, any terms that include off-diagonal elements automatically vanish, greatly simplifying any post-Hartree-Fock methods. From this point, any calculations will use the Hartree-Fock basis unless stated otherwise, and prime symbols will be omitted.

2.6 Configuration-Interaction

The most generic way to write a correlated wave function in a given basis is as a linear combination of all possible Slater determinants. In normal-ordered form, this expansion

can, in principle, consist of the $0p$ - $0h$ reference state and all possible Np - Nh excitations up to Ap - Ah excitations,

$$|\Psi_\nu\rangle = \sum_{\nu_i}^{\mathcal{N}} C_{\nu_i} |\Phi_{\nu_i}\rangle = C_0 |\Phi_0\rangle + \sum_{N=1}^A \left(\frac{1}{N!}\right)^2 \sum_{\substack{a_1 \dots a_N \\ i_1 \dots i_N}} C_{i_1 \dots i_N}^{a_1 \dots a_N} |\Phi_{i_1 \dots i_N}^{a_1 \dots a_N}\rangle. \quad (2.43)$$

Using this form of the wave function in Eq. (2.43), the Schrödinger equation can be reformulated as a standard matrix eigenvalue problem,

$$\begin{aligned} \hat{H}_N |\Psi_\nu\rangle &= \Delta E_\nu |\Psi_\nu\rangle \quad \longrightarrow \quad \langle \Psi_\mu | \hat{H}_N | \Psi_\nu \rangle = \Delta E_\nu \langle \Psi_\mu | \Psi_\nu \rangle \\ &= \sum_{\mu_i \nu_i} C_{\mu_i}^* \langle \Phi_{\mu_i} | \hat{H}_N | \Phi_{\nu_i} \rangle C_{\nu_i} = \Delta E_\nu \sum_{\mu_i \nu_i} C_{\mu_i}^* C_{\nu_i} \delta_{\mu_i \nu_i} \\ &\longrightarrow \mathbf{C}_\mu^T \left(\langle \Phi_{\mu_i} | \hat{H}_N | \Phi_{\nu_i} \rangle - \Delta E_\nu \mathbf{I} \right) \mathbf{C}_\nu = 0. \end{aligned} \quad (2.44)$$

In this case, the matrix elements are Hamiltonian terms that connect two Slater determinants, and the eigenvectors are the ground and excited states in the form of Eq. (2.43). The matrix elements can be found with the help of the Slater-Condon rules [85, 29] which, because the Hamiltonian is restricted to one- and two-body terms, require that any terms connecting Slater determinants which differ by more than two single-particle states vanish. Also, because the one-body Hamiltonian is diagonal in the Hatree-Fock basis, it only contributes to diagonal elements the CI matrix. Some examples of these matrix elements

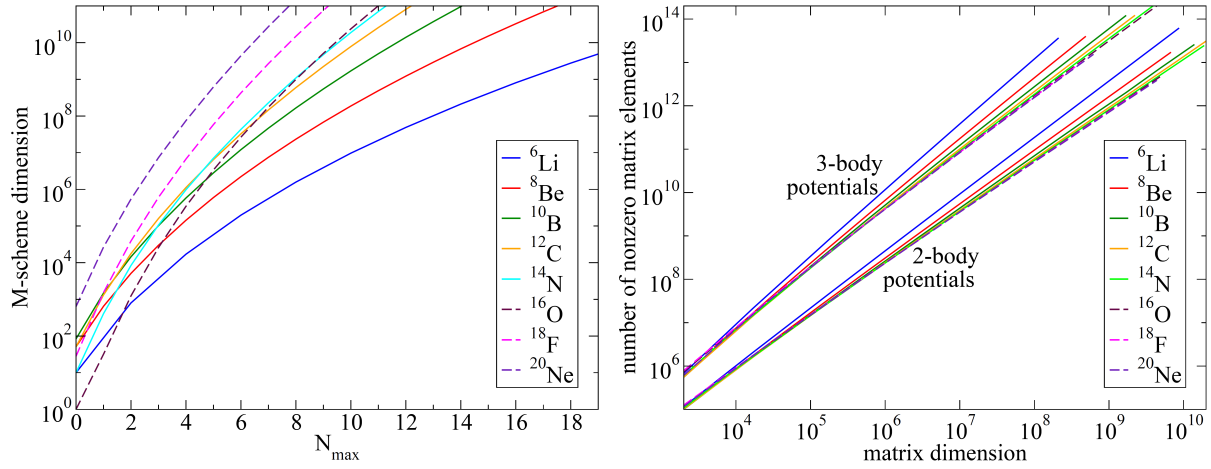


Figure 2.3: Scaling of the matrix size and number of non-zero matrix elements for nuclear CI calculations of light nuclei. Even for modest N_{\max} , the memory requirements approach the limit of petascale supercomputers (10^{10}). Figure taken from [81].

are,

$$\langle \Phi_i^a | \hat{H} | \Phi_i^a \rangle = \varepsilon_a - \varepsilon_i - V_{ia}^{ia} \quad (2.45)$$

$$\langle \Phi_{ij}^{ab} | \hat{H} | \Phi_{ij}^{cd} \rangle = V_{cd}^{ab} \quad (2.46)$$

$$\langle \Phi_{ijk}^{abc} | \hat{H} | \Phi_{ijl}^{abd} \rangle = -V_{kd}^{lc} \quad (2.47)$$

Because the configuration-interaction method exhaustively captures all the correlations of a many-body system, it is considered an “exact” method within a certain model space and becomes truly exact as the number of single-particle states is increased to infinity. However, there is a price to pay for this exactness. The number of Slater determinants, \mathcal{N} , in model space scales factorially according to Eq. (2.5) and the configuration-interaction matrix scales as \mathcal{N}^2 . For sufficiently-sized model spaces, the memory required for this matrix quickly becomes unmanigable even for the largest supercomputers.

However, for a reference state that is a good approximation to the true ground state, few-body excitations generally dominate the wave functions for low-lying states [83]. This

can be exploited by truncating the expansion in Eq. (2.43). Owing to the two-body nature of the interaction, the lowest appropriate truncation is also at the two-body level, known as configuration interaction with singles and doubles (CISD),

$$|\Psi_\nu\rangle = C_0|\Phi_0\rangle + \sum_{ai} C_i^a |\Phi_i^a\rangle + \frac{1}{4} \sum_{abij} C_{ij}^{ab} |\Phi_{ij}^{ab}\rangle. \quad (2.48)$$

This is a very straightforward and tractable way to approximate the many-body Schrödinger equation, and it can be systematically improved by adding more excitations such as triples (CISDT) or triples and quadruples (CISDTQ). But the drawback to this simplicity is that any truncated CI method is not size-extensive such that any extensive property of a system, like the energy, would scale with the size of the system. A desirable many-body method will be both systematically improvable and size-extensive while maintaining computational feasibility.

2.7 Many-Body Perturbation Theory

One many-body method that is both size-extensive and systematically improvable treats particle-particle interactions as a perturbation to the mean-field potential and is known as many-body perturbation theory (MBPT) [67, 53, 54, 82]. The Hamiltonian is partitioned into a diagonal piece and the interaction piece,

$$\begin{aligned} \hat{H} &= \hat{H}_0 + \hat{V}, \quad \text{with} \\ \hat{H}_0 &= E_0 + \sum_p f_p^p \left\{ \hat{a}_p^\dagger \hat{a}_p \right\} \quad \text{and} \\ \hat{V} &= \frac{1}{4} \sum_{pqrs} V_{rs}^{pq} \left\{ \hat{a}_p^\dagger \hat{a}_q^\dagger \hat{a}_s \hat{a}_r \right\} \end{aligned} \quad (2.49)$$

When not in the Hartree-Fock basis, the interaction piece has the additional off-diagonal Fock term, $\sum_{p \neq q} f_q^p \{ \hat{a}_p^\dagger \hat{a}_q \}$. This means that the reference state is an eigenstate of the zero-order piece of the Hamiltonian,

$$\hat{H}_0 |\Phi_0\rangle = \left(E_0 + \sum_i f_i^i \{ \hat{a}_i^\dagger \hat{a}_i \} \right) |\Phi_0\rangle = \left(E_0 + \sum_i \varepsilon_i \right) |\Phi_0\rangle = E_0^{(0)} |\Phi_0\rangle \quad (2.50)$$

.

Using *intermediate normalization*, which sets $\langle \Phi_0 | \Psi \rangle = 1$, the Schrödinger equation, Eq. (2.1) for the ground state, becomes,

$$\begin{aligned} \langle \Phi_0 | (\hat{H}_0 + \hat{V}) | \Psi \rangle &= \langle \Phi_0 | \hat{H}_0 | \Psi \rangle + \langle \Phi_0 | \hat{V} | \Psi \rangle = E \langle \Phi | \Psi \rangle \\ &= E^{(0)} \langle \Phi | \Psi \rangle + \langle \Phi_0 | \hat{V} | \Psi \rangle = E^{(0)} + \langle \Phi_0 | \hat{V} | \Psi \rangle = E. \end{aligned} \quad (2.51)$$

Next, the projection operators \hat{P} and \hat{Q} can be introduced,

$$\hat{P} = |\Phi_0\rangle \langle \Phi_0|, \quad (2.52)$$

$$\hat{Q} = \sum_{n \neq 0} |\Phi_n\rangle \langle \Phi_n| = 1 - |\Phi_0\rangle \langle \Phi_0|. \quad (2.53)$$

The \hat{P} operator isolates the reference-state component of any Slater determinant while the \hat{Q} operator isolates all components *except* the reference-state component out of any Slater determinant. Both these operators are idempotent, which means that $\hat{P}^2 = \hat{P}$ and $\hat{Q}^2 = \hat{Q}$, and because of intermediate normalization, the correlated wave function can be written as $|\Psi\rangle = (\hat{P} + \hat{Q})|\Psi\rangle = |\Phi\rangle + \hat{Q}|\Psi\rangle$. Also, both operators commute with the unperturbed part of the Hamiltonian, $\hat{H}_0 \hat{P} = \hat{P} \hat{H}_0$ and $\hat{H}_0 \hat{Q} = \hat{Q} \hat{H}_0$. These identities can be applied to an alternate version of the Schrödinger equation which defines a particular version of perturba-

tion theory known as Raleigh-Schrödinger perturbation theory (RSPT). In this version, the zeroth-order energy $E^{(0)}$ is added to both sides of the Schrödinger equation. Acting with \hat{Q} and rearranging terms gives,

$$\begin{aligned}\hat{Q}(E^{(0)} - \hat{H}_0)|\Psi\rangle &= \hat{Q}(E^{(0)} + \hat{V} - E)|\Psi\rangle \\ \hat{Q}(E^{(0)} - \hat{H}_0)\hat{Q}|\Psi\rangle &= \hat{Q}(\hat{V} - \Delta E_0)|\Psi\rangle,\end{aligned}\tag{2.54}$$

where $\Delta E_0 \equiv E - E^{(0)} = \langle \Phi_0 | \hat{V} | \Psi \rangle$. The operator $\hat{Q}(E^{(0)} - \hat{H}_0)\hat{Q}$ is invertible because $(E^{(0)} - \hat{H}_0)^{-1}$ is never singular in Q -space. Therefore, the operator $\hat{R}_0 = \hat{Q}(E^{(0)} - \hat{H}_0)^{-1}\hat{Q}$, known as the *resolvent*, can be applied to both sides to result in the generating equation for RSPT,

$$\begin{aligned}\hat{Q}(E^{(0)} - \hat{H}_0)^{-1}(E^{(0)} - \hat{H}_0)\hat{Q}|\Psi\rangle &= \hat{Q}(E^{(0)} - \hat{H}_0)^{-1}\hat{Q}(\hat{V} - \Delta E_0)|\Psi\rangle \\ \hat{Q}|\Psi\rangle &= \hat{R}_0(\hat{V} - \Delta E_0)|\Psi\rangle \\ |\Psi\rangle &= |\Phi\rangle + \hat{R}_0(\hat{V} - \Delta E_0)|\Psi\rangle\end{aligned}\tag{2.55}$$

This equation can be iterated infinitely to give the solution for the fully correlated wave function which can, in turn, be used to solve for the energy with Eq. (2.51),

$$|\Psi\rangle = \sum_{n=0}^{\infty} \left[\hat{R}_0(\hat{V} - \Delta E_0) \right]^n |\Phi_0\rangle,\tag{2.56}$$

$$\Delta E_0 = \langle \Phi_0 | \hat{V} | \Psi \rangle = \sum_{n=0}^{\infty} \langle \Phi_0 | \hat{V} \left[\hat{R}_0(\hat{V} - \Delta E_0) \right]^n |\Phi_0\rangle\tag{2.57}$$

The immediate problem with this equation is that the right-hand side of the equations contain the target energy difference ΔE_0 for which these equations are meant to solve. This

can be remedied by expanding the right-hand sides and rearranging terms. Using the fact that $\hat{R}_0 \Delta E_0 |\Phi_0\rangle = \Delta E_0 \hat{R}_0 |\Phi_0\rangle = 0$, the first-order energy $E^{(1)} = \langle \Phi_0 | \hat{V} | \Phi_0 \rangle$, and the shifted term $\tilde{V} \equiv \hat{V} - E^{(1)}$, these simplify to,

$$|\Psi\rangle - |\Phi_0\rangle = \hat{R}_0 \hat{V} |\Phi_0\rangle + \hat{R}_0 \tilde{V} \hat{R}_0 \hat{V} |\Phi_0\rangle + \hat{R}_0 \tilde{V} \hat{R}_0 \tilde{V} \hat{R}_0 \hat{V} |\Phi_0\rangle - \langle \Phi_0 | \hat{V} \hat{R}_0 \hat{V} | \Phi_0 \rangle \hat{R}_0^2 \hat{V} |\Phi_0\rangle + \dots \quad (2.58)$$

$$\Delta E_0 = \langle \Phi_0 | \hat{V} | \Phi_0 \rangle + \langle \Phi_0 | \hat{V} \hat{R}_0 \hat{V} | \Phi_0 \rangle + \langle \Phi_0 | \hat{V} \hat{R}_0 \tilde{V} \hat{R}_0 \hat{V} | \Phi_0 \rangle + \langle \Phi_0 | \hat{V} \hat{R}_0 \tilde{V} \hat{R}_0 \tilde{V} \hat{R}_0 \hat{V} | \Phi_0 \rangle - \langle \Phi_0 | \hat{V} \hat{R}_0 \hat{V} | \Phi_0 \rangle \langle \Phi_0 | \hat{V} \hat{R}_0^2 \hat{V} | \Phi_0 \rangle + \dots \quad (2.59)$$

The order of each term can be easily identified by counting the numbers of times that \hat{V} or \tilde{V} appears. At the third order in the wave function and the fourth order in the energy, *renormalization* terms make their first appearance. These terms contain separated and closed factors in the form of lower-order energy terms, such as $\langle \Phi_0 | \hat{V} \hat{R}_0 \hat{V} | \Phi_0 \rangle \equiv E^{(2)}$. Terms that do not contain normalization factors are known as *principle* terms.

A powerful application of diagrammatic techniques known as the *factorization theorem* [54, 39, 14] can immediately be used to simplify these expansions. By factoring sums of *disconnected* diagrams from the principle terms, where two or more parts of a diagram are not connected with any lines, it can be shown that they exactly cancel with the renormalization

terms at each order.

$$\begin{aligned}
& \frac{1}{16} \sum_{abcd} \frac{V_{ab}^{ij} V_{ij}^{ab} V_{cd}^{kl} V_{kl}^{cd}}{\varepsilon_{ij}^{ab} \varepsilon_{ijkl}^{abcd} \varepsilon_{kl}^{cd}} + \frac{1}{16} \sum_{abcd} \frac{V_{ab}^{ij} V_{ij}^{ab} V_{cd}^{kl} V_{kl}^{cd}}{\varepsilon_{ij}^{ab} \varepsilon_{ijkl}^{abcd} \varepsilon_{ij}^{ab}} = \frac{1}{16} \sum_{abcd} V_{ab}^{ij} V_{ij}^{ab} V_{cd}^{kl} V_{kl}^{cd} \frac{\varepsilon_{ij}^{ab} + \varepsilon_{kl}^{cd}}{(\varepsilon_{ij}^{ab})^2 \varepsilon_{ijkl}^{abcd} \varepsilon_{kl}^{cd}} \\
& = \frac{1}{4} \sum_{abij} \frac{V_{ab}^{ij} V_{ij}^{ab}}{(\varepsilon_{ij}^{ab})^2} \cdot \frac{1}{4} \sum_{cdkl} \frac{V_{cd}^{kl} V_{kl}^{cd}}{\varepsilon_{kl}^{cd}} = \langle \Psi_n^{(1)} | \Psi_n^{(1)} \rangle E_n^{(2)} \quad (2.60)
\end{aligned}$$

$$\begin{aligned}
& \frac{1}{16} \sum_{abcd} \frac{V_{ij}^{ab} V_{cd}^{kl} V_{kl}^{cd}}{\varepsilon_{kl}^{cd} \varepsilon_{ijkl}^{abcd} \varepsilon_{ij}^{ab}} |\Phi_{ij}^{ab}\rangle + \frac{1}{16} \sum_{abcd} \frac{V_{ij}^{ab} V_{cd}^{kl} V_{kl}^{cd}}{\varepsilon_{ij}^{ab} \varepsilon_{ijkl}^{abcd} \varepsilon_{ij}^{ab}} |\Phi_{ij}^{ab}\rangle = \frac{1}{16} \sum_{abcd} V_{ij}^{ab} V_{cd}^{kl} V_{kl}^{cd} \frac{\varepsilon_{ij}^{ab} + \varepsilon_{kl}^{cd}}{(\varepsilon_{ij}^{ab})^2 \varepsilon_{ijkl}^{abcd} \varepsilon_{kl}^{cd}} |\Phi_{ij}^{ab}\rangle \\
& = \frac{1}{4} \sum_{abij} \frac{V_{ij}^{ab}}{(\varepsilon_{ij}^{ab})^2} |\Phi_{ij}^{ab}\rangle \cdot \frac{1}{4} \sum_{cdkl} \frac{V_{cd}^{kl} V_{kl}^{cd}}{\varepsilon_{kl}^{cd}} = \frac{|\Psi_n^{(1)}\rangle}{\varepsilon_n} E_n^{(2)} \quad (2.61)
\end{aligned}$$

The factorization theorem is also valid with off-diagonal Fock terms and applies to the MBPT expansions of both the wave function and energy. Therefore, these can be written in terms of connected diagrams only,

$$|\Psi\rangle = \sum_{n=0}^{\infty} \left[\hat{R}_0 (\hat{V} - \Delta E_0) \right]^n |\Phi_0\rangle_C, \quad (2.62)$$

$$\Delta E_0 = \sum_{n=0}^{\infty} \langle \Phi_0 | \hat{V} \left[\hat{R}_0 (\hat{V} - \Delta E_0) \right]^n |\Phi_0\rangle_C, \quad (2.63)$$

where “C” denotes connected diagrams. This result not only simplifies the MBPT expressions, but it guarantees the size-extensivity of the MBPT wave function at each order. Also, it is a useful step towards coupled-cluster theory which reorganizes the connected diagrams from MBPT such that certain classes can be summed to infinite order.

Chapter 3

Coupled-Cluster Theory

Linked-cluster theorem,

$$|\Psi^{(1)}\rangle = \boxed{\text{diagram}} + \text{diagram} \quad (3.1)$$

$$\begin{aligned} |\Psi^{(2)}\rangle = & \text{diagram} + \text{diagram} + \boxed{\text{diagram}} + \boxed{\text{diagram}} \\ & + \boxed{\text{diagram}} + \boxed{\text{diagram}} + \boxed{\text{diagram}} + \boxed{\text{diagram}} + \boxed{\text{diagram}} \\ & + \boxed{\text{diagram}} + \boxed{\text{diagram}} + \text{diagram} + \text{diagram} + \text{diagram} \\ & + \text{diagram} + \text{diagram} + \text{diagram} + \text{diagram} + \text{diagram} \end{aligned} \quad (3.2)$$

Coupled cluster (CC) theory is based on expressing the N -particle correlated wave function $|\Psi\rangle$ using the exponential ansatz,

$$|\Psi\rangle = e^{\hat{T}} |\Phi_0\rangle,$$

where $|\Phi_0\rangle$ is the reference state as before. The cluster operator $\hat{T} \equiv \hat{T}_1 + \hat{T}_2 + \cdots + \hat{T}_N$, is

composed of k -particle k -hole excitation operators, \hat{T}_k ,

$$\hat{T}_k \equiv \left(\frac{1}{k!}\right)^2 \sum_{\substack{a_1 \dots a_k \\ i_1 \dots i_k}} t_{i_1 \dots i_k}^{a_1 \dots a_k} \left\{ \hat{a}_1^\dagger \dots \hat{a}_k^\dagger \hat{i}_k \dots \hat{i}_1 \right\}, \quad (3.3)$$

where the unknown matrix elements, $t_{i_1 \dots i_k}^{a_1 \dots a_k}$, are known as *cluster amplitudes* [82].

Using the CC ansatz, the Schrödinger equation,

$$\hat{H} e^{\hat{T}} |\Phi_0\rangle = E e^{\hat{T}} |\Phi_0\rangle, \quad (3.4)$$

can be rewritten by left-multiplying by $\langle \Phi_0 | e^{-\hat{T}}$ as,

$$\langle \Phi_0 | \bar{H} | \Phi_0 \rangle = E,$$

where we define a *coupled cluster effective Hamiltonian*,

$$\bar{H} \equiv e^{-\hat{T}} \hat{H} e^{\hat{T}}, \quad (3.5)$$

in which the wave operator, $e^{\hat{T}}$, acts as a similarity transform on the Hamiltonian in the same way that $\hat{U}(s)$ acts to transform the Hamiltonian in SRG methods. An important difference, however, is that the wave operator in CC, which contains no de-excitations, is not unitary, and thus \bar{H} is not Hermitian.

The effective Hamiltonian in Eq. (3.5) can be rewritten with commutators according to the Baker–Campbell–Hausdorff expansion as,

$$\bar{H} = \hat{H} + [\hat{H}, \hat{T}] + \frac{1}{2!} [[\hat{H}, \hat{T}], \hat{T}] + \frac{1}{3!} [[[\hat{H}, \hat{T}], \hat{T}], \hat{T}] + \frac{1}{4!} [[[[\hat{H}, \hat{T}], \hat{T}], \hat{T}], \hat{T}],$$

which terminates at four-nested commutators due to the two-body nature of the interaction. Like with IM-SRG, this commutator expression ensures that CC is size-extensive and contains only connected terms. In addition, because \hat{T} is an excitation operator, terms of the form $\hat{T}\hat{H}$ are disconnected and thus vanish [82]. Therefore the CC effective Hamiltonian can be further reduced to

$$\bar{H} = \left(\hat{H} e^{\hat{T}} \right)_c, \quad (3.6)$$

where the subscript “c” indicates that only connected terms are used.

In practice, the cluster operator \hat{T} must be truncated for calculations to be computationally feasible. In this work, we use only single and double excitations,

$$\hat{T} = \hat{T}_1 + \hat{T}_2.$$

This is known as coupled cluster with singles and doubles (CCSD), with an asymptotic computational cost that scales like IM-SRG(2). This truncation has been successfully applied to many problems in quantum chemistry [6] and nuclear physics [43]. In addition, we also truncate the three-body effective Hamiltonian terms that are induced by the similarity transformation. Fig. 3.1 shows the diagrammatic representation of Eq. (3.6) in CCSD.

The unknown cluster amplitudes in CCSD, t_i^a and t_{ij}^{ab} , are calculated by left-multiplying Eq. (3.4) by $\langle \Phi_i^a | e^{-\hat{T}}$ and $\langle \Phi_{ij}^{ab} | e^{-\hat{T}}$, respectively,

$$\langle \Phi_i^a | \bar{H} | \Phi_0 \rangle = 0, \quad (3.7)$$

$$\langle \Phi_{ij}^{ab} | \bar{H} | \Phi_0 \rangle = 0.$$

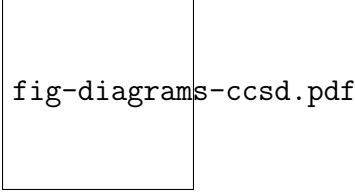


Figure 3.1: (Color online) Diagrammatic representation of \bar{H} of Eq. (3.6), excluding terms involving the one-body interaction \hat{H}_1 and first-order terms involving only the bare Hamiltonian. Open circles represent the excitation cluster operators \hat{T}_1 and \hat{T}_2 , and filled circles represent the two-body interaction \hat{H}_2 . As before, the diagrams are implicitly antisymmetrized (Hugenholtz diagrams). Lines connected to \hat{T} are always directed upward because they represent an excitation operator while the directions of external lines connected to \hat{H}_2 are unconstrained.

After the Fock matrix has been diagonalized, the diagonal components of Eq. (3.7) can be separated and, after expanding the exponent in Eq. (3.6), the non-vanishing terms of the CCSD amplitude equations become,

$$\begin{aligned} \langle \Phi_i^a | \left[\hat{H}_2 \left(\hat{T}_1 + \hat{T}_2 + \hat{T}_1 \hat{T}_2 + \frac{1}{2!} \hat{T}_1^2 + \frac{1}{3!} \hat{T}_1^3 \right) \right]_c | \Phi_0 \rangle &= \varepsilon_i^a t_i^a \\ \langle \Phi_{ij}^{ab} | \left[\hat{H}_2 \left(1 + \hat{T}_1 + \hat{T}_2 + \frac{1}{2} \hat{T}_1^2 + \hat{T}_1 \hat{T}_2 + \frac{1}{2!} \hat{T}_2^2 + \frac{1}{3!} \hat{T}_1^3 + \frac{1}{2!} \hat{T}_1^2 \hat{T}_2 + \frac{1}{4!} \hat{T}_1^4 \right) \right]_c | \Phi_0 \rangle &= \varepsilon_{ij}^{ab} t_{ij}^{ab} \end{aligned} \quad (3.8)$$

where ε are the Møller–Plesset denominators from Eq. (??). As usual, these non-linear equations are solved using an iterative procedure where the cluster amplitudes on the right-hand side of Eq. (3.8) are updated by calculating the terms on the left-hand side until a fixed point is reached. Like the HF iterative procedure, employing convergence acceleration techniques can reduce the number of CC iterations required.

$$E(\hat{T}, \hat{L}) = \langle \Phi_0 | \hat{L} e^{-\hat{T}} \hat{H} e^{\hat{T}} | \Phi_0 \rangle = \langle \Phi_0 | \hat{L} \bar{H} | \Phi_0 \rangle \quad (3.9)$$

$$\hat{L} \equiv \lambda_0 + \hat{L}_1 + \hat{L}_2 + \cdots + \hat{L}_N \quad (3.10)$$

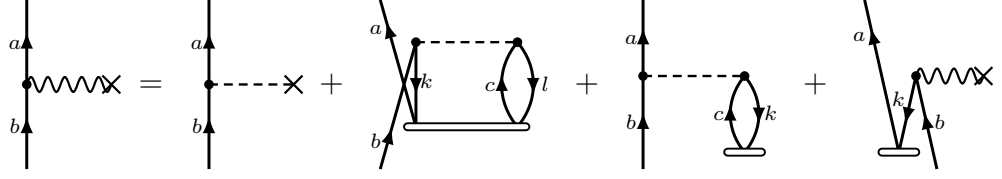
$$\hat{L}_k \equiv \left(\frac{1}{k!}\right)^2 \sum_{\substack{a_1 \dots a_k \\ i_1 \dots i_k}} \lambda_{a_1 \dots a_k}^{i_1 \dots i_k} \left\{ \hat{i}_1^\dagger \dots \hat{i}_k^\dagger \hat{a}_k \dots \hat{a}_1 \right\}, \quad (3.11)$$

$$\begin{aligned} \langle \Phi_0 | \hat{L} \left[\bar{H}, \left\{ \hat{a}^\dagger \hat{i} \right\} \right] | \Phi_0 \rangle &= 0, \\ \langle \Phi_0 | \hat{L} \left[\bar{H}, \left\{ \hat{a}^\dagger \hat{b}^\dagger \hat{j} \hat{i} \right\} \right] | \Phi_0 \rangle &= 0. \end{aligned} \quad (3.12)$$

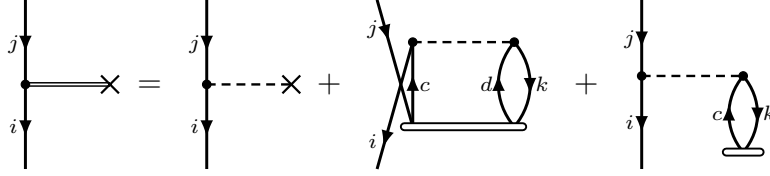
$$\begin{aligned} \langle \Phi_0 | \hat{L} \bar{H} | \Phi_i^a \rangle &= \omega \langle \Phi_0 | \hat{L} | \Phi_i^a \rangle, \\ \langle \Phi_0 | \hat{L} \bar{H} | \Phi_{ij}^{ab} \rangle &= \omega \langle \Phi_0 | \hat{L} | \Phi_{ij}^{ab} \rangle. \end{aligned} \quad (3.13)$$

$$\begin{aligned} \Delta E_{CCSD} &= \text{diagram 1} + \text{diagram 2} + \boxed{\text{diagram 3} \times} \\ &= \frac{1}{4} \sum_{klcd} V_{cd}^{kl} t_{kl}^{cd} + \frac{1}{2} \sum_{klcd} V_{cd}^{kl} t_k^c t_l^d + \boxed{\sum_{kc} f_c^k t_k^c} \end{aligned} \quad (3.14)$$

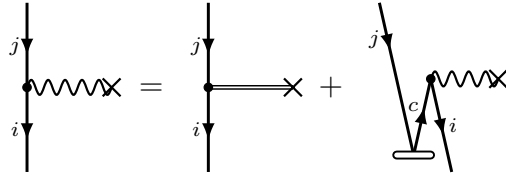
$$\begin{aligned} \text{diagram 4} &= \boxed{\text{diagram 5} \times} + \text{diagram 6} \\ X_a^i &= \boxed{f_a^i} + \sum_{kc} V_{ac}^{ik} t_k^c \end{aligned} \quad (3.15)$$



$$X_b^a = f_b^a - \frac{1}{2} \sum_{klc} V_{bc}^{kl} t_{kl}^{ac} + \sum_{kc} V_{cb}^{ka} t_k^c - \sum_k X_b^k t_k^a \quad (3.16)$$



$$X_j^i = f_j^i + \frac{1}{2} \sum_{kcd} V_{cd}^{ik} t_{jk}^{cd} + \sum_{kc} V_{jc}^{ik} t_k^c \quad (3.17)$$



$$X_j^i = X_j^i + \sum_c X_c^i t_j^c \quad (3.18)$$

$$\begin{aligned}
X_i^a = 0 = & \boxed{f_i^a} + \sum_c X_c^a t_i^c - \sum_k X_i'^k t_k^a + \sum_{kc} V_{ci}^{ka} t_k^c \\
& + \frac{1}{2} \sum_{kcd} V_{cd}^{ka} t_{ki}^{cd} - \frac{1}{2} \sum_{klc} V_{ic}^{kl} t_{kl}^{ac} + \sum_{kc} X_c^k t_{ik}^{ac}
\end{aligned} \tag{3.19}$$

$$X_{bc}^{ia} = V_{bc}^{ia} - \frac{1}{2} \sum_k V_{bc}^{ik} t_k^a \tag{3.20}$$

$$X_{bc}^{ia} = V_{bc}^{ia} - \sum_k V_{bc}^{ik} t_k^a \tag{3.21}$$

Diagrammatic equation (3.22): A double line exchange between two vertices (left) is equal to a dashed line exchange (middle) plus a term with a coefficient $\frac{1}{2}$ multiplied by a diagram with a loop and a single line exchange (right).

$$X_{ka}^{ij} = V_{ka}^{ij} + \frac{1}{2} \sum_c V_{ca}^{ij} t_k^c \quad (3.22)$$

Diagrammatic equation (3.23): A wavy line exchange between two vertices (left) is equal to a dashed line exchange (middle) plus a term with a coefficient 1 multiplied by a diagram with a loop and a single line exchange (right).

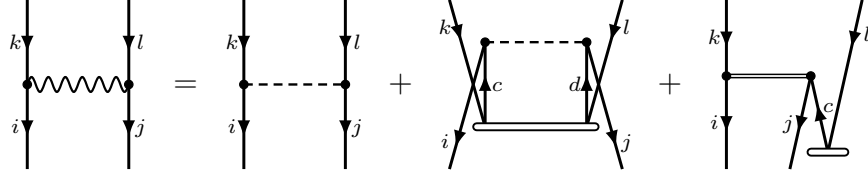
$$X_{ka}^{ij} = V_{ka}^{ij} + \sum_c V_{ca}^{ij} t_k^c \quad (3.23)$$

Diagrammatic equation (3.24): A double line exchange between two vertices (left) is equal to a dashed line exchange (middle) plus a term with a coefficient 1 multiplied by a diagram with a loop and a double line exchange (right).

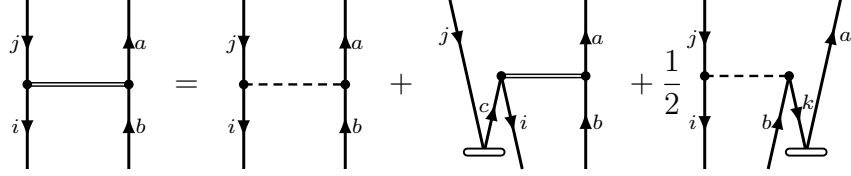
$$X_{cd}^{ab} = V_{cd}^{ab} - \hat{P}(ab) \sum_k X_{cd}^{kb} t_k^a \quad (3.24)$$

Diagrammatic equation (3.25): A wavy line exchange between two vertices (left) is equal to a double line exchange (middle) plus a term with a coefficient $\frac{1}{2}$ multiplied by a diagram with a loop and a double line exchange (right).

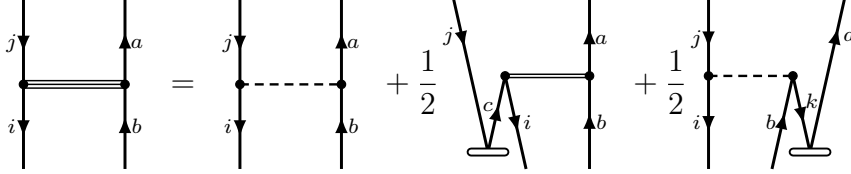
$$X_{cd}^{ab} = X_{cd}^{ab} + \frac{1}{2} \sum_{kl} V_{cd}^{kl} t_{kl}^{ab} \quad (3.25)$$



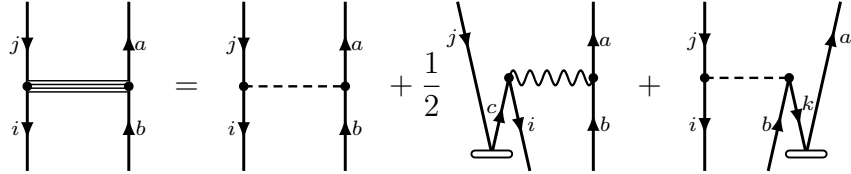
$$X_{kl}^{ij} = V_{kl}^{ij} + \frac{1}{2} \sum_{cd} V_{cd}^{ij} t_{kl}^{cd} + \hat{P}(kl) \sum_c X_{kc}^{ij} t_l^c \quad (3.26)$$



$$X_{jb}^{ia} = V_{jb}^{ia} + \sum_c X_{cb}^{ia} t_j^c - \frac{1}{2} \sum_k V_{jb}^{ik} t_k^a \quad (3.27)$$



$$X_{jb}^{ia} = V_{jb}^{ia} + \frac{1}{2} \sum_c X_{cb}^{ia} t_j^c - \frac{1}{2} \sum_k V_{jb}^{ik} t_k^a \quad (3.28)$$



$$X_{jb}^{ia} = V_{jb}^{ia} + \frac{1}{2} \sum_c X_{cb}^{ia} t_j^c - \sum_k V_{jb}^{ik} t_k^a \quad (3.29)$$

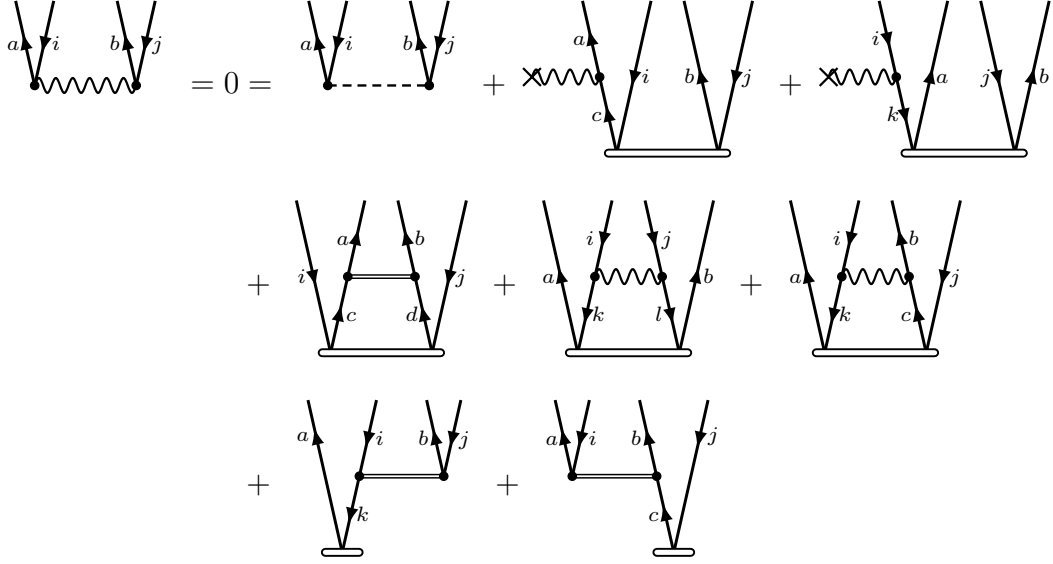
$$X_{jb}^{ia} = X_{jb}^{iia} - \left(\frac{1}{2}\right) \sum_{kc} V_{cb}^{ik} t_{jk}^{ca} + \frac{1}{2} \sum_c X_{cb}^{ia} t_j^c \quad (3.30)$$

$$X_{ic}^{ab} = V_{ic}^{ab} + \frac{1}{2} \sum_d V_{dc}^{ab} t_i^d - \hat{P}(ab) \sum_k X_{ic}^{kb} t_k^a \quad (3.31)$$

$$X_{ic}^{ab} = V_{ic}^{ab} + \sum_d V_{dc}^{ab} t_i^d - \hat{P}(ab) \sum_k X_{ic}^{kb} t_k^a - \sum_k X_c^k t_{ik}^{ab} + \hat{P}(ab) \sum_{kd} X_{dc}^{kb} t_{ik}^{ad} + \frac{1}{2} \sum_{kl} X_{ic}^{kl} t_{kl}^{ab} \quad (3.32)$$

$$X_{jk}^{ia} = V_{jk}^{ia} - \frac{1}{2} \sum_l V_{jk}^{il} t_l^a \quad (3.33)$$

$$\begin{aligned} X_{jk}^{ia} = & V_{jk}^{ia} - \sum_l V_{jk}^{il} t_l^a + \hat{P}(jk) \sum_c X_{jc}^{ia} t_c^k \\ & + \hat{P}(jk) \sum_{lc} X_{jc}^{il} t_{lk}^{ca} + \frac{1}{2} \sum_{cd} X_{cd}^{ia} t_{jk}^{cd} + \sum_c X_c^i t_{jk}^{ca} \end{aligned} \quad (3.34)$$



$$\begin{aligned}
X_{ij}^{ab} = 0 &= V_{ij}^{ab} + \hat{P}(ab) \sum_c X_c^a t_{ij}^{cb} - \hat{P}(ij) \sum_k X_i^k t_{kj}^{ab} \\
&+ \frac{1}{2} \sum_{cd} X_{cd}^{ab} t_{ij}^{cd} + \frac{1}{2} \sum_{kl} X_{ij}^{kl} t_{kl}^{ab} - \hat{P}(ab|ij) \sum_{kc} X_{ic}^{kb} t_{kj}^{ac} \\
&- \hat{P}(ab) \sum_k X_{ij}^{kb} t_k^a + \hat{P}(ij) \sum_c X_{ic}^{ab} t_j^c
\end{aligned} \tag{3.35}$$

$$\begin{aligned}
0 = & \text{Diagram 1} + \text{Diagram 2} + \text{Diagram 3} + \text{Diagram 4} + \text{Diagram 5} \\
& + \text{Diagram 6} + \text{Diagram 7} + \text{Diagram 8} \\
= & X_a^i + \sum_c \lambda_c^i X_a^c - \sum_k \lambda_a^k X_k^i + \sum_{kc} \lambda_c^k X_{ak}^{ic} + \frac{1}{2} \sum_{kcd} \lambda_{cd}^{ik} X_{ak}^{cd} \\
& - \frac{1}{2} \sum_{klc} \lambda_{ac}^{kl} X_{kl}^{ic} - \frac{1}{2} \sum_{jklcd} \lambda_{cd}^{jl} X_{aj}^{ik} t_{kl}^{cd} + \frac{1}{2} \sum_{klbcd} \lambda_{bc}^{kl} X_{ad}^{ic} t_{kl}^{bd}
\end{aligned} \tag{3.36}$$

$$\begin{aligned}
0 = & \text{Diagram 1} + \text{Diagram 2} + \text{Diagram 3} + \text{Diagram 4} \\
& + \text{Diagram 5} + \text{Diagram 6} + \text{Diagram 7} + \text{Diagram 8} \\
& + \text{Diagram 9} + \text{Diagram 10} + \text{Diagram 11} \\
= & V_{ab}^{ij} + \hat{P}(ab|ij) \lambda_a^i X_b^j - \hat{P}(ab) \sum_k \lambda_a^k X_{kb}^{ij} + \hat{P}(ij) \sum_c \lambda_c^i X_{ab}^{cj} \\
& + \hat{P}(ab) \sum_c \lambda_{ac}^{ij} X_b^c - \hat{P}(ij) \sum_k \lambda_{ab}^{ik} X_k^j + \frac{1}{2} \sum_{cd} \lambda_{cd}^{ij} X_{ab}^{cd} + \frac{1}{2} \sum_{kl} \lambda_{ab}^{kl} X_{kl}^{ij} \\
& - \hat{P}(ab|ij) \sum_{kc} \lambda_{ac}^{kj} X_{kb}^{ic} - \hat{P}(ab) \frac{1}{2} \sum_{klcd} \lambda_{ad}^{kl} V_{cb}^{ij} t_{kl}^{cd} - \hat{P}(ij) \frac{1}{2} \sum_{klcd} \lambda_{cd}^{il} V_{ab}^{kj} t_{kl}^{cd} \quad (3.37)
\end{aligned}$$

3.1 Connection to MBPT

The factorization theorem. (hughenoltz 1957, frantz and mills 1960, brandow 1967, 1977).

A sum over all the time orderings between a pair of disconnected diagrams is equal to the product of those two diagrams.

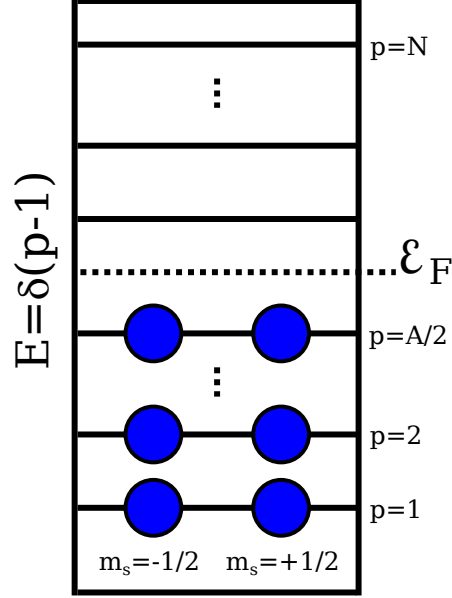


Figure 3.2: Correlation energy for the pairing model with exact diagonalization, MBPT2 and perturbation theory to third order MBPT3 for a range of interaction values. A canonical Hartree-Fock basis has been employed in all MBPT calculations.

3.2 Solving the Coupled Cluster Equations

3.3 Example: Pairing Model

It's beneficial to illustrate a simplified example of coupled cluster theory. For this purpose, we turn our attention to the simple pairing model. This pairing model will use a model space of N shells, each with two opposite spin orbitals. With a closed-shell reference states, the Hamiltonian is restricted to interact only between unbroken pairs, which can be written as,

$$^{(1)}\hat{H} = \delta \sum_{pm_p} (p-1) \hat{a}_{pm_p}^\dagger \hat{a}_{pm_p} \quad (3.38)$$

$$^{(2)}\hat{H} = -\frac{1}{2}g \sum_{pq} \hat{a}_{p+}^\dagger \hat{a}_{p-}^\dagger \hat{a}_{q-} \hat{a}_{q+} \quad (3.39)$$

Table 3.1: Single-particle states and their quantum numbers and their energies from Eq. (3.40). The degeneracy for every quantum number p is equal to 2 due to the two possible spin values.

State Label	p	$2s_z$	E	type
0	1	1	$-g/2$	hole
1	1	-1	$-g/2$	hole
2	2	1	$1-g/2$	hole
3	2	-1	$1-g/2$	hole
4	3	1	2	particle
5	3	-1	2	particle
6	4	1	3	particle
7	4	-1	3	particle

which represents a basic pairing model with p levels, each having a spin degeneracy of 2. The form of the coupled cluster equations uses single-particle states that are eigenstates of the Hartree-Fock operator, $(\hat{u} + \hat{u}_{\text{HF}})|p\rangle = \epsilon_p|p\rangle$. In the pairing model, this condition is already fulfilled. All we have to do is define the lowest N_{Fermi} states as holes and compute the Hartree-Fock energies,

$$\epsilon_{pm_p} = {}^{(1)}H_{pm_p}^{pm_p} + \sum_{im_i} {}^{(2)}H_{pm_p im_i}^{pm_p im_i} \quad (3.40)$$

To be more specific, let us look at the pairing model with four particles and eight single-particle states. These states (with $\delta = 1.0$) could be labeled as shown in Table 5.1. The Hamiltonian matrix for this four-particle problem with no broken pairs is defined by six possible Slater determinants, one representing the ground state and zero-particle-zero-hole excitations $0p-0h$, four representing various $2p-2h$ excitations and finally one representing

a $4p - 4h$ excitation. Problem ?? gives us for this specific problem

$$H = \begin{bmatrix} 2\delta - g & -g/2 & -g/2 & -g/2 & -g/2 & 0 \\ -g/2 & 4\delta - g & -g/2 & -g/2 & -0 & -g/2 \\ -g/2 & -g/2 & 6\delta - g & 0 & -g/2 & -g/2 \\ -g/2 & -g/2 & 0 & 6\delta - g & -g/2 & -g/2 \\ -g/2 & 0 & -g/2 & -g/2 & 8\delta - g & -g/2 \\ 0 & -g/2 & -g/2 & -g/2 & -g/2 & 10\delta - g \end{bmatrix} \quad (3.41)$$

It plots the correlation energy, that is the difference between the ground state energy and the reference energy. Furthermore, for the pairing model we have added results from perturbation theory to second order (MBPT2) and third order in the interaction MBPT3. Second order perturbation theory includes diagram (2) of Fig. ?? while MBPT3 includes diagrams (3), (4), (5), (8) and (9) as well. Note that diagram (3) is zero for the pairing model and that diagrams (8) and (9) do not contribute either if we work with a canonical Hartree-Fock basis. In the case of the simple pairing model it is easy to calculate ΔE_{MBPT2} analytically. This is a very useful check of our codes since this analytical expression can also be used to check our first CCD iteration. We restate this expression here but restrict the sums over single-particle states

$$\Delta E_{MBPT2} = \frac{1}{4} \sum_{abij} \frac{\langle ij|\hat{v}|ab\rangle\langle\langle|ab|\hat{v}|ij\rangle}{\epsilon_{ij}^{ab}} = \sum_{a<b, i<j} \frac{\langle ij|\hat{v}|ab\rangle\langle\langle|ab|\hat{v}|ij\rangle}{\epsilon_{ij}^{ab}}$$

For our pairing example we obtain the following result

$$\Delta E_{MBPT2} = \frac{\langle 01|\hat{v}|45\rangle^2}{\epsilon_{01}^{45}} + \frac{\langle 01|\hat{v}|67\rangle^2}{\epsilon_{01}^{67}} + \frac{\langle 23|\hat{v}|45\rangle^2}{\epsilon_{23}^{45}} + \frac{\langle 23|\hat{v}|67\rangle^2}{\epsilon_{23}^{67}},$$

which translates into

$$\Delta E_{MBPT2} = -\frac{g^2}{4} \left(\frac{1}{4+g} + \frac{1}{6+g} + \frac{1}{2+g} + \frac{1}{4+g} \right).$$

This expression can be used to check the results for any value of g and provides thereby an important test of our codes.

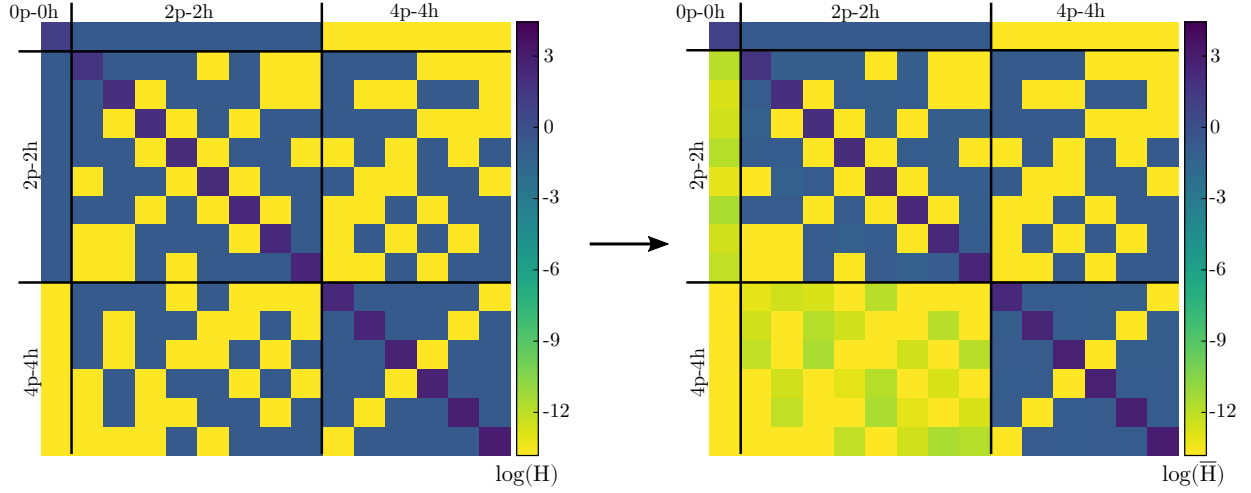


Figure 3.3: ab-initio progress blah blah blah

3.4 Example: Infinite Matter

Infinite nuclear or neutron matter is a homogeneous system and the one-particle wave functions are given by plane wave functions normalized to a volume Ω for a box with length L (the limit $L \rightarrow \infty$ is to be taken after we have computed various expectation values)

$$\psi_{\mathbf{k}\sigma}(\mathbf{r}) = \frac{1}{\sqrt{\Omega}} \exp(i\mathbf{k}\mathbf{r})\xi_{\sigma}$$

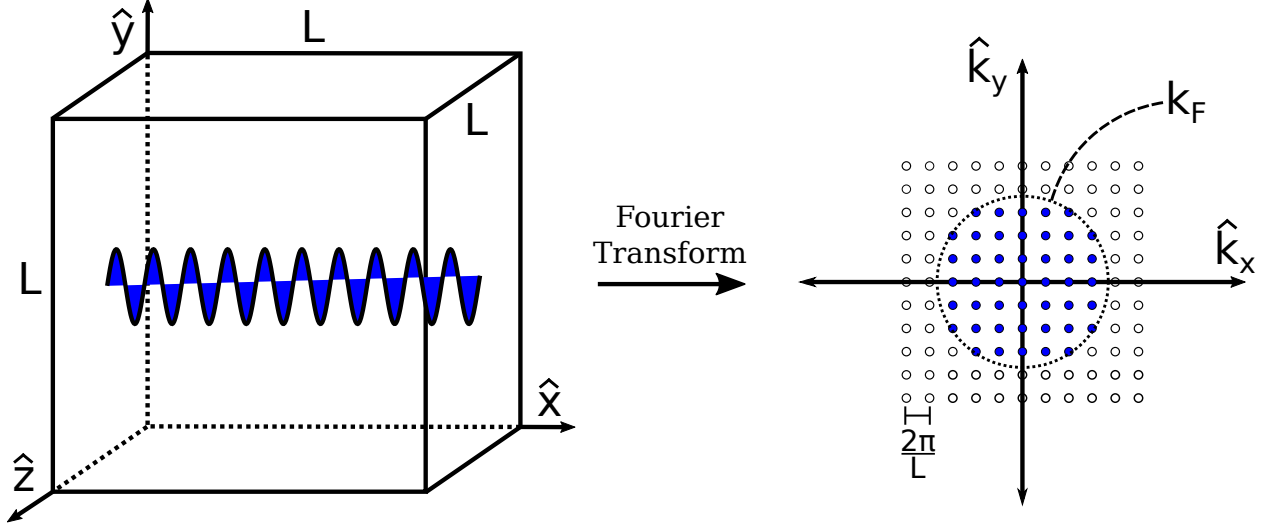


Figure 3.4: Correlation energy for the pairing model with exact diagonalization, MBPT2 and perturbation theory to third order MBPT3 for a range of interaction values. A canonical Hartree-Fock basis has been employed in all MBPT calculations.

where \mathbf{k} is the wave number and ξ_σ is the spin function for either spin up or down nucleons

$$\xi_{\sigma=+1/2} = \begin{pmatrix} 1 \\ 0 \end{pmatrix} \quad \xi_{\sigma=-1/2} = \begin{pmatrix} 0 \\ 1 \end{pmatrix}.$$

As an interesting aside, the recent works of Binder *et al* [?] and McElvain and Haxton [?] offer new perspectives on the construction of effective Hamiltonians and choices of basis functions.

We focus first on the kinetic energy operator. We assume that we have periodic boundary conditions which limit the allowed wave numbers to

$$k_i = \frac{2\pi n_i}{L} \quad i = x, y, z \quad n_i = 0, \pm 1, \pm 2, \dots$$

The operator for the kinetic energy can be written as

$$\hat{T} = \sum_{\mathbf{p}\sigma p} \frac{\hbar^2 k_p^2}{2m} a_{\mathbf{p}\sigma p}^\dagger a_{\mathbf{p}\sigma p}.$$

When using periodic boundary conditions, the discrete-momentum single-particle basis functions (excluding spin and/or isospin degrees of freedom) result in the following single-particle energy

$$\varepsilon_{n_x, n_y, n_z} = \frac{\hbar^2}{2m} \left(\frac{2\pi}{L} \right)^2 (n_x^2 + n_y^2 + n_z^2) = \frac{\hbar^2}{2m} (k_{n_x}^2 + k_{n_y}^2 + k_{n_z}^2),$$

for a three-dimensional system with

$$k_{n_i} = \frac{2\pi n_i}{L}, \quad n_i = 0, \pm 1, \pm 2, \dots,$$

We will select the single-particle basis such that both the occupied and unoccupied single-particle states have a closed-shell structure. This means that all single-particle states corresponding to energies below a chosen cutoff are included in the basis. We study only the unpolarized spin phase, in which all orbitals are occupied with one spin-up and one spin-down fermion (neutrons and protons in our case). With the kinetic energy rewritten in terms of the discretized momenta we can set up a list (assuming identical particles one and including spin up and spin down solutions) of single-particle energies with momentum quantum numbers such that $n_x^2 + n_y^2 + n_z^2 \leq 3$, as shown in for example Table 3.2

Continuing in this way we get for $n_x^2 + n_y^2 + n_z^2 = 4$ a total of 12 additional states, resulting in 66 as a new magic number. For the lowest six energy values the degeneracy in energy gives us 2, 14, 38, 54, 66 and 114 as magic numbers. These numbers will then define our Fermi

Table 3.2: Total number of particle filling $N_{\uparrow\downarrow}$ for various $n_x^2 + n_y^2 + n_z^2$ values for one spin-1/2 fermion species. Borrowing from nuclear shell-model terminology, filled shells corresponds to all single-particle states for one $n_x^2 + n_y^2 + n_z^2$ value being occupied. For matter with both protons and neutrons, the filling degree increased with a factor of 2.

$n_x^2 + n_y^2 + n_z^2$	n_x	n_y	n_z	$N_{\uparrow\downarrow}$
0	0	0	0	2
1	-1	0	0	14
1	1	0	0	
1	0	-1	0	
1	0	1	0	
1	0	0	-1	
1	0	0	1	
2	-1	-1	0	38
2	-1	1	0	
2	1	-1	0	
2	1	1	0	
2	-1	0	-1	
2	-1	0	1	
2	1	0	-1	
2	1	0	1	
2	0	-1	-1	
2	0	-1	1	
2	0	1	-1	
2	0	1	1	
3	-1	-1	-1	54
3	-1	-1	1	
3	-1	1	-1	
3	-1	1	1	
3	1	-1	-1	
3	1	-1	1	
3	1	1	-1	
3	1	1	1	

level when we compute the energy in a Cartesian basis. When performing calculations based on many-body perturbation theory, coupled cluster theory or other many-body methods, we need then to add states above the Fermi level in order to sum over single-particle states which are not occupied.

If we wish to study infinite nuclear matter with both protons and neutrons, the above magic numbers become 4, 28, 76, 108, 132, 228,

Every number of particles for filled shells defines also the number of particles to be used in a given calculation. The number of particles can in turn be used to define the density ρ (or the Fermi momentum) of the system via

$$\rho = g \frac{k_F^3}{6\pi^2},$$

where k_F is the Fermi momentum and the degeneracy g , which is two for one type of spin-1/2 particles and four for symmetric nuclear matter. With the density defined and having fixed the number of particles A and the Fermi momentum k_F , we can define the length L of the box used with periodic boundary contributions via the relation

$$V = L^3 = \frac{A}{\rho}.$$

With L we can to define the spacing between various k -values given by

$$\Delta k = \frac{2\pi}{L}.$$

Here, A is the number of nucleons. If we deal with the electron gas only, this needs to be replaced by the number of electrons N . Exercise ?? deals with the set up of a program

that establishes the single-particle basis for nuclear matter calculations with input a given number of nucleons and a user specified density or Fermi momentum.

3.4.1 Two-body interaction

As mentioned above, we will employ a plane wave basis for our calculations of infinite matter properties. With a cartesian basis we can calculate directly the various matrix elements. However, a cartesian basis represents an approximation to the thermodynamical limit. In order to compare the stability of our basis with results from the thermodynamical limit, it is convenient to rewrite the nucleon-nucleon interaction in terms of a partial wave expansion. This will allow us to compute the Hartree-Fock energy of the ground state in the thermodynamical limit (with the caveat that we need to limit the number of partial waves). In order to find the expressions for the Hartree-Fock energy in a partial wave basis, we will find it convenient to rewrite our two-body force in terms of the relative and center-of-mass motion momenta.

The direct matrix element, with single-particle three-dimensional momenta \mathbf{k}_p , spin σ_p and isospin τ_p , is defined as

$$\langle \mathbf{k}_p \sigma_p \tau_p \mathbf{k}_q \sigma_q \tau_q | \hat{v} | \mathbf{k}_r \sigma_r \tau_r \mathbf{k}_s \sigma_s \tau_s \rangle,$$

or in a more compact form as $\langle \mathbf{pq} | \hat{v} | \mathbf{rs} \rangle$ where the boldfaced letters \mathbf{p} etc represent the relevant quantum numbers, here momentum, spin and isospin. Introducing the relative momentum

$$\mathbf{k} = \frac{1}{2} (\mathbf{k}_p - \mathbf{k}_q),$$

and the center-of-mass momentum

$$\mathbf{K} = \mathbf{k}_p + \mathbf{k}_q,$$

we have

$$\langle \mathbf{k}_p \sigma_p \tau_p \mathbf{k}_q \sigma_q \tau_q | \hat{v} | \mathbf{k}_r \sigma_r \tau_r \mathbf{k}_s \sigma_s \tau_s \rangle = \langle \mathbf{k} \mathbf{K} \sigma_p \tau_p \sigma_q \tau_q | \hat{v} | \mathbf{k}' \mathbf{K}' \sigma_r \tau_r \sigma_s \tau_s \rangle.$$

The nucleon-nucleon interaction conserves the total momentum and charge, implying that the above uncoupled matrix element reads

$$\langle \mathbf{k} \mathbf{K} \sigma_p \tau_p \sigma_q \tau_q | \hat{v} | \mathbf{k}' \mathbf{K}' \sigma_r \tau_r \sigma_s \tau_s \rangle = \delta_{T_z, T'_z} \delta(\mathbf{K} - \mathbf{K}') \langle \mathbf{k} T_z S_z = (\sigma_a + \sigma_b) | \hat{v} | \mathbf{k}' T'_z S'_z = (\sigma_c + \sigma_d) \rangle,$$

where we have defined the isospin projections $T_z = \tau_p + \tau_q$ and $T'_z = \tau_r + \tau_s$. Defining $\hat{v} = \hat{v}(\mathbf{k}, \mathbf{k}')$, we can rewrite the previous equation in a more compact form as

$$\delta_{T_z, T'_z} \delta(\mathbf{K} - \mathbf{K}') \langle \mathbf{k} T_z S_z = (\sigma_p + \sigma_q) | \hat{v} | \mathbf{k}' T'_z S'_z = (\sigma_r + \sigma_s) \rangle = \delta_{T_z, T'_z} \delta(\mathbf{K} - \mathbf{K}') \langle T_z S_z | \hat{v}(\mathbf{k}, \mathbf{k}') | T'_z S'_z \rangle.$$

These matrix elements can in turn be rewritten in terms of the total two-body quantum numbers for the spin S of two spin-1/2 fermions as

$$\langle \mathbf{k} T_z S_z | \hat{v}(\mathbf{k}, \mathbf{k}') | \mathbf{k}' T'_z S'_z \rangle = \sum_{SS'} \langle \frac{1}{2} \sigma_p \frac{1}{2} \sigma_q | S S_z \rangle \langle \frac{1}{2} \sigma_r \frac{1}{2} \sigma_s | S' S'_z \rangle \langle \mathbf{k} T_z S S_z | \hat{v}(\mathbf{k}, \mathbf{k}') | \mathbf{k} T'_z S' S'_z \rangle$$

The coefficients $\langle \frac{1}{2} \sigma_p \frac{1}{2} \sigma_q | S S_z \rangle$ are so-called Clebsch-Gordan recoupling coefficients. We will assume that our interactions conserve charge. We will refer to $T_z = 0$ as the pn (proton-neutron) channel, $T_z = -1$ as the pp (proton-proton) channel and $T_z = 1$ as the nn (neutron-neutron) channel.

The nucleon-nucleon force is often derived and analyzed theoretically in terms of a partial wave expansion. A state with linear momentum \mathbf{k} can be written in terms of spherical harmonics Y_{lm} as

$$|\mathbf{k}\rangle = \sum_{l=0}^{\infty} \sum_{m=-l}^l i^l Y_{lm} \langle \hat{k} | kl m_l \rangle.$$

In terms of the relative and center-of-mass momenta \mathbf{k} and \mathbf{K} , the potential in momentum space is related to the nonlocal operator $V(\mathbf{r}, \mathbf{r}')$ by

$$\langle \mathbf{k}' \mathbf{K}' | \hat{v} | \mathbf{k}' \mathbf{K}' \rangle = \int d\mathbf{r} d\mathbf{r}' e^{-i\mathbf{k}' \mathbf{r}'} V(\mathbf{r}', \mathbf{r}) e^{i\mathbf{k} \mathbf{r}} \delta(\mathbf{K}, \mathbf{K}').$$

We will assume that the interaction is spherically symmetric and use the partial wave expansion of the plane waves in terms of spherical harmonics. This means that we can separate the radial part of the wave function from its angular dependence. The wave function of the relative motion is described in terms of plane waves as

$$e^{i\mathbf{k} \mathbf{r}} = \langle \mathbf{r} | \mathbf{k} \rangle = 4\pi \sum_{lm} i^l j_l(kr) Y_{lm}^*(\hat{\mathbf{k}}) Y_{lm}(\hat{\mathbf{r}}),$$

where j_l is a spherical Bessel function and Y_{lm} the spherical harmonic. This partial wave basis is useful for defining the operator for the nucleon-nucleon interaction, which is symmetric with respect to rotations, parity and isospin transformations. These symmetries imply that the interaction is diagonal with respect to the quantum numbers of total angular momentum J , spin S and isospin T . Using the above plane wave expansion, and coupling to final J , S and T we get

$$\langle \mathbf{k}' | V | \mathbf{k} \rangle = (4\pi)^2 \sum_{JM} \sum_{lm} \sum_{l'm'} i^{l+l'} Y_{lm}^*(\hat{\mathbf{k}}) Y_{l'm'}(\hat{\mathbf{k}}') C_{m'M_{SM}}^{l'SJ} C_{mM_{SM}}^{l'SJ} \langle k'l' ST JM | V | kl ST JM \rangle,$$

where we have defined

$$\langle k'l'STJM|V|klSTJM\rangle = \int j_{l'}(k'r')\langle l'STJM|V(r',r)|lSTJM\rangle j_l(kr)r'^2 dr' r^2 dr.$$

We have omitted the momentum of the center-of-mass motion \mathbf{K} and the corresponding orbital momentum L , since the interaction is diagonal in these variables.

The interaction we will use for these calculations is a semirealistic nucleon-nucleon potential known as the Minnesota potential [?] which has the form, $V_\alpha(r) = V_\alpha \exp(-\alpha r^2)$. The spin and isospin dependence of the Minnesota potential is given by,

$$V(r) = \frac{1}{2} \left(V_R + \frac{1}{2} (1 + P_{12}^\sigma) V_T + \frac{1}{2} (1 - P_{12}^\sigma) V_S \right) (1 - P_{12}^\sigma P_{12}^\tau),$$

where $P_{12}^\sigma = \frac{1}{2} (1 + \sigma_1 \cdot \sigma_2)$ and $P_{12}^\tau = \frac{1}{2} (1 + \tau_1 \cdot \tau_2)$ are the spin and isospin exchange operators, respectively. A Fourier transform to momentum space of the radial part $V_\alpha(r)$ is rather simple, see problem ??, since the radial depends only on the magnitude of the relative distance and thereby the relative momentum $\vec{q} = \frac{1}{2} (\vec{k}_p - \vec{k}_q - \vec{k}_r + \vec{k}_s)$. Omitting spin and isospin dependencies, the momentum space version of the interaction reads

$$\langle \mathbf{k}_p \mathbf{k}_q | V_\alpha | \mathbf{k}_r \mathbf{k}_s \rangle = \frac{V_\alpha}{L^3} \left(\frac{\pi}{\alpha} \right)^{3/2} \exp\left(\frac{-q^2}{4\alpha}\right) \delta_{\vec{k}_p + \vec{k}_q, \vec{k}_r + \vec{k}_s}$$

The various parameters defining the interaction model used in this work are listed in Table 3.3.

In these calculations we approximated our problem with periodic boundary conditions, $\phi(x_i) = \phi(x_i + L)$, but we could have chosen anti-periodic boundary conditions, $\phi(x_i) = -\phi(x_i + L)$. The difference between these two shows how the correlation energy contains

Table 3.3: Parameters used to define the Minnesota interaction model [?].

α	V_α in MeV	κ_α in fm^{-2}
R	200	1.487
T	178	0.639
S	91.85	0.465

finite-size effects [?, ?, ?, ?]. One solution to this problem is by integrating over solutions between periodic and anti-periodic conditions, known as twist-averaging [?]. First, we multiply the single-particle states by a phase for each direction, characterized by a twist-angle, θ_i .

$$\phi_{\vec{k}}(\vec{x} + \vec{L}) \rightarrow e^{i\vec{\theta}} \phi_{\vec{k}}(\vec{x}) \quad (3.42)$$

$\theta_i = 0$ for PBC and $\theta_i = \pi$ for APBC

$$\vec{k} \rightarrow \vec{k} + \frac{\vec{\theta}}{L} \quad (3.43)$$

$$\epsilon_{\vec{k}} \rightarrow \epsilon_{\vec{k}} + \frac{\pi}{L} \vec{k} \cdot \vec{\theta} + \frac{\pi^2}{L^2} \quad (3.44)$$

Adding these phases changes the single-particle energies, the correction of which disappear as $L \rightarrow \infty$, depending on $\vec{\theta}$ and thus changes the shell structure so that hole states can jump up to particle states and *vice versa*. It is thence necessary to fill hole states separately for each $\vec{\theta}$. Integration over a quantity is approximated by a weighted sum, such as Gauss-Legendre quadrature, over the quantity for each set of twist angles. The algorithm becomes then

Build mesh points and weights for each direction i : $\{\theta_i, w_i\}$ $E_{\text{twist}} = 0$ $(\theta_x, w_x) \in \{\theta_x, w_x\}$
 $(\theta_y, w_y) \in \{\theta_y, w_y\}$ $(\theta_z, w_z) \in \{\theta_z, w_z\}$ Build Basis States with $k_i \rightarrow k_i + \frac{\theta_i}{L}$ Order States
by Energy and Fill Holes Get Result E (T,HF,CCD) $E_{\text{twist}} = E_{\text{twist}} + \frac{1}{\pi^3} w_x w_y w_z E$ This
technique gives results which depend much less on the particle number, but requires a full

calculation for each set of twist angles, which can grow very quickly. For example, using 10 twist angles in each direction requires 1000 calculations. To see the effects of twist averaging, it is easy to calculate the kinetic energy per particle and the Hartree-Fock energy per particle, which avoids the full CCD calculation. These calculations can be compared to the exact values for infinite matter, which are calculated by integrating the the relevent values up to the fermi surface. The kinetic energy is given by

$$T_{\text{inf}} = \frac{3\hbar^2 k_f^2}{10m},$$

while the potential energy to first order (corresponding to the Hartree-Fock contribution) reads

$$\text{HF}_{\text{inf}} = \frac{1}{(2\pi)^6} \frac{L^3}{2\rho} \int_0^{k_f} d\vec{k}_1 \int_0^{k_f} d\vec{k}_2 \langle \vec{k}_1 \vec{k}_2 | \hat{v} | \vec{k}_1 \vec{k}_2 | . \rangle$$

With all these ingredients, we can now compute the final CCD energy and thereby the equation of state for infinite neutron matter. Figure ?? displays the total CCD energy (including the reference energy) as well as the reference energy obtained with the Minnesota interaction model. The computations have been performed with $N = 66$ neutrons and a maximum number of single-particle states constrained by $N_{\text{max}} = 36$. This corresponds to 2377 single-particle states.

We see from this figure that the correlations brought by coupled cluster theory are at the order of 10% roughly of the reference energy. It means that for this system (neutrons only) with the Minnesota potential, higher-order correlations can most likely be treated in a perturbative way. Many-body perturbation theory to second order gives results which are very close to our CCD results, as seen in Table 3.4. For low densities we observe a good agreement while higher densities bring in particle-particle correlations that become

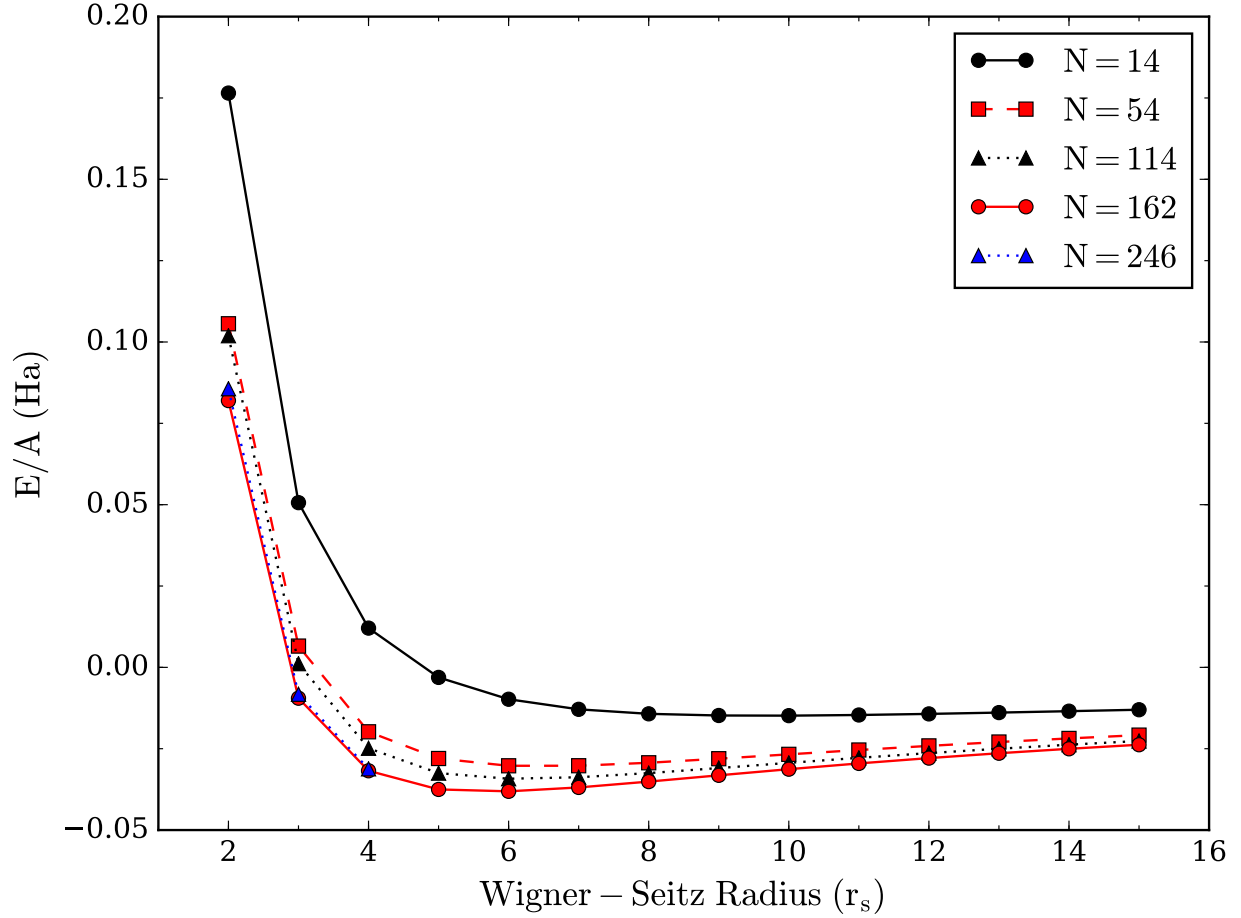


Figure 3.5: Energy per particle for pure neutron matter as function of density from coupled cluster calculations with doubles correlations only. The reference energy is included for comparison. The results have been obtained with Minnesota interaction model using periodic boundary conditions and $N = 66$ neutrons and single-particle states up to $N_{max} = 36$, resulting in a total of 2377 single-particle states.

more important as the density increases. Coupled cluster theory sums to infinite order for example particle-particle correlations and with increasing densities this is reflected in differences between the two many-body approximations. The above results agree well with the recent coupled cluster calculations of Refs. [?, ?], obtained with interaction models from effective field theory. With the inclusion of proton correlations as well as other potential models we may expect larger differences between different methods and interactions. In chapters 9, 10 and 11 we compare the above results with those obtained with Monte Carlo

Table 3.4: CCD and MBPT2 results for infinite neutron matter with $N = 66$ neutrons and a maximum number of single-particle states constrained by $N_{max} = 36$.

Density $\rho \text{ fm}^{-3}$	E_{MBPT2}	E_{CCD}
0.04	6.472	6.468
0.06	7.919	7.932
0.08	9.075	9.136
1.0	9.577	10.074
1.2	10.430	10.885
1.4	11.212	11.565
1.6	11.853	12.136
1.8	12.377	12.612
2.0	12.799	13.004

methods, the in-medium renormalization group approach and Green's function theory.

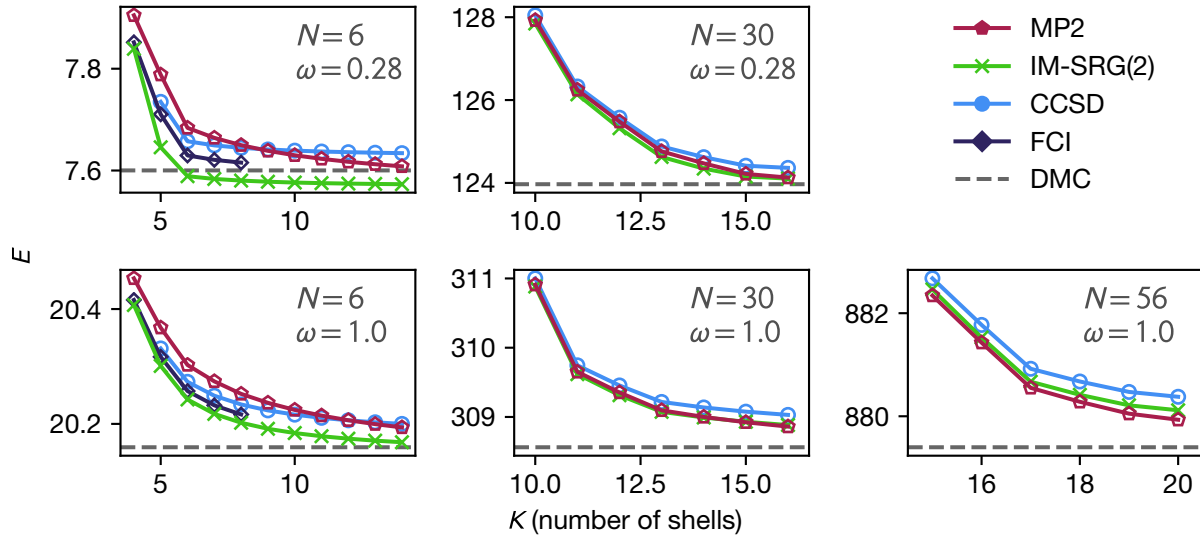


Figure 3.6: Energy per particle for pure neutron matter as function of density from coupled cluster calculations with doubles correlations only. The reference energy is included for comparison. The results have been obtained with Minnesota interaction model using periodic boundary conditions and $N = 66$ neutrons and single-particle states up to $N_{max} = 36$, resulting in a total of 2377 single-particle states.

Chapter 4

Equation-of-Motion Method

$$\hat{H} = H_{\emptyset} + \sum_{pq} H_{pq} \left\{ \hat{a}_p^\dagger \hat{a}_q \right\} + \frac{1}{4} \sum_{pqrs} H_{pqrs} \left\{ \hat{a}_p^\dagger \hat{a}_q^\dagger \hat{a}_s \hat{a}_r \right\}, \quad (4.1)$$

Particle attached and particle removed equations-of-motion (EOM) methods can be coupled with either IM-SRG or CC calculations. The principal idea is that one may construct a ladder operator \hat{X} that promotes the N -particle ground state to any state in the $N + 1$ or $N - 1$ spectrum,

$$|\Psi_u^{(N\pm 1)}\rangle = \hat{X}_u^{(N\pm 1)} |\Psi_0^{(N)}\rangle, \quad (4.2)$$

where \hat{X} is in principle a linear combination of excitation (+) and de-excitation (−) operators that change particle number by one,

$$\hat{X}_u^{(N+1)} = \sum_a x_a^{(u,+)} \left\{ \hat{a}_a^\dagger \right\} + \frac{1}{2} \sum_{abi} x_{abi}^{(u,+)} \left\{ \hat{a}_a^\dagger \hat{a}_b^\dagger \hat{a}_i \right\} + \cdots, \quad (4.3)$$

$$\hat{X}_u^{(N-1)} = \sum_i x_i^{(u,-)} \left\{ \hat{a}_i \right\} + \frac{1}{2} \sum_{ija} x_{aij}^{(u,-)} \left\{ \hat{a}_a^\dagger \hat{a}_j \hat{a}_i \right\} + \cdots. \quad (4.4)$$

Here, $x_p^{(u,\pm)}$ and $x_{pqr}^{(u,\pm)}$ are the normal-ordered matrix elements of $\hat{X}_u^{(N\pm 1)}$, defined analogously to Eq. (4.1).

Substitution of Eq. (4.2) into the energy eigenvalue problem

$$\hat{H} |\Psi_u^{(N\pm 1)}\rangle = E_u^{(N\pm 1)} |\Psi_u^{(N\pm 1)}\rangle,$$

gives

$$[\hat{H}, \hat{X}_u^{(N\pm 1)}]|\Psi_0^{(N)}\rangle = \pm \varepsilon_u^{(\pm)} \hat{X}_u^{(N\pm 1)}|\Psi_0^{(N)}\rangle, \quad (4.5)$$

which constitutes a generalized eigenvalue problem for the amplitudes x , where $\varepsilon_u^{(\pm)}$ are the single-particle addition (+) and removal (−) energies. The quality of this calculation depends on the ansatz for the N -particle ground state, as well as the systematically improvable truncation on the ladder operators. In this work we include 1p and 2p1h excitations in the $N + 1$ ladder operator and likewise 1h and 2h1p operators for the $N - 1$ ladder operators.

After a single-reference ground state IM-SRG calculation, the Hamiltonian has been rotated such that the reference state is an eigenfunction with corresponding eigenvalue $E_0^{(N)}$, which is the correlated N -particle ground state energy. The EOM equation is therefore

$$[\bar{H}, \bar{X}_u^{(N\pm 1)}]|\Phi_0^{(N)}\rangle = \pm \varepsilon_u^{(\pm)} \bar{X}_u^{(N\pm 1)}|\Phi_0^{(N)}\rangle, \quad (4.6)$$

where bars denote rotated operators. Now the reference state is used in place of the bare correlated ground state. The ground state IM-SRG procedure has implicitly re-summed contributions from higher order excitations (3-particle-2-hole, 2-particle-3-hole, 2-particle-3-hole, 4-particle-3-hole, ...) into the lower order amplitudes of the ladder operators (1-particle-0-hole, 0-particle-1-hole, 2-particle-1-hole, 1-particle-2-hole).

Despite these gains, the EOM calculation is still a partial diagonalization method, limited by the truncation to 2-particle-1-hole and 1-particle-2-hole operators. We expect $N + 1$ (or $N - 1$) states to be described appropriately by EOM-IM-SRG if their wavefunctions are dominated by 1-particle-0-hole (or 0-particle-1-hole) contributions in the rotated frame. We

use partial norms of the EOM ladder operators to estimate these contributions:

$$n_{1\text{-particle}} = \sqrt{\sum_a |\bar{x}_a^{(+)}|^2}, \quad (4.7)$$

$$n_{1\text{-hole}} = \sqrt{\sum_i |\bar{x}_i^{(-)}|^2}. \quad (4.8)$$

Large single particle partial norms indicate that the EOM truncation is reasonable for the relevant state. States with lower single particle norms should be treated with a higher EOM approximation, which can be accomplished directly or perturbatively [72].

Like EOM-IM-SRG, the equations-of-motion technique can be applied after a CC ground-state calculation, by using the CC effective Hamiltonian. Here, the non-Hermitian nature of \bar{H}_{CC} becomes apparent. In this case, in addition to constructing excitation ladder operators Eq. (4.3) and Eq. (4.4) that correspond to the right-eigenvectors of the generalized eigenvalue problem Eq. (4.6), there exist analogous de-excitation ladder operators, $\hat{L}^{(N+1)}$ and $\hat{L}^{(N-1)}$, that correspond to the left-eigenvectors,

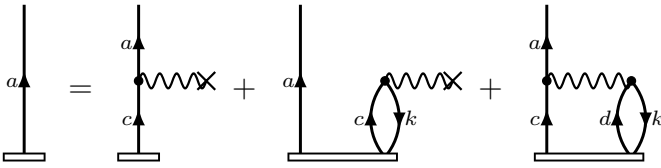
$$\begin{aligned} \hat{L}_u^{(N+1)} &= \sum_a l_a^{(u,+)} \{\hat{a}_a\} + \frac{1}{2} \sum_{iab} l_{iab}^{(u,+)} \{\hat{a}_i^\dagger \hat{a}_b \hat{a}_a\} + \dots, \\ \hat{L}_u^{(N-1)} &= \sum_i l_i^{(u,-)} \{\hat{a}_i^\dagger\} + \frac{1}{2} \sum_{ija} l_{ija}^{(u,-)} \{\hat{a}_i^\dagger \hat{a}_j^\dagger \hat{a}_a\} + \dots, \end{aligned}$$

where $l_p^{(u,\pm)}$ and $l_{pqr}^{(u,\pm)}$ are likewise the normal-ordered matrix elements of $\hat{L}_u^{(N\pm 1)}$. These left-eigenvectors satisfy the left-eigenvalue problem, with left-eigenvalues $\varepsilon_u^{(\pm)}$, analogous to Eq. (4.6),

$$\langle \Phi_0^{(N)} | [\bar{H}, \bar{L}_u^{(N\pm 1)}] = \pm \varepsilon_u^{(\pm)} \langle \Phi_0^{(N)} | \bar{L}_u^{(N\pm 1)}$$

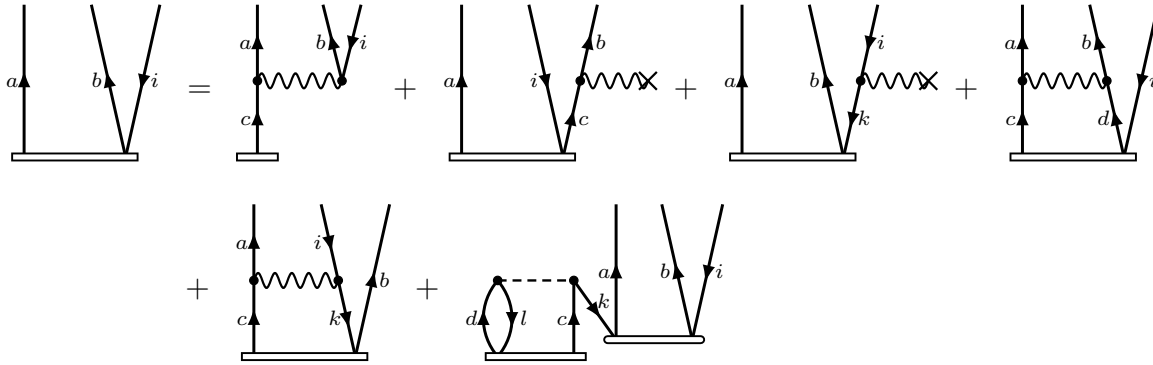
and form a bi-orthogonal set with the right-eigenvectors, $\langle \bar{L}_u^{(N\pm 1)} | \bar{X}_v^{(N\pm 1)} \rangle = \delta_{uv}$.

In this paper, because the effective Hamiltonian is real, the corresponding left- and right-eigenvalues are equal. In addition, while the the left- and right-eigenvectors are generally not equivalent, the differences in their single-particle Eq. (4.7) or single-hole Eq. (4.8) natures are, in practice, not significant. Therefore, only the right-eigenvectors are used in this paper.



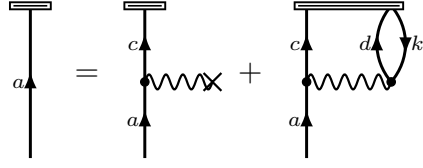
The diagrammatic equation (4.9) shows a single-particle state (a vertical line with an upward arrow labeled 'a') equal to a sum of four diagrams. The first diagram is a vertical line with an upward arrow labeled 'a' and a downward arrow labeled 'c' at the bottom. The second diagram is a vertical line with an upward arrow labeled 'a' and a downward arrow labeled 'c' at the bottom, with a wavy line connecting them and a cross at the end. The third diagram is a vertical line with an upward arrow labeled 'a' and a downward arrow labeled 'c' at the bottom, with a wavy line connecting them and a loop labeled 'k' at the end. The fourth diagram is a vertical line with an upward arrow labeled 'a' and a downward arrow labeled 'c' at the bottom, with a wavy line connecting them and a loop labeled 'd' and 'k' at the end.

$$\omega_k r^a = \sum_c X_c^a r^c + \sum_{kc} X_c^k r_k^{ac} + \frac{1}{2} \sum_{kcd} X_{cd}^{ak} r_k^{cd} \quad (4.9)$$

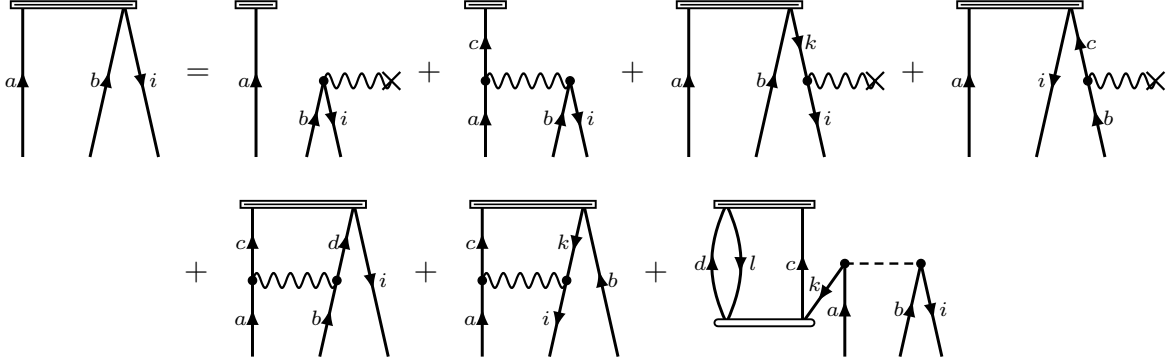


The diagrammatic equation (4.10) shows a two-particle state (two vertical lines with upward arrows labeled 'a' and 'b', and a downward arrow labeled 'i' at the bottom) equal to a sum of seven diagrams. The first four diagrams are similar to the ones in (4.9) but with an additional downward arrow labeled 'i' at the bottom. The fifth diagram is a vertical line with an upward arrow labeled 'a' and a downward arrow labeled 'c' at the bottom, with a wavy line connecting them and a loop labeled 'k' and 'l' at the end. The sixth diagram is a vertical line with an upward arrow labeled 'a' and a downward arrow labeled 'c' at the bottom, with a wavy line connecting them and a loop labeled 'd' and 'l' at the end. The seventh diagram is a vertical line with an upward arrow labeled 'a' and a downward arrow labeled 'c' at the bottom, with a wavy line connecting them and a loop labeled 'd' and 'l' at the end.

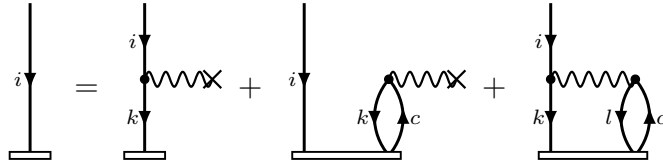
$$\begin{aligned} \omega_k r_i^{ab} = & \sum_c X_{ci}^{ab} r^c + \hat{P}(ab) \sum_c X_c^b r_i^{ac} - \sum_k X_i^k r_k^{ab} + \frac{1}{2} \sum_{cd} X_{cd}^{ab} r_i^{cd} \\ & - \hat{P}(ab) \sum_{kc} X_{ci}^{ak} r_k^{cb} - \frac{1}{2} \sum_{klcd} V_{cd}^{kl} t_{ki}^{ab} r_l^{cd} \end{aligned} \quad (4.10)$$



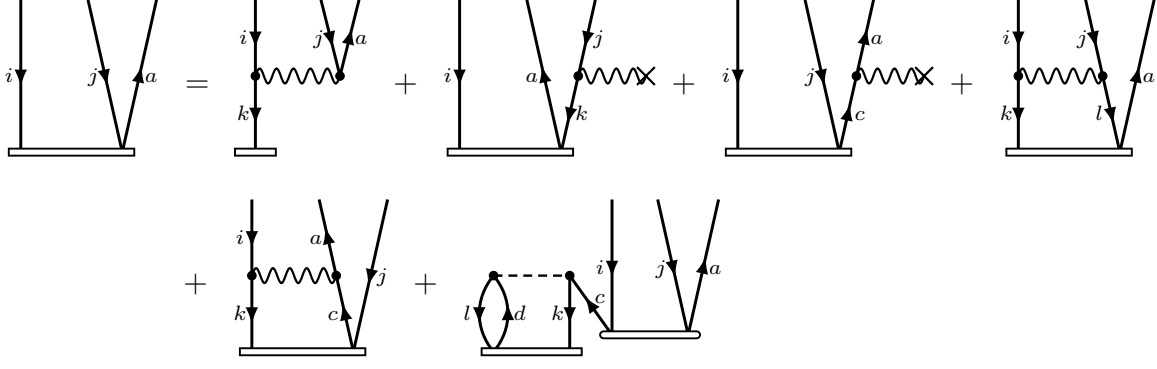
$$E_k l_a = \sum_c l_c X_a^c + \frac{1}{2} \sum_{kcd} l_{cd}^k X_{ak}^{cd} \quad (4.11)$$



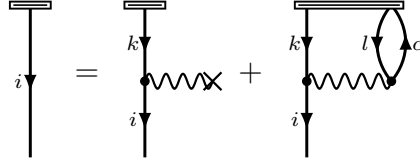
$$\begin{aligned} E_k l_{ab}^i &= \hat{P}(ab) l_a X_b^i + \sum_c l_c X_{ab}^{ci} - \sum_k l_{ab}^k X_k^i + \hat{P}(ab) \sum_c l_{ac}^i X_b^c \\ &+ \frac{1}{2} \sum_{cd} l_{cd}^i X_{ab}^{cd} - \hat{P}(ab) \sum_{kc} l_{cb}^k X_{ak}^{ci} - \frac{1}{2} \sum_{klcd} l_{cd}^l V_{ab}^{ki} t_{kl}^{cd} \end{aligned} \quad (4.12)$$



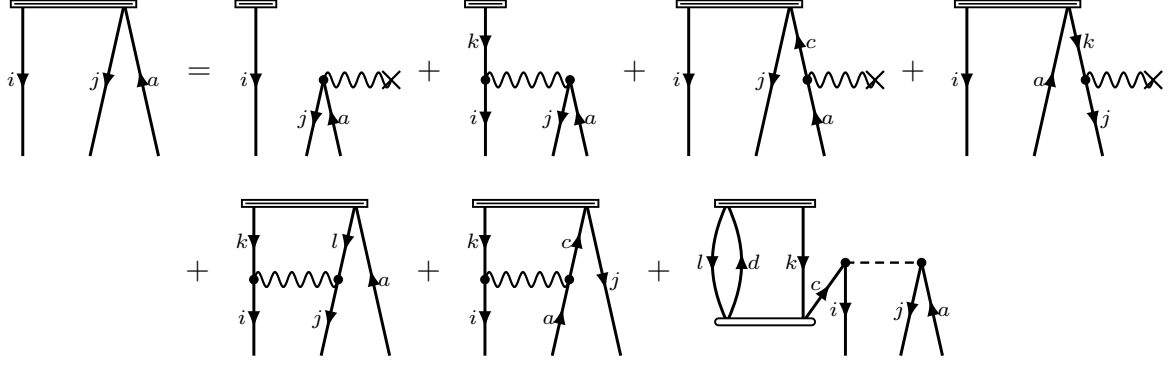
$$\omega_k r_i = - \sum_k X_i^k r_k + \sum_{kc} X_c^k r_{ik}^c - \frac{1}{2} \sum_{klc} X_{ic}^{kl} r_{kl}^c \quad (4.13)$$



$$\begin{aligned}
\omega_k r_{ij}^a = & - \sum_k X_{ij}^{ka} r_k - \hat{P}(ij) \sum_k X_j^k r_{ik}^a + \sum_c X_c^a r_{ij}^c + \frac{1}{2} \sum_{kl} X_{ij}^{kl} r_{kl}^a \\
& - \hat{P}(ij) \sum_{kc} X_{ci}^{ak} r_{kj}^c - \frac{1}{2} \sum_{klcd} V_{cd}^{kl} t_{ij}^{ca} r_{kl}^d
\end{aligned} \tag{4.14}$$



$$E_k l^i = - \sum_k l^k X_k^i - \frac{1}{2} \sum_{klc} l_c^{kl} X_{kl}^{ic} \tag{4.15}$$



$$\begin{aligned}
E_k l_a^{ij} = & \hat{P}(ij) l^i X_a^j - \sum_k l^k X_{ka}^{ij} + \sum_c l_c^{ij} X_a^c - \hat{P}(ij) \sum_k l_a^{ik} X_k^j \\
& + \frac{1}{2} \sum_{cd} l_a^{kl} X_{kl}^{ij} - \hat{P}(ij) \sum_{kc} l_c^{kj} X_{ak}^{ci} - \frac{1}{2} \sum_{klcd} l_d^{kl} V_{ca}^{ij} t_{kl}^{cd}
\end{aligned} \tag{4.16}$$

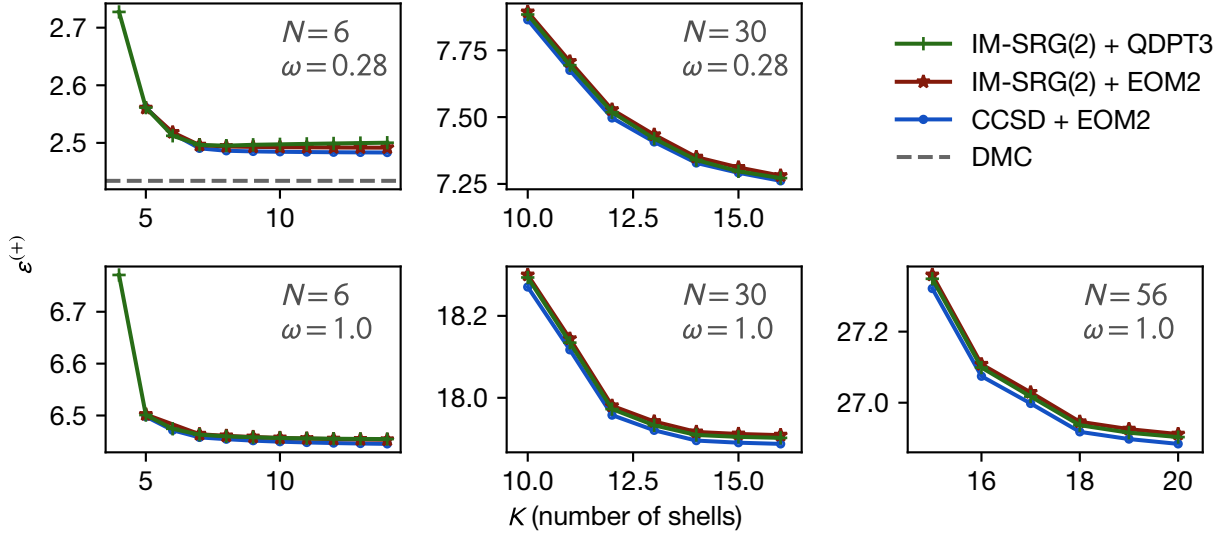


Figure 4.1: Progress of ab-initio nuclear structure from calculations of ground-state energies with NN+3N interactions. Early progress was approximately linear as the problem size scaled with Moore's law while more recent progress has taken advantage of new algorithms which have outpaced Moore's law. Data taken from [51].

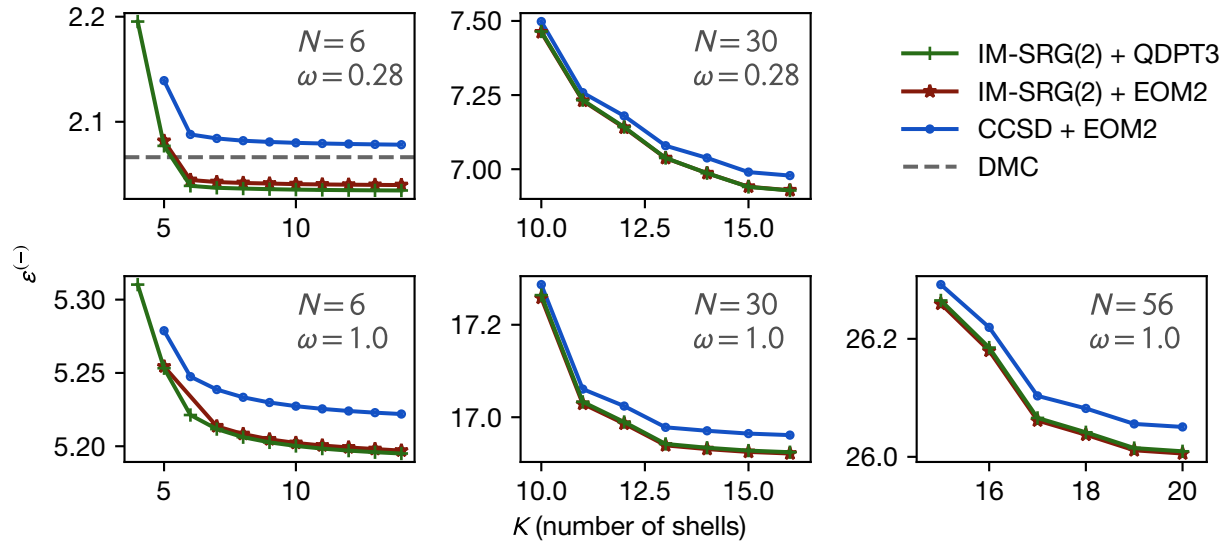
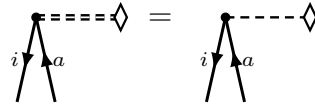


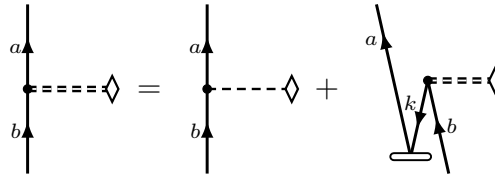
Figure 4.2: Progress of ab-initio nuclear structure from calculations of ground-state energies with NN+3N interactions. Early progress was approximately linear as the problem size scaled with Moore's law while more recent progress has taken advantage of new algorithms which have outpaced Moore's law. Data taken from [51].

Chapter 5

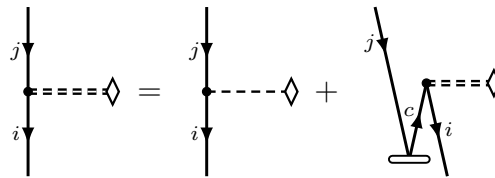
Effective Operators



$$\lambda \bar{O}_a^i = \lambda O_a^i \quad (5.1)$$



$$\lambda \bar{O}_b^a = \lambda O_b^a - \sum_k \lambda \bar{O}_b^k t_k^a \quad (5.2)$$



$$\lambda \bar{O}_j^i = \lambda O_j^i + \sum_c \lambda \bar{O}_c^i t_j^c \quad (5.3)$$

$$\lambda \bar{O}_i^a = \lambda O_i^a + \sum_c \lambda \bar{O}_c^a t_i^c - \sum_k \lambda \bar{O}_i^k t_k^a + \sum_{kc} \lambda \bar{O}_c^k t_{ik}^{ac} \quad (5.4)$$

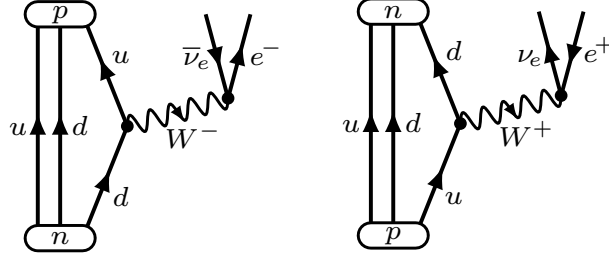
$$\lambda \bar{O}_{ic}^{ab} = - \sum_k \lambda \bar{O}_c^k t_{ik}^{ab} \quad (5.5)$$

$$\lambda \bar{O}_{jk}^{ia} = \sum_c \lambda \bar{O}_c^i t_{jk}^{ca} \quad (5.6)$$

$$\lambda \bar{O}_{ij}^{ab} = \hat{P}(ab) \sum_c \lambda \bar{O}_c^a t_{ij}^{cb} - \hat{P}(ij) \sum_k \lambda \bar{O}_i^k t_{kj}^{ab} \quad (5.7)$$

Decay Type	$\Delta J = J_F - J_I$	$\pi_F \pi_I$
Fermi	0	+1
Gamow-Teller	1 ($J_F = 0$ or $J_I = 0$)	+1
Gamow-Teller	0,1 ($J_F > 0$ and $J_I > 0$)	+1

Table 5.1: Single-particle states and their quantum numbers and their energies from Eq. (3.40). The degeneracy for every quantum number p is equal to 2 due to the two possible spin values.

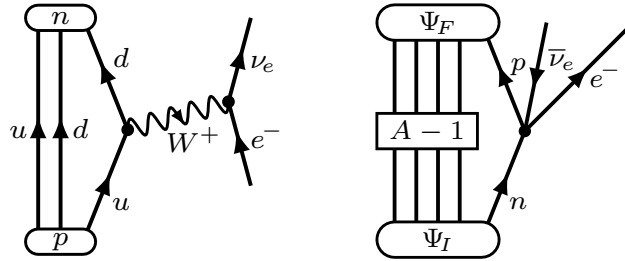


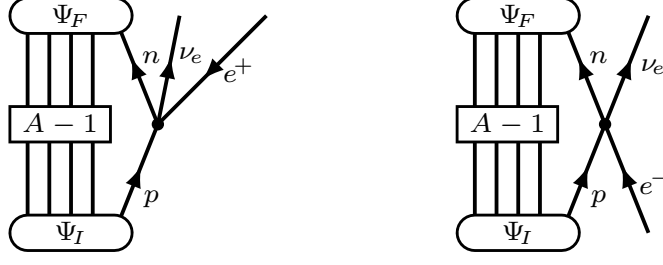
5.1 Beta Decay

$$\beta^- \text{ decay :} \quad n \longrightarrow p + e^- + \bar{\nu}_e \quad (5.8)$$

$$\beta^+ \text{ decay :} \quad p \longrightarrow n + e^+ + \nu_e \quad (5.9)$$

$$\text{Electron capture :} \quad p + e^- \longrightarrow n + \nu_e \quad (5.10)$$





5.2 Sum Rules

$$\begin{aligned}
\sum_F [B_{F-}^{I,F} - B_{F-}^{I,F}] &= \sum_F \left[|\langle F | \sum_i \tau_i^- | I \rangle|^2 - |\langle F | \sum_i \tau_i^+ | I \rangle|^2 \right] \\
&= \sum_F \left[\langle I | \sum_i \tau_i^+ | F \rangle \langle F | \sum_i \tau_i^- | I \rangle - \langle I | \sum_i \tau_i^- | F \rangle \langle F | \sum_i \tau_i^+ | I \rangle \right] \\
&= \langle I | (\sum_i \tau_i^+) (\sum_j \tau_j^-) - (\sum_i \tau_i^-) (\sum_j \tau_j^+) | I \rangle = \langle I | 2 \sum_i \tau_i^z | I \rangle = (N_I - Z_I) \quad (5.11)
\end{aligned}$$

$$\begin{aligned}
\sum_F [B_{GT-}^{I,F} - B_{GT-}^{I,F}] &= \sum_{F,\mu} \left[|\langle F | \sum_i \sigma_i^\mu \tau_i^- | I \rangle|^2 - |\langle F | \sum_i \sigma_i^\mu \tau_i^+ | I \rangle|^2 \right] \\
&= \sum_{F,\mu} \left[\langle I | \sum_i \sigma_i^\mu \tau_i^+ | F \rangle \langle F | \sum_i \sigma_i^\mu \tau_i^- | I \rangle - \langle I | \sum_i \sigma_i^\mu \tau_i^- | F \rangle \langle F | \sum_i \sigma_i^\mu \tau_i^+ | I \rangle \right] \\
&= \sum_\mu \left[\langle I | (\sum_i \sigma_i^\mu \tau_i^+) (\sum_j \sigma_j^\mu \tau_j^-) - (\sum_i \sigma_i^\mu \tau_i^-) (\sum_j \sigma_j^\mu \tau_j^+) | I \rangle \right] \\
&= \sum_\mu \left[\langle I | \sum_i \sigma_{i,\mu}^2 (\tau_{i,+} \tau_{i,-} - \tau_{i,-} \tau_{i,+}) | I \rangle \right] = 3 \langle I | \sum_i (\tau_{i,+} \tau_{i,-} - \tau_{i,-} \tau_{i,+}) | I \rangle \\
&= 3 \langle I | 2 \sum_i \tau_i^z | I \rangle = 3 (N_I - Z_I) \quad (5.12)
\end{aligned}$$

$$\sum_F \left[B_{F-}^{I,F} - B_{F-}^{I,F} \right] = (N_I - Z_I) \quad (5.13)$$

$$\sum_F \left[B_{GT-}^{I,F} - B_{GT-}^{I,F} \right] = 3 (N_I - Z_I) \quad (5.14)$$

5.3 Calculating Beta-Decay Matrix Elements

Fix these!!!!!!

$$\mathcal{M}_F \equiv \langle \mathcal{F} \| \tau \| \mathcal{I} \rangle = \delta_{J_{\mathcal{F}} J_{\mathcal{I}}} \sum_{pq} \langle p \| \hat{\tau} \| q \rangle \langle \mathcal{F} \| \hat{a}_p^\dagger \hat{a}_q \| \mathcal{I} \rangle \quad (5.15)$$

$$\mathcal{M}_{GT} \equiv \langle \mathcal{F} \| \sigma \tau \| \mathcal{I} \rangle = \sum_{pq} \langle p \| \hat{\sigma} \hat{\tau} \| q \rangle \langle \mathcal{F} \| \hat{a}_p^\dagger \hat{a}_q \| \mathcal{I} \rangle \quad (5.16)$$

$$\langle p \| \hat{\tau} \| q \rangle = \delta_{n_p n_q} \delta_{l_p l_q} \delta_{j_p j_q} \delta_{t_p t_q \pm 1} \hat{j}_p \quad (5.17)$$

$$\langle p \| \hat{\sigma} \hat{\tau} \| q \rangle = \sqrt{6} \delta_{n_p n_q} \delta_{l_p l_q} \delta_{t_p t_q \pm 1} \hat{j}_p \hat{j}_q (-1)^{l_p + j_p + \frac{3}{2}} \begin{Bmatrix} \frac{1}{2} & \frac{1}{2} & 1 \\ j_q & j_p & l_p \end{Bmatrix} \quad (5.18)$$

$$B_F \equiv \frac{g_V^2}{\hat{j}_I^2} |\mathcal{M}_F|^2 \quad (5.19)$$

$$B_F = \frac{g_V^2}{\hat{j}_I^2} \sum_{\mathcal{F}\mathcal{I}} \frac{\langle \hat{L}^{\mathcal{I}} | \tau | \hat{R}^{\mathcal{F}} \rangle \langle \hat{L}^{\mathcal{F}} | \tau | \hat{R}^{\mathcal{I}} \rangle}{\langle J_{\mathcal{I}} M_{\mathcal{I}}; \lambda - \mu | J_{\mathcal{F}} M_{\mathcal{F}} \rangle^2} \quad (5.20)$$

$$B_{GT} \equiv \frac{g_A^2}{\hat{j}_I^2} |\mathcal{M}_{GT}|^2 \quad (5.21)$$

$$B_{GT} = \frac{g_A^2}{\hat{j}_I^2} \sum_{\mathcal{F}\mathcal{I}} \frac{\langle \hat{L}^{\mathcal{I}} | \sigma \tau | \hat{R}^{\mathcal{F}} \rangle \langle \hat{L}^{\mathcal{F}} | \sigma \tau | \hat{R}^{\mathcal{I}} \rangle}{\langle J_{\mathcal{I}} M_{\mathcal{I}}; \lambda - \mu | J_{\mathcal{F}} M_{\mathcal{F}} \rangle^2} \quad (5.22)$$

$$B_{\beta-} = \langle \Phi_0 | \hat{L}^n (\hat{\beta}^-)^\dagger \hat{R}^p | \Phi_0 \rangle \langle \Phi_0 | \hat{L}^p \hat{\beta}^- \hat{R}^n | \Phi_0 \rangle \quad (5.23)$$

$$B_{\beta-} = \langle \Phi_0 | \hat{L}_p (\hat{\beta}^-)^\dagger \hat{R}_n | \Phi_0 \rangle \langle \Phi_0 | \hat{L}_n \hat{\beta}^- \hat{R}_p | \Phi_0 \rangle \quad (5.24)$$

$$B_{\beta-} = \langle \Phi_0 | \hat{L}_p^n (\hat{\beta}^-)^\dagger \hat{R}_0 | \Phi_0 \rangle \langle \Phi_0 | \hat{L}_0 \hat{\beta}^- \hat{R}_p^n | \Phi_0 \rangle \quad (5.25)$$

$$B_{\beta-} = \langle \Phi_0 | \hat{L}_0 (\hat{\beta}^-)^\dagger \hat{R}_n^p | \Phi_0 \rangle \langle \Phi_0 | \hat{L}_n^p \hat{\beta}^- \hat{R}_0 | \Phi_0 \rangle \quad (5.26)$$

$$B_{\beta+} = \langle \Phi_0 | \hat{L}^p (\hat{\beta}^+)^\dagger \hat{R}^n | \Phi_0 \rangle \langle \Phi_0 | \hat{L}^n \hat{\beta}^+ \hat{R}^p | \Phi_0 \rangle \quad (5.27)$$

$$B_{\beta+} = \langle \Phi_0 | \hat{L}_n (\hat{\beta}^+)^\dagger \hat{R}_p | \Phi_0 \rangle \langle \Phi_0 | \hat{L}_p \hat{\beta}^+ \hat{R}_n | \Phi_0 \rangle \quad (5.28)$$

$$B_{\beta+} = \langle \Phi_0 | \hat{L}_n^p (\hat{\beta}^+)^\dagger \hat{R}_0 | \Phi_0 \rangle \langle \Phi_0 | \hat{L}_0 \hat{\beta}^+ \hat{R}_n^p | \Phi_0 \rangle \quad (5.29)$$

$$B_{\beta+} = \langle \Phi_0 | \hat{L}_0 (\hat{\beta}^+)^\dagger \hat{R}_p^n | \Phi_0 \rangle \langle \Phi_0 | \hat{L}_p^n \hat{\beta}^+ \hat{R}_0 | \Phi_0 \rangle \quad (5.30)$$

Quenching [45, 96, 61, 71]

Chapter 6

Conclusions and Perspectives

Chapter 7

Instructions

If you want to use this class, it's probably a good idea to use the source code of this example document as a starting point.

7.1 Preamble

The document class may be declared using `\documentclass[<type>]{msudissertation}`, where `<type>` is either `dissertation` (default) or `thesis`. The class is based on the `book` class and thus inherits all its structural conventions. The WikiBooks has more information about this: https://en.wikibooks.org/wiki/LaTeX/Document_Structure .

Afterward, you can load your packages. Among those, you may find the following packages useful:

- `\usepackage{hyperref}`: provides hyperlinks (`\url`) and PDF bookmarks
- `\usepackage{pdflscape}`: provides `\begin{landscape}` ... `\end{landscape}`
- `\usepackage{titling}`: provides `\thetitle`, `\theauthor`, and `\thedata`

Refer to their official documentation on CTAN for more details.

To set the title, author, degree program, and date, include the following commands in your preamble:

- `\title{<title>}`

- `\author{<name>}`
- `\def\thedegreeprogram{<subject>---<degree>}`
- `\date{<year>}` (optional) Per university guidelines, the date must be contain only a 4-digit year. If omitted, it defaults to the current year, which could be undesirable if you want the reproduce the document years later.

The rest of the document is divided into three major parts, preceded the special markers `\frontmatter`, `\mainmatter`, and `\appendix` respectively.

7.2 Front matter

In the front matter, certain chapter names have been endowed with special meanings, e.g. `\chapter{Abstract}` or `\chapter{Copyright}`. This is what allows them to have unique formatting. They must be spelled and capitalized exactly as written in the source code of this example, unless otherwise specified. Given that the `\chapter` command has been imbued with some rather fragile (read: hacky) logic, try not to sneeze on them too hard.

The front matter in this example is a lot more packed than your typical dissertation or thesis, because a lot of the chapters are optional and have been filled with placeholder text. They can be safely deleted if neither you nor the university guidelines require them.

7.3 Main matter

The main matter is the most uninteresting part of this template, because it's almost the same as your vanilla book class. Just write `\chapter{<chapter>}` and `\section{<section>}` like you normally do.

Chapter 8

Appendix

You can have as many appendices as you want, or none at all. If you do have *at least one*, use the `\appendix` macro to create a cover page with the correct grammatical number depending on how many you have, and adjusts the table of contents according to university guidelines. After this macro, all uses of `\chapter{<chapter>}` will create an appendix chapter instead of a regular chapter. Do *not* use `\appendix` if you have no appendices at all.

At the very end, there is the mandatory bibliography. Here, I’m assuming you want to use the traditional `natbib`. If so, start by selecting a `\bibliographystyle{<style>}`. If you don’t like calling it “Bibliography”, you can pick a more suitable title using the syntax `\renewcommand{\bibname}{<title>}` as long as it conforms to university guidelines. Afterward, you can write `\bibliography{<name>}` where `<name>` is the path to the `.bib` database without the file extension.

And that’s it! The remaining part of this document is full of placeholder text so you can stop reading now.

Chapter 9

Lorem ipsum

Lorem ipsum dolor sit amet, consectetur adipiscing elit. Ut et leo non tortor viverra sodales. Ut condimentum odio orci, a varius sapien vehicula quis. Pellentesque a lacus sed sem gravida scelerisque. Nunc rutrum ornare fringilla. Donec ac lorem non leo tincidunt finibus quis in lectus.[30]

Pellentesque ac consequat leo. Nulla vel aliquet ex. Nulla non faucibus sapien, eu portitor ligula:

$$I = \int_{-\infty}^{\infty} \frac{x}{1 + e^{-x^2/2}} dx \quad (9.1)$$

Class aptent taciti sociosqu ad litora torquent per conubia nostra, per inceptos himenaeos. In odio metus, maximus sed dictum vel, rhoncus id ante. Phasellus viverra sodales neque ut pulvinar.

Sed neque metus, elementum at risus in, imperdiet iaculis dolor. Vivamus quis libero quis dui finibus imperdiet. Nunc mollis odio eget nibh volutpat interdum. Praesent non felis in sem luctus gravida.

9.1 Pellentesque Scelerisque

Pellentesque scelerisque justo in pellentesque iaculis. Nunc in elementum tortor. Vestibulum tincidunt lacus ac libero gravida, sit amet rhoncus risus iaculis. Sed rhoncus nisl ac felis

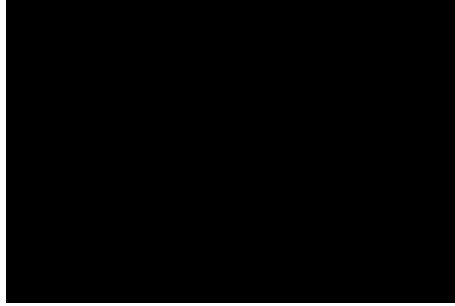


Figure 9.1: Lorem ipsum dolor sit amet, consectetur adipiscing elit. Ut et leo non tortor viverra sodales.

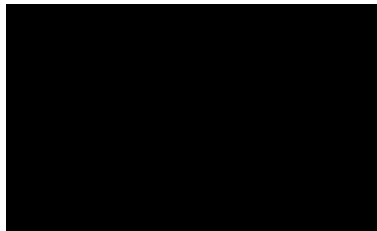


Figure 9.2: Ut condimentum odio orci, a varius sapien vehicula quis.

auctor efficitur. Nulla vel lorem bibendum, laoreet risus vel, euismod odio. Sed a justo augue. Sed sed viverra magna. Etiam vestibulum tellus ut consequat ultricies. Pellentesque mattis odio ac ipsum luctus, ac laoreet ex efficitur. Sed tincidunt, est id viverra ullamcorper, orci dolor accumsan erat, id accumsan tortor est quis ante. Integer pretium elit a ligula tristique imperdiet.

In vitae elit massa. Morbi fermentum arcu quis tristique pretium. Suspendisse potenti. Suspendisse at nisi nec sem dignissim mattis finibus ac sem. Aenean lobortis volutpat turpis, a lacinia ante pellentesque eget. Vivamus fermentum tempus viverra. Sed sollicitudin cursus rutrum. [30]

9.1.1 Fusce Convallis

Fusce convallis placerat porta. Nam porta euismod justo, nec efficitur erat tincidunt non. Proin viverra sagittis nibh, ac rhoncus nibh condimentum in. Nunc tristique augue quis ante

dapibus, sit amet porta purus molestie. Pellentesque sagittis tincidunt eros, eget fermentum nibh viverra dapibus. Phasellus id dignissim sapien. Mauris eget interdum sapien, in hendrerit ante.

Fusce sed eros sem. Mauris posuere egestas risus et sollicitudin. Suspendisse posuere nec lectus a iaculis. In tincidunt nisl consequat sem feugiat mollis. Vivamus ante libero, lobortis id erat vel, fringilla sodales justo. Mauris vel iaculis lectus, non vehicula ipsum. Praesent mollis convallis nibh in ornare. Fusce tincidunt libero sit amet efficitur convallis.

9.2 Curabitur

Curabitur dignissim orci quis orci blandit blandit.¹ Cras cursus tellus quam, sed lacinia nisi scelerisque posuere. Vestibulum sed lacinia orci, id sagittis lorem. Etiam lacinia elementum tortor, ut rutrum tellus laoreet sit amet. Etiam dignissim sagittis sapien in dignissim. Vestibulum ante ipsum primis in faucibus orci luctus et ultrices posuere cubilia Curae; Nullam blandit est vel diam hendrerit posuere. Maecenas nec arcu eu dui semper porttitor.

¹Aenean a semper dolor.

X	O	
O	X	
O		X

Table 9.1: Nulla suscipit ultricies massa at sagittis.

Suspendisse aliquet vel orci volutpat imperdiet. Aenean et ex a nisl volutpat ultrices. Duis pellentesque mi vitae maximus sagittis. Quisque dignissim ante pulvinar, porta odio sed, hendrerit ante. Mauris euismod enim ac nibh laoreet, vel eleifend lacus euismod. Fusce bibendum malesuada magna vitae efficitur.

APPENDICES

Appendix A

Etiam a Convallis

Your appendix goes here.

—

Lorem ipsum dolor sit amet, consectetur adipiscing elit. Sed cursus, ex vitae sagittis tempor, risus ipsum ultrices elit, vel eleifend magna ex in tellus. Proin congue mattis sem, eget gravida tellus iaculis nec. Sed consectetur varius quam convallis tincidunt. Aliquam congue augue vitae lacus dignissim, efficitur condimentum magna lacinia.

Etiam a convallis quam, in feugiat purus. Mauris porta magna ipsum, ac pharetra nisl tristique ac. Nullam consectetur finibus tortor, eget ultrices libero auctor a. Cras facilisis sapien metus, at accumsan ex auctor a. Pellentesque varius non dolor vitae rhoncus. Cras eget ante vitae magna aliquam condimentum. Vestibulum ante ipsum primis in faucibus orci luctus et ultrices posuere cubilia Curae; Donec molestie est consequat maximus dictum.[30]

Nunc Nec Ultrices Justo

Nunc nec ultrices justo, nec rhoncus urna. Proin sagittis tempor purus, nec pulvinar leo varius eget. Etiam a nisi nec neque dignissim molestie. Ut tincidunt vel diam sed imperdiet. Praesent a auctor turpis, in semper ipsum. Sed eu erat interdum, sagittis lectus nec, fringilla felis. Nunc lacus lacus, scelerisque eu mollis ac, ultrices a leo. Aliquam mattis felis enim, in cursus augue dignissim eget. Aenean fermentum mi id facilisis pulvinar.[30]

Aliquam aliquam, lorem elementum mollis ornare, augue felis tristique est, a blandit velit
dui a orci. Sed id nisl dictum, tincidunt dui quis, gravida felis. Curabitur vitae erat at lacus
volutpat iaculis ut ut enim. Nullam vel venenatis metus. Sed rutrum est at lectus elementum
viverra. Nulla sed enim risus.

Appendix B

Nulla Feugiat

1	2	3
4	5	6
7	8	9

Table B.1: Lorem ipsum dolor sit amet, consectetur adipiscing elit. Nulla feugiat ante quis consectetur pellentesque. In tincidunt orci in justo tempor, non tempor metus congue.[30]

Appendix C

Diagrammatic Rules

Appendix D

Angular Momentum Coupling

Two angular momenta, $|j_1 m_1\rangle$ and $|j_2 m_2\rangle$, can be coupled into a state with total angular momentum J and projection M , $|j_1 j_2; JM\rangle$. The coupled state is written as a linear combination of uncoupled states, $|j_1 m_1; j_2 m_2\rangle$.

$$|j_1 j_2; JM\rangle = \sum_{m_1+m_2=M} \langle j_1 m_1; j_2 m_2 | JM \rangle |j_1 m_1; j_2 m_2\rangle \quad (\text{D.1})$$

The coefficients in this expansion, $\langle j_1 m_1; j_2 m_2 | JM \rangle$, are called the Clebsch-Gordon coefficients. They have the symmetry property that introduces a relative phase between states with different coupling orders.

$$\langle j_2 m_2; j_1 m_1 | JM \rangle = (-1)^{j_1+j_2-J} \langle j_1 m_1; j_2 m_2 | JM \rangle \quad (\text{D.2})$$

Appendix E

Coupled Two-Body State

A two-body state relative to some reference vacuum, $|\Phi\rangle$, involving either particles or holes, can be written as the result of acting with the appropriate particle or hole creation operators, $|pq\rangle = p^\dagger q^\dagger |\Phi\rangle$. The letters $\{p, q, r, s, \dots\}$ denote generic particle or hole states, $\{a, b, c, d, \dots\}$ denote particle states, and $\{i, j, k, l, \dots\}$ denote hole states. These M -scheme states, with total angular momentum projection M , can be used to build J -scheme states which are coupled to a total angular momentum J . The generic j -coupled states corresponding to the orbits of p and q are given by $\{\alpha, \beta, \gamma, \dots\}$.

$$|\alpha\beta; JM\rangle = \frac{\sqrt{1 + \delta_{\alpha\beta} (-1)^J}}{1 + \delta_{\alpha\beta}} \left[\alpha^\dagger \beta^\dagger \right]_{JM} |\Phi\rangle = \frac{\sqrt{1 + \delta_{\alpha\beta} (-1)^J}}{1 + \delta_{\alpha\beta}} \sum_{\substack{p \in \alpha \\ q \in \beta}} \langle j_p m_p j_q m_q | JM \rangle p^\dagger q^\dagger |\Phi\rangle \quad (\text{E.1})$$

When the states α and β are coupled in the reverse order, each Clebsch-Gordon coefficient acquires the same phase factor as Eqn. (2) when p and q are switched. Therefore the coupled states show a similar symmetry property as the Clebsch-Gordon coefficients depending on the order of α and β . An additional factor of (-1) comes from anti-commutating the creation operators involved, which must commute because they are only of the particle/hole creation type.

$$|\beta\alpha; JM\rangle = (-1)^{j_\alpha + j_\beta - J + 1} |\alpha\beta; JM\rangle \quad (\text{E.2})$$

Appendix F

Convergence Acceleration: Direct-Inversion of the Iterative Subspace

Direct-Inversion of the Iterative Subspace (DIIS) is an extension to the damping method to help stabilize and accelerate the convergence. In the damping method, the input amplitude vector to iteration $i + 1$ is a mixture of the output of the two previous iterations, $\tilde{\mathbf{t}}_{i+1} = \alpha \mathbf{t}_i + (1 - \alpha) \mathbf{t}_{i-1}$, where the CCD step is $\mathcal{F}(\tilde{\mathbf{t}}_i) = \mathbf{t}_i$. In DIIS, the input amplitude vector to iteration $i + 1$ is a linear combination of the last l vectors, $\tilde{\mathbf{t}}_{i+1} = \sum_{m=i-l+1}^i c_m \mathbf{t}_m$. Rewriting the vectors as the exact solution, $\mathcal{F}(\mathbf{t}^*) = \mathbf{t}^*$ or $\tilde{\mathbf{t}}_i = \mathbf{t}_i$, plus an error term, $\mathbf{t}_i = \mathbf{t}^* + \mathbf{r}_i$, the interpolated vector can be rewritten, $\tilde{\mathbf{t}}_{i+1} = \sum_{m=i-l+1}^i c_m (\mathbf{t}^* + \mathbf{r}_m) = \sum_{m=i-l+1}^i c_m \mathbf{t}^* + \sum_{m=i-l+1}^i c_m \mathbf{r}_m$. Equating this to the exact solution and minimizing the error vector gives, $\mathbf{t}^* = \lim \left(\sum_{m=i-l+1}^i c_m \mathbf{t}^* + \sum_{m=i-l+1}^i c_m \mathbf{r}_m \right) = \sum_{m=i-l+1}^i c_m \mathbf{t}^*$, so that $\sum_{m=i-l+1}^i c_m = 1$. Therefore, the task is to minimize the norm of the error vector, $\tilde{\mathbf{r}}_{i+1}^\dagger \tilde{\mathbf{r}}_{i+1} = \sum_{m,n=i-l+1}^i c_m c_n \mathbf{r}_m^\dagger \mathbf{r}_n$, with the constraint that the sum of the coefficients is one, $\min \left(\sum_{m,n=i-l+1}^i c_m c_n \mathbf{r}_m^\dagger \mathbf{r}_n - \lambda \left(1 - \sum_{m=i-l+1}^i c_m \right) \right)$. This can be rewritten as a matrix equation with matrix $B_{ij} = \mathbf{r}_i^\dagger \mathbf{r}_j$, $\mathcal{L} = \sum_{m,n=i-l+1}^i c_m c_n B_{mn} - \lambda \left(1 - \sum_{m=i-l+1}^i c_m \right)$.

$$\frac{\partial \mathcal{L}}{\partial c_k} = 0 = \sum_{n=i-l+1}^i c_n B_{kn} + \sum_{m=i-l+1}^i c_m B_{mk} + \lambda = 2 \sum_{n=i-l+1}^i c_n B_{kn} + \lambda \quad (\text{F.1})$$

$$(\text{F.2})$$

Appendix G

CCSD Diagrams

The following diagrams represent the different contributions to the CCSD cluster amplitudes *without* directly building the effective Hamiltonian, \bar{H} . The boxed diagrams are automatically zero in a Hartree-Fock basis.

$$\begin{aligned}
 \hat{f}_N \hat{t}_1 |\Phi_0\rangle_c &= \boxed{\text{diagram 1}} + \text{diagram 2} + \text{diagram 3} \\
 &= \boxed{f_i^a} - \sum_k f_i^k t_k^a + \sum_c f_c^a t_i^c
 \end{aligned} \tag{G.1}$$

The diagrams in equation (G.1) are as follows:
 - **Diagram 1 (boxed):** A vertex with two incoming lines labeled a and i , and a dashed line extending to the right ending in a cross (X).
 - **Diagram 2:** A vertex with two incoming lines labeled a and i , and two outgoing lines labeled k and c . The vertex is connected to a horizontal bar below it.
 - **Diagram 3:** A vertex with two incoming lines labeled i and c , and two outgoing lines labeled a and k . The vertex is connected to a horizontal bar below it.

$$\begin{aligned}
 \hat{V}_N \hat{t}_1 |\Phi_0\rangle_c &= \text{diagram 4} \\
 &= - \sum_{kc} V_{ic}^{ka} t_k^c
 \end{aligned} \tag{G.2}$$

The diagram in equation (G.2) is as follows:
 - **Diagram 4:** A vertex with two incoming lines labeled a and i , and two outgoing lines labeled c and k . The vertex is connected to a horizontal bar below it. A dashed line extends from the vertex to the right, ending in a cross (X).

$$\begin{aligned}
\hat{f}_N \hat{t}_2 |\Phi_0\rangle_c &= \text{Diagram 1} \\
&= \sum_{kc} \boxed{f_c^k t_{ki}^{ac}} \quad (G.3)
\end{aligned}$$

Diagram 1: A dashed box containing a diagram. On the left, a horizontal dashed line with an 'X' at its left end. A vertical line segment connects this dashed line to a vertex. From this vertex, a curved line with an arrow labeled 'c' goes down to a horizontal line, and another curved line with an arrow labeled 'k' goes up to a vertex. From this second vertex, a line with an arrow labeled 'a' goes up and to the right, and another line with an arrow labeled 'i' goes up and to the right. The horizontal line at the bottom is a thick horizontal bar.

$$\begin{aligned}
\hat{V}_N \hat{t}_2 |\Phi_0\rangle_c &= \text{Diagram 2} + \text{Diagram 3} \\
&= \frac{1}{2} \sum_{kcd} V_{cd}^{ka} t_{ki}^{cd} + \frac{1}{2} \sum_{klc} V_{ic}^{kl} t_{kl}^{ca} \quad (G.4)
\end{aligned}$$

Diagram 2: A dashed box containing a diagram. On the left, a horizontal dashed line with an 'X' at its left end. A vertical line segment connects this dashed line to a vertex. From this vertex, a curved line with an arrow labeled 'c' goes down to a horizontal line, and another curved line with an arrow labeled 'k' goes up to a vertex. From this second vertex, a line with an arrow labeled 'a' goes up and to the right, and another line with an arrow labeled 'i' goes up and to the right. The horizontal line at the bottom is a thick horizontal bar.

Diagram 3: A dashed box containing a diagram. On the left, a horizontal dashed line with an 'X' at its left end. A vertical line segment connects this dashed line to a vertex. From this vertex, a curved line with an arrow labeled 'c' goes down to a horizontal line, and another curved line with an arrow labeled 'k' goes up to a vertex. From this second vertex, a line with an arrow labeled 'i' goes up and to the right, and another line with an arrow labeled 'a' goes up and to the right. The horizontal line at the bottom is a thick horizontal bar.

$$\begin{aligned}
\hat{f}_N \hat{t}_1^2 |\Phi_0\rangle_c &= \text{Diagram 4} \\
&= \sum_{kcd} \boxed{f_d^l t_l^a t_i^d} \quad (G.5)
\end{aligned}$$

Diagram 4: A dashed box containing a diagram. On the left, a horizontal dashed line with an 'X' at its left end. A vertical line segment connects this dashed line to a vertex. From this vertex, a line with an arrow labeled 'a' goes up and to the right, and another line with an arrow labeled 'l' goes up and to the right. From this second vertex, a line with an arrow labeled 'd' goes up and to the right, and another line with an arrow labeled 'i' goes up and to the right. The horizontal line at the bottom is a thick horizontal bar.

$$\begin{aligned}
\hat{V}_N \hat{t}_1^2 |\Phi_0\rangle_c &= \text{diagram 1} + \text{diagram 2} \\
&= \sum_{kcd} V_{cd}^{ka} t_k^c t_i^d + \sum_{klc} V_{ic}^{kl} t_k^c t_l^a
\end{aligned} \tag{G.6}$$

The first diagram shows a loop with vertices \$c\$ and \$d\$, and external lines \$a\$ and \$i\$. The second diagram shows a loop with vertices \$c\$ and \$l\$, and external lines \$i\$ and \$a\$.

$$\begin{aligned}
\hat{V}_N \hat{t}_1 \hat{t}_2 |\Phi_0\rangle_c &= \text{diagram 1} + \text{diagram 2} + \text{diagram 3} \\
&= -\frac{1}{2} \sum_{klcd} V_{cd}^{kl} t_{ki}^{cd} t_l^a - \frac{1}{2} \sum_{klcd} V_{cd}^{kl} t_{kl}^{ca} t_i^d + \sum_{klcd} V_{cd}^{kl} t_{il}^{ad} t_k^c
\end{aligned} \tag{G.7}$$

The diagrams represent various combinations of loops and external lines. The first two diagrams show loops with vertices \$c\$ and \$d\$, and external lines \$a\$ and \$i\$. The third diagram shows a loop with vertices \$c\$ and \$l\$, and external lines \$a\$ and \$i\$.

$$\begin{aligned}
\hat{V}_N \hat{t}_1^3 |\Phi_0\rangle_c &= \text{diagram 1} \\
&= - \sum_{klcd} V_{cd}^{kl} t_k^c t_i^d t_l^a
\end{aligned} \tag{G.8}$$

The diagram shows a loop with vertices \$c\$ and \$d\$, and external lines \$a\$ and \$i\$.

$$\begin{aligned}
\hat{V}_N |\Phi_0\rangle_c &= \text{diagram 1} \\
&= V_{ij}^{ab}
\end{aligned} \tag{G.9}$$

The diagram shows two vertices \$i\$ and \$j\$ connected by a dashed line, with external lines \$a\$ and \$b\$.

$$\begin{aligned}
\hat{f}_N \hat{t}_2 |\Phi_0\rangle_c &= \text{Diagram 1} + \text{Diagram 2} \\
&= \hat{P}(ab) \sum_c f_c^b t_{ij}^{ac} - \hat{P}(ij) \sum_k f_j^k t_{ik}^{ab}
\end{aligned} \tag{G.10}$$

The diagrams show two terms. The first term is a vertex with four external lines: two incoming from the left (labeled i and a) and two outgoing to the right (labeled j and b). A dashed line connects the two internal vertices, with a cross at the right end. The second term is similar, but the incoming lines are labeled a and i , and the outgoing lines are labeled b and j . The dashed line connects the two internal vertices, with a cross at the right end.

$$\begin{aligned}
\hat{V}_N \hat{t}_1 |\Phi_0\rangle_c &= \text{Diagram 1} + \text{Diagram 2} \\
&= -\hat{P}(ab) \sum_k V_{ij}^{kb} t_k^a + \hat{P}(ij) \sum_c V_{cj}^{ab} t_i^c
\end{aligned} \tag{G.11}$$

The diagrams show two terms. The first term is a vertex with four external lines: two incoming from the left (labeled a and i) and two outgoing to the right (labeled j and b). A dashed line connects the two internal vertices, with a cross at the right end. The second term is similar, but the incoming lines are labeled i and a , and the outgoing lines are labeled j and b . The dashed line connects the two internal vertices, with a cross at the right end.

$$\begin{aligned}
\hat{V}_N \hat{t}_2 |\Phi_0\rangle_c &= \text{Diagram 1} + \text{Diagram 2} + \text{Diagram 3} \\
&= \frac{1}{2} \sum_{kl} V_{ij}^{kl} t_{kl}^{ab} + \frac{1}{2} \sum_{cd} V_{cd}^{ab} t_{ij}^{cd} - \hat{P}(ij|ab) \sum_{kc} V_{ic}^{kb} t_{kj}^{ac}
\end{aligned} \tag{G.12}$$

The diagrams show three terms. The first term is a vertex with four external lines: two incoming from the left (labeled a and i) and two outgoing to the right (labeled j and b). A dashed line connects the two internal vertices, with a cross at the right end. The second term is similar, but the incoming lines are labeled i and a , and the outgoing lines are labeled j and b . The dashed line connects the two internal vertices, with a cross at the right end. The third term is similar, but the incoming lines are labeled a and i , and the outgoing lines are labeled b and j . The dashed line connects the two internal vertices, with a cross at the right end.

$$\begin{aligned}
\hat{V}_N \hat{t}_1^2 |\Phi_0\rangle_c &= \text{Diagram 1} + \text{Diagram 2} + \text{Diagram 3} \\
&= \sum_{kl} V_{ij}^{kl} t_k^a t_l^b + \sum_{cd} V_{cd}^{ab} t_i^c t_j^d - \hat{P}(ij|ab) \sum_{kc} V_{ic}^{kb} t_k^a t_j^c
\end{aligned} \tag{G.13}$$

The diagrams show three terms. The first term is a vertex with four external lines: two incoming from the left (labeled a and i) and two outgoing to the right (labeled j and b). A dashed line connects the two internal vertices, with a cross at the right end. The second term is similar, but the incoming lines are labeled i and a , and the outgoing lines are labeled j and b . The dashed line connects the two internal vertices, with a cross at the right end. The third term is similar, but the incoming lines are labeled a and i , and the outgoing lines are labeled b and j . The dashed line connects the two internal vertices, with a cross at the right end.

$$\begin{aligned}
\hat{V}_N \hat{t}_2^2 |\Phi_0\rangle_c &= \text{Diagram 1} + \text{Diagram 2} + \text{Diagram 3} \\
&+ \text{Diagram 4} \\
&= \frac{1}{4} \sum_{klcd} V_{cd}^{kl} t_{kl}^{ab} t_{ij}^{cd} + \hat{P}(ab) \sum_{klcd} V_{cd}^{kl} t_{lj}^{ac} t_{ki}^{bd} - \hat{P}(ij) \frac{1}{2} \sum_{klcd} V_{cd}^{kl} t_{lj}^{ab} t_{ki}^{cd} \\
&- \hat{P}(ab) \frac{1}{2} \sum_{klcd} V_{cd}^{kl} t_{ij}^{db} t_{kl}^{ca} \tag{G.14}
\end{aligned}$$

$$\begin{aligned}
\hat{f}_N \hat{t}_1 \hat{t}_2 |\Phi_0\rangle_c &= \text{Diagram 5} + \text{Diagram 6} \\
&= - \left[\hat{P}(ab) \sum_{kc} f_c^k t_k^a t_{ij}^{cb} \right] - \left[\hat{P}(ij) \sum_{kc} f_c^k t_i^c t_{kj}^{ab} \right] \tag{G.15}
\end{aligned}$$

$$\begin{aligned}
\hat{V}_N \hat{t}_1 \hat{t}_2 |\Phi_0\rangle_c = & \text{Diagram 1} + \text{Diagram 2} + \text{Diagram 3} \\
& + \text{Diagram 4} + \text{Diagram 5} + \text{Diagram 6} \\
= & \hat{P}(ij|ab) \sum_{kcd} V_{cd}^{ka} t_{jk}^{bc} t_i^d - \hat{P}(ij|ab) \sum_{klc} V_{ci}^{kl} t_{jk}^{bc} t_l^a - \hat{P}(ab) \frac{1}{2} \sum_{kcd} V_{cd}^{kb} t_{ij}^{cd} t_k^a \\
& + \hat{P}(ij) \frac{1}{2} \sum_{klc} V_{cj}^{kl} t_{kl}^{ab} t_i^c + \hat{P}(ab) \sum_{kcd} V_{cd}^{ka} t_k^c t_{ij}^{db} - \hat{P}(ij) \sum_{klc} V_{ci}^{kl} t_k^c t_{lj}^{ab} \quad (\text{G.16})
\end{aligned}$$

$$\begin{aligned}
\hat{V}_N \hat{t}_1^3 |\Phi_0\rangle_c = & \text{Diagram 7} + \text{Diagram 8} \\
= & -\hat{P}(ij|ab) \sum_{kcd} V_{cd}^{kb} t_k^a t_i^c t_j^d + \hat{P}(ij|ab) \sum_{klc} V_{cj}^{kl} t_i^c t_k^a t_l^b \quad (\text{G.17})
\end{aligned}$$

$$\begin{aligned}
\hat{V}_N \hat{t}_1^2 \hat{t}_2 |\Phi_0\rangle_c = & \text{Diagram 1} + \text{Diagram 2} + \text{Diagram 3} \\
& + \text{Diagram 4} + \text{Diagram 5} \\
= & \frac{1}{2} \sum_{klcd} V_{cd}^{kl} t_{kl}^{ab} t_i^c t_j^d + \frac{1}{2} \sum_{klcd} V_{cd}^{kl} t_{ij}^{cd} t_k^a t_l^b + \hat{P}(ij|ab) \sum_{klcd} V_{cd}^{kl} t_{lj}^{ac} t_k^b t_i^d \\
& - \hat{P}(ij) \frac{1}{2} \sum_{klcd} V_{cd}^{kl} t_{lj}^{ab} t_k^c t_i^d - \hat{P}(ab) \frac{1}{2} \sum_{klcd} V_{cd}^{kl} t_{ij}^{db} t_k^c t_l^a
\end{aligned} \tag{G.18}$$

$$\begin{aligned}
\hat{V}_N \hat{t}_1^4 |\Phi_0\rangle_c = & \text{Diagram 6} \\
= & \sum_{klcd} V_{cd}^{kl} t_k^a t_l^b t_i^c t_j^d
\end{aligned} \tag{G.19}$$

Appendix H

Computational Implementation

The sums involved in building the CC effective Hamiltonian, solving the CC equations, solving the EOM-CC equations, and building effective operators can all be reformulated as matrix-matrix multiplications and thus performed with efficient LAPACK and BLAS routines. To take advantage of this efficiency, the various cluster amplitudes and matrix elements must be grouped into structures with similar index structure. An additional benefit to these structures is that angular-momentum-coupling coefficients are automatically removed by summing over Clebsch-Gordon coefficients ($\sum_{m_1 m_2} C_{m_1 m_2 M}^{j_1 j_2 J} C_{m_1 m_2 M'}^{j_1 j_2 J'} = \delta_{JJ'} \delta_{MM'}$).

Structure Definitions

The matrix structures are based on channels that separate states with different symmetries depending on a system's conserved quantum numbers, given by $\vec{\xi}$, so that $|p\rangle \in \vec{\xi}_3$. This separation can be applied to direct two-body states ($|pq\rangle \rightarrow \vec{\xi}_p + \vec{\xi}_q \in \vec{\xi}_1$) and cross two-body states ($|p\bar{q}\rangle \rightarrow \vec{\xi}_p - \vec{\xi}_q \in \vec{\xi}_2$). Additionally, cross three-body states can be separated as one-body states ($|pq\bar{s}\rangle \rightarrow \vec{\xi}_p + \vec{\xi}_q - \vec{\xi}_r \in \vec{\xi}_3$).

For a one-body operator $A_q^p \left\{ \hat{a}_p^\dagger \hat{a}_q \right\}$, there is a direct-channel matrix element and a cross-channel matrix element,

$$\mathbf{A}_1 = A_q^p \quad \mathbf{A}_2 = A^{p\bar{q}} \quad (\text{H.1})$$

For a two-body operator $A_{rs}^{pq} \left\{ \hat{a}_p^\dagger \hat{a}_q^\dagger \hat{a}_s \hat{a}_r \right\}$, there is a direct-channel matrix element, four cross-channel matrix elements, and four one-channel matrix elements,

$$\begin{aligned} \mathbf{A}_1 &= A_{rs}^{pq} \\ \mathbf{A}_{2_1} &= A_{r\bar{q}}^{p\bar{s}} \quad \mathbf{A}_{2_2} = A_{s\bar{p}}^{q\bar{r}} \quad \mathbf{A}_{2_3} = A_{s\bar{q}}^{p\bar{r}} \quad \mathbf{A}_{2_4} = A_{r\bar{p}}^{q\bar{s}} \\ \mathbf{A}_{3_1} &= A_{rs\bar{q}}^p \quad \mathbf{A}_{3_2} = A_{rs\bar{p}}^q \quad \mathbf{A}_{3_3} = A_r^{pq\bar{s}} \quad \mathbf{A}_{3_4} = A_s^{pq\bar{r}} \end{aligned} \quad (\text{H.2})$$

For an EOM operator of the form $A_r^{pq} \left\{ \hat{a}_p^\dagger \hat{a}_q^\dagger \hat{a}_r \right\}$, there is a direct-channel matrix element, a one-channel matrix element, and two cross-channel matrix elements,

$$\begin{aligned} \mathbf{A}_1 &= A_r^{pq} & \mathbf{A}_3 &= A_r^{pq\bar{r}} \\ \mathbf{A}_{2_1} &= A_{r\bar{q}}^p & \mathbf{A}_{2_2} &= A_{r\bar{p}}^q \end{aligned} \quad (\text{H.3})$$

EOM operators of the form $A_{qr}^p \left\{ \hat{a}_p^\dagger \hat{a}_r \hat{a}_q \right\}$ has similar structures,

$$\begin{aligned} \mathbf{A}_1 &= A_{qr}^p & \mathbf{A}_3 &= A_{qr\bar{p}} \\ \mathbf{A}_{2_1} &= A_q^{p\bar{r}} & \mathbf{A}_{2_2} &= A_r^{p\bar{q}} \end{aligned} \quad (\text{H.4})$$

\bar{H} , Matrix Form

$$\begin{aligned} X_a^i &= \begin{bmatrix} f_a^i \end{bmatrix} + V_{c\bar{k}}^{i\bar{a}} t^{c\bar{k}} \\ \mathbf{X}_2^{hp} &\leftarrow \begin{bmatrix} \mathbf{f}_2^{hp} \end{bmatrix} + \mathbf{V}_{23}^{hhpp} \cdot \mathbf{t}_2 \end{aligned} \quad (\text{H.5})$$

$$\begin{aligned}
X_b^a &= f_b^a - \frac{1}{2} t_{kl\bar{c}}^a V_b^{kl\bar{c}} + V_{c\bar{k}}^{a\bar{b}} t^{c\bar{k}} - t_k^a X_b^k \\
\mathbf{X}_3^{pp} &\longleftarrow -\frac{1}{2} \mathbf{t}_{31} \cdot \mathbf{V}_{33}^{hhpp} - \mathbf{t}_3 \cdot \mathbf{X}_3^{hp} \\
\mathbf{X}_2^{pp} &\longleftarrow \mathbf{f}_2^{pp} + \mathbf{V}_{24}^{hppp} \cdot \mathbf{t}_2
\end{aligned} \tag{H.6}$$

$$\begin{aligned}
X_j^i &= f_j^i + \frac{1}{2} V_{cd\bar{k}}^i t_j^{cd\bar{k}} + V_{c\bar{k}}^{i\bar{j}} t^{c\bar{k}} \\
\mathbf{X}'_3^{hh} &\longleftarrow \frac{1}{2} \mathbf{V}_{31}^{hhpp} \cdot \mathbf{t}_{33} \\
\mathbf{X}'_2^{hh} &\longleftarrow \mathbf{f}_2^{hh} + \mathbf{V}_{23}^{hhhp} \cdot \mathbf{t}_2
\end{aligned} \tag{H.7}$$

$$\begin{aligned}
X_j^i &= f_j^i + \frac{1}{2} V_{cd\bar{k}}^i t_j^{cd\bar{k}} + V_{c\bar{k}}^{i\bar{j}} t^{c\bar{k}} + X_c^{i_t c} t_j^c \\
\mathbf{X}_3^{hh} &\longleftarrow \frac{1}{2} \mathbf{V}_{31}^{hhpp} \cdot \mathbf{t}_{33} + \mathbf{X}_3^{hp} \cdot \mathbf{t}_3 \\
\mathbf{X}'_2^{hh} &\longleftarrow \mathbf{f}_2^{hh} + \mathbf{V}_{23}^{hhhp} \cdot \mathbf{t}_2
\end{aligned} \tag{H.8}$$

$$\begin{aligned}
X_i^a &= \left[\tilde{f}_i^a \right] + X_c^a t_i^c - t_k^a X_i^k - V_{c\bar{k}}^{a\bar{i}} t^{c\bar{k}} + \frac{1}{2} V_{cd\bar{k}}^a t_i^{cd\bar{k}} - \frac{1}{2} t_{kl\bar{c}}^a V_i^{kl\bar{c}} + t_{k\bar{c}}^{a\bar{i}} X^{k\bar{c}} \\
\mathbf{X}_3^{ph} &\longleftarrow \mathbf{X}_3^{pp} \cdot \mathbf{t}_3 - \mathbf{t}_3 \cdot \mathbf{X}'_3^{hh} + \frac{1}{2} \mathbf{V}_{32}^{hppp} \cdot \mathbf{t}_{34} - \frac{1}{2} \mathbf{t}_{31} \cdot \mathbf{V}_{33}^{hhhp} \\
\mathbf{X}_2^{ph} &\longleftarrow \left[\overset{\sim}{\mathbf{f}}_2^{ph} \right] - \mathbf{V}_{22}^{hphp} \cdot \mathbf{t}_2 + \mathbf{t}_{23} \cdot \mathbf{X}_2^{hp}
\end{aligned} \tag{H.9}$$

$$\begin{aligned}
X_{bc}^{ia} &= V_{bc}^{ia} - \frac{1}{2} t_k^a V_{bc\bar{i}}^k \\
\mathbf{X}'_{32}^{hppp} &\longleftarrow \mathbf{V}_{32}^{hppp} - \frac{1}{2} \mathbf{t}_3 \cdot \mathbf{V}_{32}^{hhpp}
\end{aligned} \tag{H.10}$$

$$\begin{aligned}
X_{bc}^{ia} &= V_{bc}^{ia} - t_k^a V_{bc\bar{i}}^k \\
\mathbf{X}_{32}^{hppp} &\longleftarrow \mathbf{V}_{32}^{hppp} - \mathbf{t}_3 \cdot \mathbf{V}_{32}^{hhpp}
\end{aligned} \tag{H.11}$$

$$\begin{aligned}
X_{ka}^{ij} &= V_{ka}^{ij} + \frac{1}{2} V_c^{ij\bar{a}} t_k^c \\
\mathbf{X}_{33}'^{hhhp} &\longleftarrow \mathbf{V}_{ka}^{ij} + \frac{1}{2} \mathbf{V}_{33}^{hhpp} \cdot \mathbf{t}_3
\end{aligned} \tag{H.12}$$

$$\begin{aligned}
X_{ka}^{ij} &= V_{ka}^{ij} + V_c^{ij\bar{a}} t_k^c \\
\mathbf{X}_{33}^{hhhp} &\longleftarrow \mathbf{V}_{ka}^{ij} + \mathbf{V}_{33}^{hhpp} \cdot \mathbf{t}_3
\end{aligned} \tag{H.13}$$

$$\begin{aligned}
X_{cd}'^{ab} &= V_{cd}^{ab} - \hat{P}(ab) t_k^a X_{cd\bar{b}}'^k \\
\mathbf{X}_1'^{pppp} &\longleftarrow \mathbf{V}_1^{pppp} \\
\mathbf{X}_{31(2)}'^{pppp} &\longleftarrow \mp \mathbf{t}_3 \cdot \mathbf{X}_{31}'^{hhpp}
\end{aligned} \tag{H.14}$$

$$\begin{aligned}
X_{cd}^{ab} &= X_{cd}'^{ab} + \frac{1}{2} t_{kl}^{ab} V_{cd}^{kl} \\
\mathbf{X}_1^{pppp} &\longleftarrow \mathbf{X}_1'^{pppp} + \frac{1}{2} \mathbf{t}_1 \cdot \mathbf{V}_1^{hhpp}
\end{aligned} \tag{H.15}$$

$$\begin{aligned}
X_{kl}^{ij} &= V_{kl}^{ij} + \frac{1}{2} V_{cd}^{ij} t_{kl}^{cd} + \hat{P}(kl) X_c^{ij\bar{k}} t_l^c \\
\mathbf{X}_1^{hhhh} &\longleftarrow \mathbf{V}_1^{hhhh} + \frac{1}{2} \mathbf{V}_1^{hhpp} \cdot \mathbf{t}_1 \\
\mathbf{X}_{33(4)}^{hhhh} &\longleftarrow \mp \mathbf{X}_{34}'^{hhhp} \cdot \mathbf{t}_3
\end{aligned} \tag{H.16}$$

$$\begin{aligned}
X_{jb}^{ia} &= V_{jb}^{ia} + X_c^{iab} t_j^c - \frac{1}{2} t_k^a V_{jb\bar{i}}^k \\
\mathbf{X}_{21}^{hph\bar{p}} &\longleftarrow \mathbf{V}_{21}^{hph\bar{p}} \\
\mathbf{X}_{33}^{hph\bar{p}} &\longleftarrow \mathbf{X}_{33}^{hppp} \cdot \mathbf{t}_3 \\
\mathbf{X}_{32}^{hph\bar{p}} &\longleftarrow -\frac{1}{2} \mathbf{t}_3 \cdot \mathbf{V}_{32}^{hhhp}
\end{aligned} \tag{H.17}$$

$$\begin{aligned}
X_{jb}^{\prime\prime ia} &= V_{jb}^{ia} + \frac{1}{2} X_c^{iab} t_j^c - \frac{1}{2} t_k^a V_{jb\bar{i}}^k \\
\mathbf{X}_{21}^{\prime\prime hph\bar{p}} &\longleftarrow \mathbf{V}_{21}^{hph\bar{p}} \\
\mathbf{X}_{33}^{\prime\prime hph\bar{p}} &\longleftarrow \frac{1}{2} \mathbf{X}_{33}^{hppp} \cdot \mathbf{t}_3 \\
\mathbf{X}_{32}^{\prime\prime hph\bar{p}} &\longleftarrow -\frac{1}{2} \mathbf{t}_3 \cdot \mathbf{V}_{32}^{hhhp}
\end{aligned} \tag{H.18}$$

$$\begin{aligned}
X_{jb}^{\prime\prime\prime ia} &= V_{jb}^{ia} + \frac{1}{2} X_c^{iab} t_j^c - t_k^a V_{jb\bar{i}}^k \\
\mathbf{X}_{21}^{\prime\prime\prime hph\bar{p}} &\longleftarrow \mathbf{V}_{21}^{hph\bar{p}} \\
\mathbf{X}_{33}^{\prime\prime\prime hph\bar{p}} &\longleftarrow \frac{1}{2} \mathbf{X}_{33}^{hppp} \cdot \mathbf{t}_3 \\
\mathbf{X}_{32}^{\prime\prime\prime hph\bar{p}} &\longleftarrow -\mathbf{t}_3 \cdot \mathbf{V}_{32}^{hhhp}
\end{aligned} \tag{H.19}$$

$$\begin{aligned}
X_{jb}^{ia} &= V_{jb}^{ia} + X_c^{iab} t_j^c - t_k^a V_{jb\bar{i}}^k - \left(\frac{1}{2}\right) V_{c\bar{k}}^{i\bar{b}} t_{j\bar{a}}^{ck} \\
\mathbf{X}_{21}^{hph\bar{p}} &\longleftarrow \mathbf{V}_{21}^{hph\bar{p}} - \left(\frac{1}{2}\right) \mathbf{V}_{21}^{hhpp} \mathbf{t}_{21} \\
\mathbf{X}_{33}^{hph\bar{p}} &\longleftarrow \mathbf{X}_{33}^{hppp} \cdot \mathbf{t}_3 \\
\mathbf{X}_{32}^{hph\bar{p}} &\longleftarrow -\mathbf{t}_3 \cdot \mathbf{V}_{32}^{hhhp}
\end{aligned} \tag{H.20}$$

$$\begin{aligned}
X'^{ab}_{ic} &= V^{ab}_{ic} + \frac{1}{2}V^{ab\bar{c}}_d t^d_i - \hat{P}(ab) t^a_k X''^k_{ic\bar{b}} \\
\mathbf{X}'^{pphp}_{33} &\longleftarrow \mathbf{V}^{pphp}_{33} + \frac{1}{2}\mathbf{V}^{pppp}_{33} \cdot \mathbf{t}_3 \\
\mathbf{X}'^{pphp}_{31(2)} &\longleftarrow \mp \mathbf{t}_3 \cdot \mathbf{X}''^{hphp}_{31}
\end{aligned} \tag{H.21}$$

$$\begin{aligned}
X^{ab}_{ic} &= V^{ab}_{ic} + V^{ab\bar{c}}_d \mathbf{t}^d_i - \hat{P}(ab) t^a_k X'^k_{ic\bar{b}} - t^{ab\bar{i}}_k X^k_c + \hat{P}(ab) t^{a\bar{i}}_{k\bar{d}} X^{k\bar{d}}_{c\bar{b}} + \frac{1}{2}t^{ab}_{kl} X^{kl}_{ic} \\
\mathbf{X}^{pphp}_{33} &\longleftarrow \mathbf{V}^{pphp}_{33} + \mathbf{V}^{pppp}_{33} \cdot \mathbf{t}_3 \\
\mathbf{X}^{pphp}_{31(2)} &\longleftarrow \mp \mathbf{t}_3 \cdot \mathbf{X}^{hphp}_{31} \\
\mathbf{X}^{pphp}_{34} &\longleftarrow -\mathbf{t}_{34} \cdot \mathbf{X}^{hp}_3 \\
\mathbf{X}^{pphp}_{22(3)} &\longleftarrow \mp \mathbf{t}_{23} \cdot \mathbf{X}^{hppp}_{23} \\
\mathbf{X}^{pphp}_1 &\longleftarrow \frac{1}{2}\mathbf{t}_1 \cdot \mathbf{X}^{hhhp}_1
\end{aligned} \tag{H.22}$$

$$\begin{aligned}
X'^{ia}_{jk} &= V^{ia}_{jk} - \frac{1}{2}t^a_l V^l_{jk\bar{i}} \\
\mathbf{X}'^{hphh}_{32} &\longleftarrow \mathbf{V}^{hphh}_{32} - \frac{1}{2}\mathbf{t}_3 \cdot \mathbf{V}^{hhhh}_{32}
\end{aligned} \tag{H.23}$$

$$\begin{aligned}
X_{jk}^{ia} &= V_{jk}^{ia} - t_l^a V_{jk\bar{i}}^l + \hat{P}(jk) X_c^{''ia\bar{j}} t_k^c + \hat{P}(jk) X_{cl}^{i\bar{j}} t_{k\bar{a}}^{cl} + \frac{1}{2} X_{cd}^{ia} t_{jk}^{cd} + X_c^{ie} t_{jk\bar{a}}^e \\
\mathbf{X}_{32}^{hphh} &\longleftarrow \mathbf{V}_{32}^{hphh} - \mathbf{t}_3 \cdot \mathbf{V}_{32}^{hhhh} \\
\mathbf{X}_{33(4)}^{hphh} &\longleftarrow \mp \mathbf{X}_{34}^{''hphp} \cdot \mathbf{t}_3 \\
\mathbf{X}_{21(3)}^{hphh} &\longleftarrow \mp \mathbf{X}_{23}^{hhhp} \cdot \mathbf{t}_{23} \\
\mathbf{X}_1^{hphh} &\longleftarrow \frac{1}{2} \mathbf{X}_1^{hppp} \cdot \mathbf{t}_1 \\
\mathbf{X}_{31}^{hphh} &\longleftarrow \mathbf{X}_3^{hp} \cdot \mathbf{t}_{31}
\end{aligned} \tag{H.24}$$

$$\begin{aligned}
X_{ij}^{ab} &= V_{ij}^{ab} + \hat{P}(ab) X_c^a t_{ij\bar{b}}^c - \hat{P}(ij) t_k^{ab\bar{j}} X_i^k + \frac{1}{2} X_{cd}^{ab} t_{ij}^{cd} + \frac{1}{2} t_{kl}^{ab} X_{ij}^{kl} - \hat{P}(ab|ij) t_{k\bar{c}}^{a\bar{j}} X_{i\bar{b}}^{k\bar{c}} - \hat{P}(ab) t_k^a X_{ij\bar{b}}'^k + \hat{P}(ij) t_{k\bar{c}}^{a\bar{j}} X_{i\bar{b}}^{k\bar{c}} \\
\mathbf{X}_1^{pphh} &\longleftarrow \mathbf{V}_1^{pphh} + \frac{1}{2} \mathbf{X}_1^{pppp} \cdot \mathbf{t}_1 + \frac{1}{2} \mathbf{t}_1 \cdot \mathbf{X}_1^{hhhh} \\
\mathbf{X}_{31(2)}^{pphh} &\longleftarrow \pm \mathbf{X}_3^{pp} \cdot \mathbf{t}_{31} \mp \mathbf{t}_3 \mathbf{X}_{31}^{hphh} \\
\mathbf{X}_{33(4)}^{pphh} &\longleftarrow \mp \mathbf{t}_{33} \cdot \mathbf{X}_3^{hh} \pm \mathbf{X}_{34}^{pphp} \mathbf{t}_3 \\
\mathbf{X}_{21(2)}^{pphh} &\longleftarrow -\mathbf{t}_{21} \cdot \mathbf{X}_{21}^{hphp} \\
\mathbf{X}_{23(4)}^{pphh} &\longleftarrow \mathbf{t}_{21} \cdot \mathbf{X}_{21}^{hphp}
\end{aligned} \tag{H.25}$$

\hat{L} , Matrix Form

$$\begin{aligned}
0 &= X_a^i + \lambda_c^i X_a^c - X_k^i \lambda_a^k - X_{k\bar{c}}^{i\bar{a}} \lambda^{k\bar{c}} - \frac{1}{2} \lambda_{cd\bar{k}}^i X_a^{cd\bar{k}} - \frac{1}{2} X_{kl\bar{c}}^i \lambda_a^{kl\bar{c}} + \frac{1}{2} X_{j\bar{k}}^{i\bar{a}} \left(\lambda_{cd\bar{l}}^j t_k^{cd\bar{l}} \right)^{j\bar{k}} - \frac{1}{2} X_{d\bar{c}}^{i\bar{a}} \left(t_{kl\bar{b}}^d \lambda_c^{kl\bar{b}} \right)^{d\bar{c}} \\
\lambda_3 &\leftarrow X_3^{hp} + \lambda_3 X_3^{pp} - X_3^{hh} \lambda_3 - \frac{1}{2} \lambda_{31} X_{34}^{pphp} - \frac{1}{2} X_{31}^{hphh} \lambda_{33} \\
\lambda_2 &\leftarrow -X_{21}^{hphp} \lambda_2 + \frac{1}{2} X_{21}^{hhhp} \left(\lambda_{31} t_{33} \right)_2 - \frac{1}{2} X_{23}^{hppp} \left(t_{32} \lambda_{33} \right)_2
\end{aligned} \tag{H.26}$$

$$\begin{aligned}
0 &= V_{ab}^{ij} + \hat{P}(ab|ij) \left(\lambda_a^i X_b^j \right)_{ab}^{ij} - \hat{P}(ab) X_k^{ij\bar{b}} \lambda_a^k - \hat{P}(ij) \lambda_c^i X_{ab\bar{j}}^c - \hat{P}(ab) \lambda_c^{ij\bar{a}} X_b^c + \hat{P}(ij) X_k^j \lambda_{ab\bar{i}}^k + \frac{1}{2} \lambda_{ca}^{ij} \\
\lambda_1 &\leftarrow V_{\text{hhpp}1} + \hat{P} \left(\lambda_3 X_{\text{hp}3} \right)_1 + \frac{1}{2} \lambda_1 X_{\text{pppp}1} + \frac{1}{2} X_{\text{hhhh}1} \lambda_1 \\
\lambda_{3_{3(4)}} &\leftarrow \mp X_{\text{hhhp}3} \lambda_3 \pm \lambda_{3_3} X_{\text{pp}3} \mp \frac{1}{2} V_{\text{hhpp}3} \left(t_{3_1} \lambda_{3_3} \right) \\
\lambda_{3_{1(2)}} &\leftarrow \mp \lambda_3 X_{\text{hppp}3_2} \mp X_{\text{hh}3} \lambda_{3_1} \mp \frac{1}{2} \left(\lambda_{3_1} t_{3_3} \right) V_{\text{hhpp}3_1} \\
\lambda_{2_{1(2)}} &\leftarrow -X_{\text{hphp}2_1} \lambda_{2_1} \\
\lambda_{2_{3(4)}} &\leftarrow X_{\text{hphp}2_1} \lambda_{2_1}
\end{aligned}$$

\hat{R}_k^+ , Matrix Form

$$\begin{aligned}
\omega_k r^a &= X_c^a r^c + r_{k\bar{c}}^a X^{k\bar{c}} - \frac{1}{2} X_{cd\bar{k}}^a r^{cd\bar{k}} \\
\omega_k \mathbf{r} &\leftarrow \mathbf{X}_3^{pp} \cdot \mathbf{r} + \mathbf{r}_{2_1} \cdot \mathbf{X}_2^{hp} - \frac{1}{2} \mathbf{X}_{3_2}^{hpp} \cdot \mathbf{r}_3
\end{aligned} \tag{H.27}$$

$$\begin{aligned}
\omega_k r_i^{ab} &= -X_c^{ab\bar{i}} r^c + \hat{P}(ab) X_c^b r_{i\bar{a}}^c - r_k^{ab} X_i^k + \frac{1}{2} X_{cd}^{ab} r_i^{cd} - \hat{P}(ab) r_{k\bar{c}}^b X_{i\bar{a}}^{k\bar{c}} - \frac{1}{2} t_k^{ab\bar{i}} V_{cd\bar{l}}^k r^{cd\bar{l}} \\
\omega_k \mathbf{r}_3 &\leftarrow -\mathbf{X}_{3_4}^{pphp} \cdot \mathbf{r} - \frac{1}{2} \mathbf{t}_{3_3} \cdot \mathbf{V}_{3_1}^{hpp} \cdot \mathbf{r}_3 \\
\omega_k \mathbf{r}_{2_{1(2)}} &\leftarrow \mp \mathbf{X}_3^{pp} \cdot \mathbf{r}_{2_2} \pm \mathbf{r}_{2_2} \cdot \mathbf{X}_{2_1}^{hphp} \\
\omega_k \mathbf{r}_1 &\leftarrow -\mathbf{r}_1 \cdot \mathbf{X}_3^{hh} + \frac{1}{2} \mathbf{X}_1^{pppp} \cdot \mathbf{r}_1
\end{aligned} \tag{H.28}$$

\hat{L}_k^+ , Matrix Form

The difference for the left eigenproblem is that disconnected term is computed as an outer product rather than with matrix-matrix multiplication.

$$\begin{aligned}
E_k l_a &= l_c X_a^c - \frac{1}{2} l_{cd\bar{k}} X_a^{cd\bar{k}} \\
E_k \mathbf{l} &\longleftarrow \mathbf{l} \cdot \mathbf{X}_3^{pp} - \frac{1}{2} \mathbf{l}_3 \cdot \mathbf{X}_{34}^{pphp}
\end{aligned} \tag{H.29}$$

$$\begin{aligned}
E_k l_{ab}^i &= \hat{P}(ab) l_a X^{i\bar{b}} - l_c X_{ab\bar{i}}^c - X_k^i l_{ab}^k + \hat{P}(ab) l_c^{i\bar{a}} X_b^c + \frac{1}{2} l_{cd}^i X_{ab}^{cd} - \hat{P}(ab) X_{k\bar{c}}^{i\bar{a}} l_b^{k\bar{c}} - \frac{1}{2} l_{cd\bar{l}} t_k^{cd\bar{l}} V_{ab\bar{i}}^k \\
E_k l_3 &\longleftarrow -\mathbf{l} \cdot \mathbf{X}_{32}^{hppp} - \frac{1}{2} \mathbf{l}_3 \cdot \mathbf{t}_{33} \cdot \mathbf{V}_{31}^{hhpp} \\
E_k \mathbf{l}_{21(2)} &\longleftarrow \pm \mathbf{l} \otimes \mathbf{X}_2^{hp} \mp \mathbf{l}_{22} \cdot \mathbf{X}_3^{pp} \pm \mathbf{X}_{21}^{hhpp} \cdot \mathbf{l}_{22} \\
E_k \mathbf{l}_1 &\longleftarrow -\mathbf{X}_3^{hh} \cdot \mathbf{l}_1 + \frac{1}{2} \mathbf{l}_1 \cdot \mathbf{X}_1^{pppp}
\end{aligned} \tag{H.30}$$

\hat{R}_k^- , Matrix Form

$$\begin{aligned}
\omega_k r_i &= -r_k X_i^k + X_{c\bar{k}} r_i^{c\bar{k}} - \frac{1}{2} r_{kl\bar{c}} X_i^{kl\bar{c}} \\
\omega_k \mathbf{r} &\longleftarrow -\mathbf{r} \cdot \mathbf{X}_3^{hh} + \mathbf{X}_{2'}^{hp} \cdot \mathbf{r}_{21} - \frac{1}{2} \mathbf{r}_3 \cdot \mathbf{X}_{33}^{hhhp}
\end{aligned} \tag{H.31}$$

$$\begin{aligned}
\omega_k r_{ij}^a &= -r_k X_{ij\bar{a}}^k - \hat{P}(ij) r_k^{a\bar{i}} X_j^k + X_c^a r_{ij}^c + \frac{1}{2} r_{kl}^a X_{ij}^{kl} - \hat{P}(ij) X_{c\bar{k}}^{a\bar{i}} r_j^{c\bar{k}} - \frac{1}{2} r_{kl\bar{d}} V_c^{kl\bar{d}} t_{ij\bar{a}}^c \\
\omega_k \mathbf{r}_3 &\longleftarrow -\mathbf{r} \cdot \mathbf{X}_{31}^{hphh} - \frac{1}{2} \mathbf{r}_3 \cdot \mathbf{V}_{33}^{hhpp} \cdot \mathbf{t}_{31} \\
\omega_k \mathbf{r}_{21(2)} &\longleftarrow \pm \mathbf{r}_{22} \cdot \mathbf{X}_3^{hh} \pm \mathbf{X}_{22}^{hhpp} \cdot \mathbf{r}_{22} \\
\omega_k \mathbf{r}_1 &\longleftarrow \mathbf{X}_3^{pp} \cdot \mathbf{r}_1 + \frac{1}{2} \mathbf{r}_1 \cdot \mathbf{X}_1^{hhhh}
\end{aligned} \tag{H.32}$$

$\hat{L}_k^-, \text{ Matrix Form}$

Again, the disconnected term is computed as an outer product rather than with matrix-matrix multiplication.

$$\begin{aligned} E_k l^i &= -X_k^i l^k - \frac{1}{2} X_{kl\bar{c}}^i l^{kl\bar{c}} \\ E_k \mathbf{l} &\longleftarrow -\mathbf{X}_3^{HH} \cdot \mathbf{l} - \frac{1}{2} \mathbf{X}_{31}^{hphh} \cdot \mathbf{l}_3 \end{aligned} \quad (\text{H.33})$$

$$\begin{aligned} E_k l_a^{ij} &= \hat{P}(ij) l^i X_{a\bar{j}} - X_k^{ij\bar{a}} l^k + l_c^{ij} X_a^c - \hat{P}(ij) X_k^j l_{a\bar{i}}^k + \frac{1}{2} X_{kl}^{ij} l_a^{kl} - \hat{P}(ij) l_{c\bar{k}}^j X_{a\bar{i}}^{c\bar{k}} - \frac{1}{2} V_c^{ij\bar{a}} t_{kl\bar{d}}^c l^{kl\bar{d}} \\ E_k l_3 &\longleftarrow -\mathbf{X}_{33}^{hhhp} \cdot \mathbf{l} - \frac{1}{2} \mathbf{V}_{33}^{hhpp} \cdot \mathbf{t}_{31} \cdot \mathbf{l}_3 \\ E_k \mathbf{l}_{2_{1(2)}} &\longleftarrow \pm \mathbf{l} \otimes \mathbf{X}_{2'}^{hp} \pm \mathbf{X}_3^{hh} \cdot \mathbf{l}_{22} \pm \mathbf{l}_{22} \cdot \mathbf{X}_{22}^{hphp} \\ E_k \mathbf{l}_1 &\longleftarrow \mathbf{l}_1 \cdot \mathbf{X}_3^{pp} + \frac{1}{2} \mathbf{X}_1^{hhhh} \cdot \mathbf{l}_1 \end{aligned} \quad (\text{H.34})$$

${}^\lambda \bar{O}, \text{ Matrix Form}$

$$\begin{aligned} {}^\lambda \bar{O}_a^i &= {}^\lambda O_a^i \\ {}^\lambda \bar{\mathbf{O}}_3^{hp} &\longleftarrow {}^\lambda \mathbf{O}_3^{hp} \end{aligned} \quad (\text{H.35})$$

$$\begin{aligned} {}^\lambda \bar{O}_b^a &= {}^\lambda O_b^a - t_k^{a\lambda} \bar{O}_b^k \\ {}^\lambda \bar{\mathbf{O}}_3^{pp} &\longleftarrow {}^\lambda \mathbf{O}_3^{pp} - \mathbf{t}_3 \cdot {}^\lambda \bar{\mathbf{O}}_3^{hp} \end{aligned} \quad (\text{H.36})$$

$$\begin{aligned}
\lambda \bar{O}_j^i &= \lambda O_j^i + \lambda \bar{O}_c^i t_j^c \\
\lambda \bar{\mathbf{O}}_3^{hh} &\longleftarrow \lambda \mathbf{O}_3^{hh} + \lambda \bar{\mathbf{O}}_3^{hp} \cdot \mathbf{t}_3
\end{aligned} \tag{H.37}$$

$$\begin{aligned}
\lambda \bar{O}_i^a &= \lambda O_i^a + \lambda \bar{O}_c^a t_i^c - t_k^a \lambda \bar{O}_i^k + t_{k\bar{c}}^{a\bar{i}} \lambda \bar{O}^{k\bar{c}} \\
\lambda \bar{\mathbf{O}}_3^{ph} &\longleftarrow \lambda \mathbf{O}_3^{ph} + \lambda \bar{\mathbf{O}}_3^{pp} \cdot \mathbf{t}_3 - \mathbf{t}_3 \cdot \lambda \bar{\mathbf{O}}_{hh}^3 \\
\lambda \bar{\mathbf{O}}_2^{ph} &\longleftarrow \mathbf{t}_{23} \cdot \lambda \bar{\mathbf{O}}_2^{hp}
\end{aligned} \tag{H.38}$$

$$\begin{aligned}
\lambda \bar{O}_{ic}^{ab} &= -t_k^{ab\bar{i}} \lambda \bar{O}_c^k \\
\lambda \bar{\mathbf{O}}_{34}^{pphp} &\longleftarrow -\mathbf{t}_{34} \cdot \lambda \bar{\mathbf{O}}_3^{hp}
\end{aligned} \tag{H.39}$$

$$\begin{aligned}
\lambda \bar{O}_{jk}^{ia} &= \lambda \bar{O}_c^i t_{jk\bar{a}}^c \\
\lambda \bar{\mathbf{O}}_{31}^{hphh} &\longleftarrow \lambda \bar{\mathbf{O}}_3^{hp} \cdot \mathbf{t}_{31}
\end{aligned} \tag{H.40}$$

$$\begin{aligned}
\lambda \bar{O}_{ij}^{ab} &= \hat{P}(ab) \lambda \bar{O}_c^a t_{ij\bar{b}}^c - \hat{P}(ij) t_k^{ab\bar{j}} \lambda \bar{O}_i^k \\
\lambda \bar{\mathbf{O}}_{31(2)}^{pphh} &\longleftarrow \pm \lambda \bar{\mathbf{O}}_3^{pp} \cdot \mathbf{t}_{31} \\
\lambda \bar{\mathbf{O}}_{33(4)}^{pphh} &\longleftarrow \mp \mathbf{t}_{33} \cdot \lambda \bar{\mathbf{O}}_3^{hh}
\end{aligned} \tag{H.41}$$

Appendix I

Angular Momentum Coupling

Before deriving useful equations for J-scheme angular momentum coupling, it's necessary to list some shorthand notations and definitions:

$$\hat{p} \equiv \sqrt{2j_p + 1} \quad (\text{I.1})$$

$$\sum_{\{m\}} \equiv \text{sum over all } m \quad (\text{I.2})$$

Clebsch-Gordan coefficients:

$$\langle pq|J\rangle \equiv \langle j_p m_p; j_q m_q | JM \rangle \quad (\text{I.3})$$

$$\langle p\bar{q}|J\rangle \equiv \langle j_p, m_p; j_q, -m_q | JM \rangle (-1)^{(q-m_q)} \quad (\text{I.4})$$

$$\sum_{JM} \langle pq|J\rangle \langle p'q'|J\rangle = \delta_{m_p m_{p'}} \delta_{m_q m_{q'}} \quad (\text{I.5})$$

$$\sum_{m_p m_q} \langle pq|J\rangle \langle pq|J'\rangle = \delta_{JJ'} \delta_{MM'} \quad (\text{I.6})$$

Two-body J-scheme matrix elements in terms of M-scheme matrix elements:

$$X_{rsJ}^{pqJ} = \sum_{\{m\}} X_{rm_r sm_s}^{pmpqm_q} \langle pq|J\rangle \langle rs|J\rangle \quad (\text{I.7})$$

$$X_{r\bar{q}J'}^{p\bar{s}J'} = \sum_{\{m\}} X_{rm_r sm_s}^{pmpqm_q} \langle p\bar{s}|J'\rangle \langle r\bar{q}|J'\rangle \quad (\text{I.8})$$

$$X_{rsJ\bar{q}}^p = \sum_{\{m\}} X_{rm_r sm_s}^{pmpqm_q} \langle rs|J\rangle \langle J\bar{q}|p\rangle \quad (\text{I.9})$$

$$X_r^{pqJ\bar{s}} = \sum_{\{m\}} X_{rm_r sm_s}^{pmpqm_q} \langle pq|J\rangle \langle J\bar{s}|r\rangle \quad (\text{I.10})$$

$$(\text{I.11})$$

Two-body M-scheme matrix elements in terms of J-scheme matrix elements:

$$X_{rm_r sm_s}^{pmpqm_q} = \sum_{JM} X_{rsJ}^{pqJ} \langle pq|J\rangle \langle rs|J\rangle \quad (\text{I.12})$$

$$= \sum_{J'M'} X_{r\bar{q}J'}^{p\bar{s}J'} \langle p\bar{s}|J'\rangle \langle r\bar{q}|J'\rangle \quad (\text{I.13})$$

$$= \sum_{JM} X_{rsJ\bar{q}}^p \langle rs|J\rangle \langle J\bar{q}|p\rangle \quad (\text{I.14})$$

$$= \sum_{JM} X_r^{pqJ\bar{s}} \langle pq|J\rangle \langle J\bar{s}|r\rangle \quad (\text{I.15})$$

$$(\text{I.16})$$

$$\lambda R_i^{abJ} = \lambda \mathbb{R}_i^{abJ} \frac{\langle J\bar{i}|\lambda\rangle}{\hat{\lambda}} (-1)^{2\lambda} \quad (\text{I.17})$$

$$\lambda \mathbb{R}_i^{abJ} = \sum_{J'} \lambda \mathbb{R}_{i\bar{b}J'}^a \hat{J} \hat{J}' \left\{ \begin{matrix} a & b & J \\ i & \lambda & J' \end{matrix} \right\} (-1)^{\lambda-a+J'} \quad (\text{I.18})$$

$$\lambda \mathbb{R}_{ij}^a = \sum_{J'} \lambda \mathbb{R}_i^{a\bar{j}J'} \hat{J} \hat{J}' \left\{ \begin{matrix} i & j & J \\ a & \lambda & J' \end{matrix} \right\} (-1)^{\lambda+a-J} \quad (\text{I.19})$$

REFERENCES

REFERENCES

- [1] Derivation of the brueckner many-body theory. *Proceedings of the Royal Society of London A: Mathematical, Physical and Engineering Sciences*, 239(1217):267–279, 1957.
- [2] Frank T. Avignone, Steven R. Elliott, and Jonathan Engel. Double beta decay, majorana neutrinos, and neutrino mass. *Rev. Mod. Phys.*, 80:481–516, Apr 2008.
- [3] R. F. Bacher. The interaction of configurations: $sd - p^2$. *Phys. Rev.*, 43:264–269, Feb 1933.
- [4] F.C. Barker, B.A. Brown, W. Jaus, and G. Rasche. Determination of $\nu\nu$ from fermi decays and the unitarity of the km -mixing matrix. *Nuclear Physics A*, 540(3):501 – 519, 1992.
- [5] Bruce R. Barrett, Petr Navrátil, and James P. Vary. Ab initio no core shell model. *Progress in Particle and Nuclear Physics*, 69(Supplement C):131 – 181, 2013.
- [6] Rodney J. Bartlett and Monika Musiał. Coupled-cluster theory in quantum chemistry. *Rev. Mod. Phys.*, 79:291–352, Feb 2007.
- [7] Omar Benhar, Nicola Farina, Hiroki Nakamura, Makoto Sakuda, and Ryoichi Seki. Electron- and neutrino-nucleus scattering in the impulse approximation regime. *Phys. Rev. D*, 72:053005, Sep 2005.
- [8] H. A. Bethe. Nuclear many-body problem. *Phys. Rev.*, 103:1353–1390, Sep 1956.
- [9] Sven Binder, Piotr Piecuch, Angelo Calci, Joachim Langhammer, Petr Navrátil, and Robert Roth. Extension of coupled-cluster theory with a noniterative treatment of connected triply excited clusters to three-body hamiltonians. *Phys. Rev. C*, 88:054319, Nov 2013.
- [10] R. M. Bionta, G. Blewitt, C. B. Bratton, D. Casper, A. Ciocio, R. Claus, B. Cortez, M. Crouch, S. T. Dye, S. Errede, G. W. Foster, W. Gajewski, K. S. Ganezer, M. Goldhaber, T. J. Haines, T. W. Jones, D. Kielczewska, W. R. Kropp, J. G. Learned, J. M. LoSecco, J. Matthews, R. Miller, M. S. Mudan, H. S. Park, L. R. Price, F. Reines, J. Schultz, S. Seidel, E. Shumard, D. Sinclair, H. W. Sobel, J. L. Stone, L. R. Sulak, R. Svoboda, G. Thornton, J. C. van der Velde, and C. Wuest. Observation of a neutrino burst in coincidence with supernova 1987a in the large magellanic cloud. *Phys. Rev. Lett.*, 58:1494–1496, Apr 1987.
- [11] S. K. Bogner, H. Hergert, J. D. Holt, A. Schwenk, S. Binder, A. Calci, J. Langhammer, and R. Roth. Nonperturbative shell-model interactions from the in-medium similarity renormalization group. *Phys. Rev. Lett.*, 113:142501, Oct 2014.
- [12] S. K. Bogner, H. Hergert, J. D. Holt, A. Schwenk, S. Binder, A. Calci, J. Langhammer, and R. Roth. Nonperturbative shell-model interactions from the in-medium similarity renormalization group. *Phys. Rev. Lett.*, 113:142501, Oct 2014.

- [13] S.K. Bogner, R.J. Furnstahl, and A. Schwenk. From low-momentum interactions to nuclear structure. *Progress in Particle and Nuclear Physics*, 65(1):94 – 147, 2010.
- [14] Baird H. Brandow. Linked-cluster expansions for the nuclear many-body problem. *Rev. Mod. Phys.*, 39:771–828, Oct 1967.
- [15] L. Brillouin. Les problèmes de perturbations et les champs self-consistents. *Le journal de physique et le radium*, 3(9):373–389, 1932.
- [16] B. A. Brown and B. H. Wildenthal. Corrections to the free-nucleon values of the single-particle matrix elements of the $m1$ and gamow-teller operators, from a comparison of shell-model predictions with sd-shell data. *Phys. Rev. C*, 28:2397–2413, Dec 1983.
- [17] Charles G Broyden. A class of methods for solving nonlinear simultaneous equations. *Math. Comput.*, 19(92):577–593, 1965.
- [18] K. A. Brueckner and C. A. Levinson. Approximate reduction of the many-body problem for strongly interacting particles to a problem of self-consistent fields. *Phys. Rev.*, 97:1344–1352, Mar 1955.
- [19] S. Bustabad, G. Bollen, M. Brodeur, D. L. Lincoln, S. J. Novario, M. Redshaw, R. Ringle, S. Schwarz, and A. A. Valverde. First direct determination of the ^{48}Ca double- β decay q value. *Phys. Rev. C*, 88:022501, Aug 2013.
- [20] Nicola Cabibbo. Unitary symmetry and leptonic decays. *Phys. Rev. Lett.*, 10:531–533, Jun 1963.
- [21] J. Carlson, S. Gandolfi, F. Pederiva, Steven C. Pieper, R. Schiavilla, K. E. Schmidt, and R. B. Wiringa. Quantum monte carlo methods for nuclear physics. *Rev. Mod. Phys.*, 87:1067–1118, Sep 2015.
- [22] J. Cizek and J. Paldus. Correlation problems in atomic and molecular systems iii. rederivation of the coupled-pair many-electron theory using the traditional quantum chemical methodst. *International Journal of Quantum Chemistry*, 5(4):359–379, 1971.
- [23] J. Cizek and J. Paldus. Coupled cluster approach. *Physica Scripta*, 21(3-4):251, 1980.
- [24] Jiri Cizek. On the correlation problem in atomic and molecular systems. calculation of wavefunction components in urselltype expansion using quantumfield theoretical methods. *The Journal of Chemical Physics*, 45(11):4256–4266, 1966.
- [25] D. B. Cline, G. M. Fuller, W. P. Hong, B. Meyer, and J. Wilson. Prospects for detection of a cosmologically significant neutrino mass from a galactic supernova neutrino burst using a neutral-current-based detector. *Phys. Rev. D*, 50:720–729, Jul 1994.
- [26] F. Coester. Bound states of a many-particle system. *Nuclear Physics*, 7(Supplement C):421 – 424, 1958.
- [27] F. Coester and H. Kmmel. Short-range correlations in nuclear wave functions. *Nuclear Physics*, 17(Supplement C):477 – 485, 1960.

- [28] E. U. Condon. The theory of complex spectra. *Phys. Rev.*, 36:1121–1133, Oct 1930.
- [29] E. U. Condon. The theory of complex spectra. *Phys. Rev.*, 36:1121–1133, Oct 1930.
- [30] Jane Doe and John Smith. Lorem ipsum dolor sit amet, consectetur adipiscing elit. *Lor. Ips.*, 45:123, 2000.
- [31] A. Ekström, G. R. Jansen, K. A. Wendt, G. Hagen, T. Papenbrock, S. Bacca, B. Carlsson, and D. Gazit. Effects of three-nucleon forces and two-body currents on gamow-teller strengths. *Phys. Rev. Lett.*, 113:262504, Dec 2014.
- [32] S. R. Elliott, A. A. Hahn, and M. K. Moe. Direct evidence for two-neutrino double-beta decay in ^{82}Se . *Phys. Rev. Lett.*, 59:2020–2023, Nov 1987.
- [33] Jonathan Engel. Nuclear matrix elements for double- β decay. *XXVI International Conference on Neutrino Physics and Astrophysics (Neutrino 2014)*, 1666, 2015.
- [34] E. Epelbaum, H.-W. Hammer, and Ulf-G. Meißner. Modern theory of nuclear forces. *Rev. Mod. Phys.*, 81:1773–1825, Dec 2009.
- [35] G.T. Ewan. The sudbury neutrino observatory. *Nuclear Instruments and Methods in Physics Research Section A: Accelerators, Spectrometers, Detectors and Associated Equipment*, 314(2):373 – 379, 1992.
- [36] E. Fermi. Versuch einer Theorie der β -Strahlen. I. *Zeitschrift für Physik*, 88:161–177, March 1934.
- [37] A.L. Fetter and J.D. Walecka. *Quantum Theory of Many-particle Systems*. Dover Books on Physics. Dover Publications, 2003.
- [38] V. Fock. Näherungsmethode zur lösung des quantenmechanischen mehrkörperproblems. *Zeitschrift für Physik*, 61(1):126–148, Jan 1930.
- [39] Lee M. Frantz and Robert L. Mills. Many-body basis for the optical model. *Nuclear Physics*, 15:16 – 32, 1960.
- [40] J. R. Gour, P. Piecuch, M. Hjorth-Jensen, M. Włoch, and D. J. Dean. Coupled-cluster calculations for valence systems around ^{16}O . *Phys. Rev. C*, 74:024310, Aug 2006.
- [41] K. Gulyuz, J. Ariche, G. Bollen, S. Bustabad, M. Eibach, C. Izzo, S. J. Novario, M. Redshaw, R. Ringle, R. Sandler, S. Schwarz, and A. A. Valverde. Determination of the direct double- β -decay q value of ^{96}Zr and atomic masses of $^{90-92,94,96}\text{Zr}$ and $^{92,94-98,100}\text{Mo}$. *Phys. Rev. C*, 91:055501, May 2015.
- [42] G. Hagen, A. Ekström, C. Forssén, G. R. Jansen, W. Nazarewicz, T. Papenbrock, K. A. Wendt, S. Bacca, N. Barnea, B. Carlsson, C. Drischler, K. Hebeler, M. Hjorth-Jensen, M. Miorelli, G. Orlandini, A. Schwenk, and J. Simonis. Neutron and weak-charge distributions of the ^{48}Ca nucleus. *Nature Physics*, 12:186 EP –, Nov 2015. Article.

- [43] G. Hagen, T. Papenbrock, M. Hjorth-Jensen, and D. J. Dean. Coupled-cluster computations of atomic nuclei. *Rep. Prog. in Phys.*, 77(9):096302, Sep 2014.
- [44] J. C. Hardy and I. S. Towner. Superaligned $0^+ \rightarrow 0^+$ nuclear β decays: A critical survey with tests of the conserved vector current hypothesis and the standard model. *Phys. Rev. C*, 71:055501, May 2005.
- [45] J. C. Hardy and I. S. Towner. Superaligned $0^+ \rightarrow 0^+$ nuclear β decays: A critical survey with tests of the conserved vector current hypothesis and the standard model. *Phys. Rev. C*, 71:055501, May 2005.
- [46] C.K. Hargrove, I. Batkin, M.K. Sundaresan, and J. Dubeau. A lead astronomical neutrino detector: Land. *Astroparticle Physics*, 5(2):183 – 196, 1996.
- [47] D. R. Hartree. The wave mechanics of an atom with a non-coulomb central field. part i. theory and methods. *Mathematical Proceedings of the Cambridge Philosophical Society*, 24(1):89110, 1928.
- [48] H Hergert. In-medium similarity renormalization group for closed and open-shell nuclei. *Physica Scripta*, 92(2):023002, 2017.
- [49] H. Hergert, S. Binder, A. Calci, J. Langhammer, and R. Roth. Ab initio calculations of even oxygen isotopes with chiral two-plus-three-nucleon interactions. *Phys. Rev. Lett.*, 110:242501, Jun 2013.
- [50] H. Hergert, S. K. Bogner, T. D. Morris, S. Binder, A. Calci, J. Langhammer, and R. Roth. Ab initio multireference in-medium similarity renormalization group calculations of even calcium and nickel isotopes. *Phys. Rev. C*, 90:041302, Oct 2014.
- [51] Heiko Hergert. Private communication.
- [52] K. Hirata, T. Kajita, M. Koshiba, M. Nakahata, Y. Oyama, N. Sato, A. Suzuki, M. Takita, Y. Totsuka, T. Kifune, T. Suda, K. Takahashi, T. Tanimori, K. Miyano, M. Yamada, E. W. Beier, L. R. Feldscher, S. B. Kim, A. K. Mann, F. M. Newcomer, R. Van, W. Zhang, and B. G. Cortez. Observation of a neutrino burst from the supernova sn1987a. *Phys. Rev. Lett.*, 58:1490–1493, Apr 1987.
- [53] J. Hubbard. The description of collective motions in terms of many-body perturbation theory. *Proceedings of the Royal Society of London. Series A, Mathematical and Physical Sciences*, 240(1223):539–560, 1957.
- [54] N.M. Hugenholtz. Perturbation theory of large quantum systems. *Physica*, 23(1):481 – 532, 1957.
- [55] G. R. Jansen, J. Engel, G. Hagen, P. Navratil, and A. Signoracci. Ab-initio coupled-cluster effective interactions for the shell model: Application to neutron-rich oxygen and carbon isotopes. *Phys. Rev. Lett.*, 113:142502, Oct 2014.

- [56] G. R. Jansen, M. D. Schuster, A. Signoracci, G. Hagen, and P. Navrátil. Open sd -shell nuclei from first principles. *Phys. Rev. C*, 94:011301, Jul 2016.
- [57] W. Jaus and G. Rasche. Nuclear-structure dependence of $o(\alpha)$ corrections to fermi decays and the value of the kobayashi-maskawa matrix element V_{ud} . *Phys. Rev. D*, 41:166–176, Jan 1990.
- [58] Makoto Kobayashi and Toshihide Maskawa. Cp-violation in the renormalizable theory of weak interaction. *Progress of Theoretical Physics*, 49(2):652–657, 1973.
- [59] E Kolbe, K Langanke, G Martnez-Pinedo, and P Vogel. Neutrinonucleus reactions and nuclear structure. *Journal of Physics G: Nuclear and Particle Physics*, 29(11):2569, 2003.
- [60] K. Kowalski, D. J. Dean, M. Hjorth-Jensen, T. Papenbrock, and P. Piecuch. Coupled cluster calculations of ground and excited states of nuclei. *Phys. Rev. Lett.*, 92:132501, Apr 2004.
- [61] Kuniharu Kubodera, Jean Delorme, and Mannque Rho. Axial currents in nuclei. *Phys. Rev. Lett.*, 40:755–758, Mar 1978.
- [62] H. Kmmel, K.H. Lhrmann, and J.G. Zabolitzky. Many-fermion theory in exps- (or coupled cluster) form. *Physics Reports*, 36(1):1 – 63, 1978.
- [63] K. Langanke, P. Vogel, and E. Kolbe. Signal for supernova ν_μ and ν_τ neutrinos in water Čerenkov detectors. *Phys. Rev. Lett.*, 76:2629–2632, Apr 1996.
- [64] David L. Lincoln, Jason D. Holt, Georg Bollen, Maxime Brodeur, Scott Bustabad, Jonathan Engel, Samuel J. Novario, Matthew Redshaw, Ryan Ringle, and Stefan Schwarz. First direct double- β decay q -value measurement of ^{82}Se in support of understanding the nature of the neutrino. *Phys. Rev. Lett.*, 110:012501, Jan 2013.
- [65] R. Machleidt and D.R. Entem. Chiral effective field theory and nuclear forces. *Physics Reports*, 503(1):1 – 75, 2011.
- [66] H. S. Miley, F. T. Avignone, R. L. Brodzinski, J. I. Collar, and J. H. Reeves. Suggestive evidence for the two-neutrino double- β decay of ^{76}Ge . *Phys. Rev. Lett.*, 65:3092–3095, Dec 1990.
- [67] Chr. Møller and M. S. Plesset. Note on an approximation treatment for many-electron systems. *Phys. Rev.*, 46:618–622, Oct 1934.
- [68] P. Navrátil, J. P. Vary, and B. R. Barrett. Large-basis ab initio no-core shell model and its application to ^{12}C . *Phys. Rev. C*, 62:054311, Oct 2000.
- [69] Petr Navrtil, Sofia Quaglioni, Ionel Stetcu, and Bruce R Barrett. Recent developments in no-core shell-model calculations. *Journal of Physics G: Nuclear and Particle Physics*, 36(8):083101, 2009.

- [70] W. E. Ormand and B. A. Brown. Isospin-mixing corrections for fp-shell fermi transitions. *Phys. Rev. C*, 52:2455–2460, Nov 1995.
- [71] Eulogio Oset and Mannque Rho. Axial currents in nuclei: The gamow-teller matrix element. *Phys. Rev. Lett.*, 42:47–50, Jan 1979.
- [72] N. M. Parzuchowski, T. D. Morris, and S. K. Bogner. Ab initio excited states from the in-medium similarity renormalization group. *Phys. Rev. C*, 95:044304, Apr 2017.
- [73] Piotr Piecuch, Karol Kowalski, Ian S. O. Pimienta, and Michael J. McGuire. Recent advances in electronic structure theory: Method of moments of coupled-cluster equations and renormalized coupled-cluster approaches. *International Reviews in Physical Chemistry*, 21(4):527–655, 2002.
- [74] Steven C. Pieper, , and R. B. Wiringa. Quantum monte carlo calculations of light nuclei. *Annual Review of Nuclear and Particle Science*, 51(1):53–90, 2001.
- [75] B. S. Pudliner, V. R. Pandharipande, J. Carlson, Steven C. Pieper, and R. B. Wiringa. Quantum monte carlo calculations of nuclei with $a \leq 7$. *Phys. Rev. C*, 56:1720–1750, Oct 1997.
- [76] P. Pulay. Improved scf convergence acceleration. *J. Comput. Chem.*, 3(4):556–560, 1982.
- [77] Péter Pulay. Convergence acceleration of iterative sequences. the case of scf iteration. *Chem. Phys. Lett.*, 73(2):393 – 398, 1980.
- [78] Matthew Redshaw, Georg Bollen, Maxime Brodeur, Scott Bustabad, David L. Lincoln, Samuel J. Novario, Ryan Ringle, and Stefan Schwarz. Atomic mass and double- β -decay q value of ^{48}Ca . *Phys. Rev. C*, 86:041306, Oct 2012.
- [79] Robert Roth, Joachim Langhammer, Angelo Calci, Sven Binder, and Petr Navrátil. Similarity-transformed chiral $nn + 3n$ interactions for the ab initio description of ^{12}C and ^{16}O . *Phys. Rev. Lett.*, 107:072501, Aug 2011.
- [80] H.F. Schaefer. *Quantum chemistry: the development of ab initio methods in molecular electronic structure theory*. Oxford science publications. Clarendon Press, 1984.
- [81] Meiyue Shao, Hasan Metin Aktulga, Chao Yang, Esmond G. Ng, Pieter Maris, and James P. Vary. Accelerating nuclear configuration interaction calculations through a preconditioned block iterative eigensolver. *CoRR*, abs/1609.01689, 2016.
- [82] I. Shavitt and R. J. Bartlett. *Many-Body Methods in Chemistry and Physics: MBPT and Coupled-Cluster Theory*. Cambridge Molecular Science. Cambridge University Press, 2009.
- [83] C. David Sherrill and Henry F. Schaefer. The configuration interaction method: Advances in highly correlated approaches. volume 34 of *Advances in Quantum Chemistry*, pages 143 – 269. Academic Press, 1999.

- [84] J. C. Slater. The theory of complex spectra. *Phys. Rev.*, 34:1293–1322, Nov 1929.
- [85] J. C. Slater. The theory of complex spectra. *Phys. Rev.*, 34:1293–1322, Nov 1929.
- [86] V. Somà, C. Barbieri, and T. Duguet. Ab initio gorkov-green’s function calculations of open-shell nuclei. *Phys. Rev. C*, 87:011303, Jan 2013.
- [87] V. Somà, C. Barbieri, and T. Duguet. Ab initio self-consistent gorkov-green’s function calculations of semi-magic nuclei: Numerical implementation at second order with a two-nucleon interaction. *Phys. Rev. C*, 89:024323, Feb 2014.
- [88] V. Somà, A. Cipollone, C. Barbieri, P. Navrátil, and T. Duguet. Chiral two- and three-nucleon forces along medium-mass isotope chains. *Phys. Rev. C*, 89:061301, Jun 2014.
- [89] S. R. Stroberg, A. Calci, H. Hergert, J. D. Holt, S. K. Bogner, R. Roth, and A. Schwenk. Nucleus-dependent valence-space approach to nuclear structure. *Phys. Rev. Lett.*, 118:032502, Jan 2017.
- [90] S. R. Stroberg, H. Hergert, J. D. Holt, S. K. Bogner, and A. Schwenk. Ground and excited states of doubly open-shell nuclei from ab initio valence-space hamiltonians. *Phys. Rev. C*, 93:051301, May 2016.
- [91] Jouni Suhonen and Osvaldo Civitarese. Weak-interaction and nuclear-structure aspects of nuclear double beta decay. *Physics Reports*, 300(3):123 – 214, 1998.
- [92] Jouni Suhonen and Osvaldo Civitarese. Probing the quenching of ga by single and double beta decays. *Physics Letters B*, 725(1):153 – 157, 2013.
- [93] D.J. Thouless. Stability conditions and nuclear rotations in the hartree-fock theory. *Nuclear Physics*, 21:225 – 232, 1960.
- [94] I S Towner and J C Hardy. The evaluation of v_{ud} , experiment and theory. *Journal of Physics G: Nuclear and Particle Physics*, 29(1):197, 2003.
- [95] I. S. Towner and J. C. Hardy. An Improved calculation of the isospin-symmetry-breaking corrections to superallowed Fermi beta decay. *Phys. Rev.*, C77:025501, 2008.
- [96] I. S. Towner and J. C. Hardy. Improved calculation of the isospin-symmetry-breaking corrections to superallowed fermi β decay. *Phys. Rev. C*, 77:025501, Feb 2008.
- [97] I. S. Towner and F. C. Khanna. Quenching of allowed gamow-teller β transitions in mirror nuclei. *Phys. Rev. Lett.*, 42:51–54, Jan 1979.
- [98] I.S. Towner. The nuclear-structure dependence of radiative corrections in superallowed fermi beta-decay. *Nuclear Physics A*, 540(3):478 – 500, 1992.
- [99] I.S. Towner. Quenching of spin operators in the calculation of radiative corrections for nuclear beta decay. *Physics Letters B*, 333(1):13 – 16, 1994.

- [100] K. Tsukiyama, S. K. Bogner, and A. Schwenk. In-medium similarity renormalization group for nuclei. *Phys. Rev. Lett.*, 106:222502, Jun 2011.
- [101] K. Tsukiyama, S. K. Bogner, and A. Schwenk. In-medium similarity renormalization group for open-shell nuclei. *Phys. Rev. C*, 85:061304, Jun 2012.
- [102] C. W. Ufford. Configuration interaction in complex spectra. *Phys. Rev.*, 44:732–739, Nov 1933.
- [103] E. K. Warburton and B. A. Brown. Effective interactions for the 0p1s0d nuclear shell-model space. *Phys. Rev. C*, 46:923–944, Sep 1992.
- [104] G. C. Wick. The evaluation of the collision matrix. *Phys. Rev.*, 80:268–272, Oct 1950.
- [105] B. H. Wildenthal, M. S. Curtin, and B. A. Brown. Predicted features of the beta decay of neutron-rich sd-shell nuclei. *Phys. Rev. C*, 28:1343–1366, Sep 1983.
- [106] Fred L. Wilson. Fermi’s theory of beta decay. *American Journal of Physics*, 36(12):1150–1160, 1968.
- [107] M. Włoch, D. J. Dean, J. R. Gour, M. Hjorth-Jensen, K. Kowalski, T. Papenbrock, and P. Piecuch. Ab-initio coupled-cluster study of ^{16}O . *Phys. Rev. Lett.*, 94:212501, Jun 2005.
- [108] Marta Woch, Jeffrey R Gour, Piotr Piecuch, David J Dean, Morten Hjorth-Jensen, and Thomas Papenbrock. Coupled-cluster calculations for ground and excited states of closed- and open-shell nuclei using methods of quantum chemistry. *Journal of Physics G: Nuclear and Particle Physics*, 31(8):S1291, 2005.